DEVELOPMENT AND VALIDATION OF A MICROFLUIDIC HYDROGEL PLATFORM FOR OSTEOCHONDRAL TISSUE ENGINEERING

A Dissertation
Presented to
The Academic Faculty

by

Stephen M. Goldman

In Partial Fulfillment
of the Requirements for the Degree
Doctor of Philosophy in Bioengineering in the
School of Mechanical Engineering

Georgia Institute of Technology
December 2014

DEVELOPMENT AND VALIDATION OF A MICROFLUIDIC HYDROGEL PLATFORM FOR OSTEOCHONDRAL TISSUE ENGINEERING

Approved by:

Dr. Gilda Barabino, Advisor
Department of Biomedical Engineering
Georgia Institute of Technology

Dr. Robert Guldberg
School of Mechanical Engineering
Georgia Institute of Technology

Dr. Edward Botchwey
Department of Biomedical Engineering
Georgia Institute of Technology

Dr. Johnna Temenoff
Department of Biomedical Engineering
Georgia Institute of Technology

Dr. Athanassios Sambanis
School of Chemical & Bimolecular Engineering
Georgia Institute of Technology

Dr. Spero Karas
Department of Orthopaedic Surgery
Emory University

Date Approved: October 31, 2014

To Anna for her love and support

ACKNOWLEDGEMENTS

I would like to acknowledge everyone who contributed supported me during throughout graduate school. First, I would like to thank my research advisor Dr. Gilda Barabino, for her role in my development as a scientist and engineer throughout this period of my life, and for her friendship on a personal level. I would also like to thank my committee members – Dr. Robert Guldberg, Dr. Ed Botchwey, Dr. Johnna Temenoff, Dr. Athanasios Sambanis, and Dr. Spero Karas for their insight and suggestions that helped guide me in the completion of this work. I deeply value the broad range of expertise that they contributed to this work and I am certain their advice helped to maximize the scientific impact of the work presented herein. Aside from those mentioned above, perhaps the most impactful influences during my time in graduate school have been my labmates and former suitemates from the Barabino, McIntire, and Lam Laboratories. In particular, Yueh-Hsun "Kevin" Yang deserves my greatest gratitude. Kevin was my predecessor in the Barabino Laboratory by one year, and he played a significant role in my early years in the laboratory as I was getting my feet wet in tissue engineering. Throughout the years, Kevin became my confidant, sounding board, and co-troubleshooter with regards to any experimental mishaps, of which there were more they I could have ever imagined when I started out on this journey. Finally, I need to acknowledge my family for all of their love and support throughout my time at Georgia Tech, particularly my wife Anna. Anna went through all of the ups and downs of graduate school right along with me, and despite some frustration at times, never wavered in her support of my goals. I'll never be able to fully express my gratitude for this, and I look forward to the next phase of life together.

TABLE OF CONTENTS

ACKNOWLEDGEMENTS ..... **IV**

LIST OF TABLES ..... **VII**

LIST OF FIGURES ..... **VIII**

LIST OF SYMBOLS ..... **X**

LIST OF ABBREVIATIONS ..... **XI**

SUMMARY ..... **XII**

1 INTRODUCTION **1**

1.1 MOTIVATIONS 1

1.2 RESEARCH OBJECTIVES 1

1.3 SIGNIFICANCE & SCIENTIFIC IMPACT 4

2 BACKGROUND **5**

2.1 THE OSTEOCHONDRAL UNIT 5

2.2 INTRA-ARTICULAR INJURY & TREATMENT 11

2.3 TISSUE ENGINEERING 15

2.4 OSTEOCHONDRAL TISSUE ENGINEERING 19

2.5 MICROFLUIDIC SCAFFOLDING IN TISSUE ENGINEERING 21

3 DEVELOPMENT AND VALIDATION OF A MICROFLUIDIC HYDROGEL FOR TISSUE ENGINEERING† **24**

3.1 INTRODUCTION 24

3.2 MICROFLUIDIC CONSTRUCT DESIGN 25

3.3 PARAMETRIC STUDY OF BIOPROCESSING PARAMETERS 28

3.4 MATERIALS & METHODS 30

3.5 RESULTS 34

3.6 DISCUSSION 38

3.7 CONCLUSIONS 41

4 EFFECT OF HYDRODYNAMIC LOADING ON MESENCHYMAL STEM CELL DIFFERENTIATION EFFICIENCY 42

4.1 INTRODUCTION 42

4.2 MATERIALS & METHODS 44

4.3 RESULTS 51

4.4 DISCUSSION 71

4.5 CONCLUSIONS 73

5 SPATIAL ENGINEERING OF OSTEOCHONDRAL TISSUE CONSTRUCTS THROUGH MICROFLUIDICALLY DIRECTED DIFFERENTIATION OF BOVINE MESENCHYMAL STEM CELLS 75

5.1 INTRODUCTION 75

5.2 MATERIALS & METHODS 77

5.3 RESULTS 82

5.4 DISCUSSION 87

5.5 CONCLUSIONS 89

6 FUTURE DIRECTIONS 91

7 FINAL THOUGHTS 99

APPENDIX A: MASS TRANSPORT PROPERTIES OF AGAROSE 101

APPENDIX B: BIOCHEMICAL PROTOCOLS 110

APPENDIX C: HISTOLOGY & IMMUNOHISTOCHEMISTRY 118

APPENDIX D: QUANTITATIVE RT-PCR PROTOCOLS 120

REFERENCES 125

LIST OF TABLES

Table 1.1: Parameters for Microfluidic Construct Design..... 27

Table 4.2: **Experimental Design Matrix**..... 46

Table 4.3: Parameters for Microfluidic Construct Design..... 49

Table A.1: Solute Diffusivities in Cell-Free Agarose Systems 101

Table A.2: **Solute Diffusivities in Cell-Seeded Agarose Systems** 102

Table A.3: **Solute Diffusivities in Articular Cartilage** 102

LIST OF FIGURES

Figure 2.1: Illustration of Osteochondral Unit 5

Figure 2.2: Illustration of Cartilaginous Matrix Components 7

Figure 2.3: Etiology & Incidence of PTOA 12

Figure 2.4: Overview of Osteochondral Repair Procedures 14

Figure 2.5: Bioreactor Configurations for Tissue Engineering 18

Figure 2.6: Overview of Pioneering Microfluidic Hydrogel Technologies 22

Figure 3.1: Microfluidic Construct Geometry 26

Figure 3.2: Bioprocessing Guidelines for Microfluidic Tissue Construct 29

Figure 3.3: Fabrication Process for Microfluidic Constructs 31

Figure 3.4: Biochemical Composition of Microfluidic Constructs 35

Figure 3.5: Mechanical Properties of Microfluidic Constructs 36

Figure 3.6: Histological Staining of Microfluidic Cartilage Constructs 37

Figure 4.1: Illustration of Custom Parallel-Plate Culture System 47

Figure 4.2: Expression of MSC Surface Markers 51

Figure 4.3: MSC Trilineage Induction 52

Figure 4.4: Gene Expression of Unsupplemented Static Cultures 53

Figure 4.5: Gene Expression of Unsupplemented Hydrodynamic Cultures 55

Figure 4.6: Gene Expression of TGF-β3 Supplemented Static Cultures 57

Figure 4.7: Gene Expression of BMP-2 Supplemented Static Cultures 58

Figure 4.8: 1 ng/mL BMP-2 Supplemented Hydrodynamic Cultures 60

Figure 4.9: 10 ng/mL BMP-2 Supplemented Hydrodynamic Cultures 61

Figure 4.10: 100 ng/mL BMP-2 Supplemented Hydrodynamic Cultures 62

Figure 4.11: 1 ng/mL TGF-β3 Supplemented Hydrodynamic Cultures 64

Figure 4.12: 10 ng/mL Supplemented Hydrodynamic Cultures 65

Figure 4.13: 100 ng/mL Supplemented Hydrodynamic Cultures 66

Figure 4.14: Histologic & Immunofluorescence Staining of Static Cultures 68

Figure 4.15: Histologic Staining of Low Shear Cultures 69

Figure 4.16: Histologic Staining of High Shear Cultures 70

Figure 5.1: Assembly of Microfluidic Osteochondral Constructs 79

Figure 5.2: DNA Content of Microfluidic Osteochondral Constructs 82

Figure 5.3: Differential Gene Expression of Osteochondral Constructs 83

Figure 5.4: sGAG Content of Osteochondral Constructs 84

Figure 5.5: Differential Collagen Content of Osteochondral Constructs 85

Figure 5.6: Histology & Immunofluorescence of Osteochondral Constructs 86

Figure A.1: Image Processing Algorithm for Mass Transport Measurements 106

Figure A.2: Sample Time Series of Dispersion Measurements 107

Figure A.3: Experimentally Determined Dispersion Coefficients 108

LIST OF SYMBOLS

C_0	Initial Concentration of Glucose in Culture Media
C_{out}	Concentration of Glucose in Culture Media Efflux
D_{eff}	Effective Diffusivity of Glucose in the Tissue Construct
D_{media}	Diffusivity of Glucose in the Culture Media
L_{bend}	Arc Length of Microfluidic Network Bends
$L_{channel}$	Microchannel Length Between Bends
L_{eff}	Effective Microchannel Length
N_{bend}	Number of Microfluidic Network Bends
$N_{channel}$	Number of Channels per Microfluidic Network
Q_{media}	Volumetric Flow Rate of Culture Media
R_i	Inner Radius of Microchannel
R_o	Outer Radius of Microchannel
λ	Maximum Allowable Microchannel Spacing
μ_{media}	Dynamic Viscosity of Culture Media
ν_{max}	Maximum Cellular Glucose Consumption Rate
π	Mathematical Constant
ρ_{media}	Volumetric Mass Density of Culture Media
φ	Thiele Modulus

LIST OF ABBREVIATIONS

ACI	autologous chondrocyte implantation
ACL	anterior cruciate ligament
ANOVA	analysis of variance
BM	basal medium
BMP-2	bone morphogenetic protein 2
BSA	bovine serum albumin
CCD	charge coupled device
CFD	computational fluid dynamics
DAPI	4',6-diamidino-2-phenylindole
DMEM	Dulbecco's Modified Eagle Medium
DMMB	1-9-dimethylmethylene blue
DMSO	dimethylsulfoxide
ECM	extracellular matrix
EDTA	ethylenediaminetetraacetic acid
ELISA	enzyme-linked immunosorbent assay
FITC	Fluorescein isothiocyanate
FBS	fetal bovine serum
GAG	glycosaminoglycan
MSCs	mesenchymal stem cells
OA	osteoarthritis
OATS	osteochondral autologous transfer system
PDMS	polydimethylsiloxane
PEG	polyethylene glycol
PSF	penicillin-streptomycin-fungizone
PTOA	post-traumatic osteoarthritis
SEM	standard error to the mean
TGF-β	transforming growth factor beta
VOI	volume of interest

SUMMARY

Due to the inability of intra-articular injuries to adequately self-heal, current therapies are largely focused on palliative care and restoration of joint function rather than true regeneration. Subsequently tissue engineering of chondral and osteochondral tissue constructs has emerged as a promising strategy for the repair of partial and full-thickness intra-articular defects. Unfortunately, the fabrication of large tissue constructs is plagued by poor nutrient transport to the interior of the tissue resulting in poor tissue growth and necrosis. Further, for the specific case of osteochondral grafts, the presence of two distinct tissue types offers additional challenges related to cell sourcing, scaffolding strategies, and bioprocessing. To overcome these constraints, this dissertation was focused on the development and validation of a microfluidic hydrogel platform which reduces nutrient transport limitations within an engineered tissue construct through a serpentine microfluidic network embedded within the developing tissue. To this end, a microfluidic hydrogel was designed to meet the nutrition requirements of a developing tissue and validated through the cultivation of chondral tissue constructs of clinically relevant thicknesses. Additionally, optimal bioprocessing conditions with respect to morphogen delivery and hydrodynamic loading were pursued for the production of bony and cartilaginous tissue from bone marrow derived mesenchymal stem cells. Finally, the optimal bioprocessing conditions were implemented within MSC laden microfluidic hydrogels to spatially engineer the matrix composition of a biphasic osteochondral graft through directed differentiation.

1 INTRODUCTION

1.1 Motivations

Articular Cartilage is a resilient load-bearing soft tissue which covers the ends of bones in synovial joints. It receives its functional properties from its large avascular, alymphatic, and aneural extracellular matrix primarily made up of collagens, proteoglycans, and water. The solid phase of the matrix (collagens and proteoglycans) provides the tissue with its strength to resist tensile and shearing loads, while the interaction of the proteoglycans with water in the matrix interstitial gives the tissue its resistance to compressive loads and durability. The avascular and alymphatic nature of the tissue, however, limit the tissue's ability to repair itself in the event of an acute traumatic insult. Further, severe intra-articular injuries can also impact the subchondral bone. Injuries which penetrate to the subchondral bone may result in filling of the defect with a suboptimal fibrocartilage resulting from the migration and differentiation of bone marrow progenitor cells. These sites subsequently result in a high reoccurrence of injury and progressive degeneration through a process coined post-traumatic osteoarthritis. As standard treatment of intra-articular defects are palliative in nature and do not offer true regeneration of the articular surface, novel therapeutic strategies are sought to combat these injuries through restoration of the biological and physical functions of the osteochondral unit.

1.2 Research Objectives

Tissue engineering has emerged as a promising strategy for the repair partial and full-thickness osteochondral defects. In order for engineered constructs to be clinically relevant functional criteria such as size, structure, mechanical properties, biochemical composition, immunological compatibility and integration capability must be met. Great strides toward meeting these criteria have been made such that the scientific community can now produce

constructs which approach the metrics of the native tissue for most of these criteria. The processes which produce such constructs, however, are limited in their ability to produce constructs which are simultaneously mechanically robust, adequately nourished, and of clinically relevant thickness.

Therefore, the overall goal of my dissertation was to develop and utilize a microfluidic hydrogel culture system which reduces nutrient transport limitations within engineered tissues and allows the delivery of biochemical and physical cues to modulate cell fate processes for the purpose of chondral and osteochondral defect repair. I approached this problem by addressing the following specific aims:

Specific Aim I: Parametric Design of Microfluidic Hydrogel Network for Optimal Nutrient Utilization in Tissue Engineering Constructs

Embedding a microfluidic network within the bulk of hydrogel based tissue engineering constructs offer the ability to spatiotemporally manipulate the physical and biochemical microenvironment of the resident cell population. To maximize the metabolic activity of the developing tissue, the design parameters of microfluidic network and culture conditions should be well characterized and controlled. The ***objective*** of this study is to design of the microfluidic network with regard to the number, size and spacing of channels, as well the material properties of the hydrogel, flow profile, and the seeding density of the cell source all impact the distribution and utilization of nutrients, wastes, and chemical signaling molecules in the tissue. Through the use of finite-element modeling and literature benchmarks an optimal microfludic hydrogel will be established for articular cartilage engineering. Our design will be ***validated*** by showing that our prototype produces tissue constructs which exhibit increased cell viability and proliferation, increased deposition of extracellular matrix components (collagen II, proteoglycans), and improved histological grading relative to static controls with and without embedded channels.

Specific Aim II: Determine the Effect of Hydrodynamic Loading on Chondrogenic and Osteogenic Differentiation of Mesenchymal Stem Cells

Mesenchymal Stems Cells (MSCs) are well known progenitor cells for both the chondrocyte and osteoblast lineages. The differentiation path can be modulated both by the composition of the media in which the MSCs are cultured, and by the physical environment in which the cells reside. The ***objective*** of this study, therefore, was to determine the effect of uniform superficial shear stress on the differentiation of bovine mesenchymal stems cells down the chondrogenic and osteogenic lineages. Specific Aim I provides a range of flow rates which provide for the homogeneous distribution of metabolic solutes (glucose, oxygen, growth factors) throughout the construct. Within this operating range, the flow rate was varied to elucidate the relationship between the magnitude and duration of the applied stress and the expression of chondrogenic and osteogenic markers. Additionally, cultures supplemented with inductive cytokines were assessed under static and dynamic loading conditions to elucidate synergistic effects of chemical supplementation and physical stimulation for the purpose of optimizing culture conditions for MSC differentiation. The ***working hypothesis*** of this study was that osteogenic differentiation will require exposure to a higher shear rate than chondrogenic differentiation.

Specific Aim III: Spatially Engineer Osteochondral Tissue Constructs Through Microfluidically Directed Differentiation of Mesenchymal Stem Cells

The ***objective*** of this study was to induce differential expression of chondrogenic and osteogenic markers within a continuous hydrogel construct for repairing osteochondral defects. Integrated osteochondral constructs with a differential phenotypic character were produced by incorporating independent, parallel flow structures into the bulk of the tissue construct and supplying optimized media and bioprocessing conditions differentially

within the two flow structures. The working ***hypothesis*** of this study was that the expression chondrogenic and osteogenic differentiation markers will vary according to spatial proximity to the microfluidic network doped with the appropriate induction cues.

1.3 Significance & Scientific Impact

The technological advancement and studies described herein have broad implications in the area of tissue engineering beyond the present application of chondral and osteochondral tissue engineering. It is not difficult to imagine extension of the technique to tissues of multiple cell types including vascularized tissues, tumorogenesis models, and interfacial tissue engineering (bone/tendon, bone/ligament, bone cartilage) as well as investigational drug and stem cell differentiation studies. The ability to expand the thickness of constructs produced in a high-throughput manner also opens the possibility of our technique being an enabling technology for the fulfillment cost-efficient, readily available tissue engineered substitutes for clinical implementation at hospitals around the world.

2 BACKGROUND

2.1 The Osteochondral Unit

The osteochondral unit is an apparent level organization of two distinct tissue types: the articular cartilage which provides a smooth wear resistant surface at the articulating junctions of diarthrodial joints and the subchondral trabecular bone. Between these two tissues, the mechanical and chemical makeup of the tissue varies in composition (**Figure 2.1**).

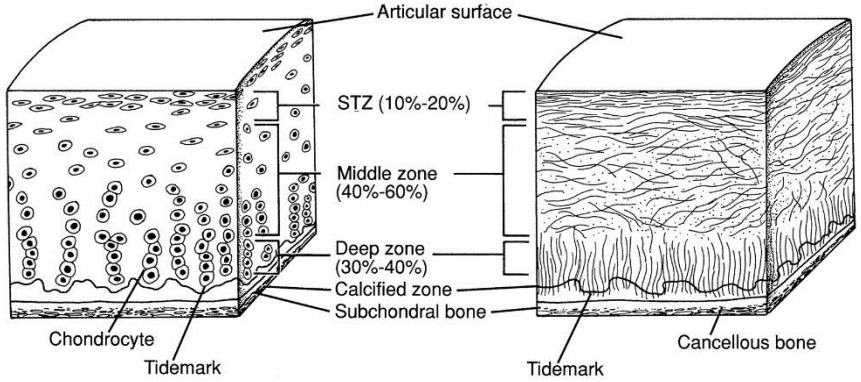

Figure 2.1: Illustration of Osteochondral Unit
The osteochondral unit consists of articular cartilage separated from a region of trabecular bone by a region of calcified cartilage. Image adapted from Buckwalter, J., Mow, V., et al. (1994). "Restoration of Injured or Degenerated Articular Cartilage." Journal of the American Academy of Orthopaedic Surgeons **2**(4): 192-201.

Described herein are the structure, composition, and function of these tissue that make them unique and are of the greatest importance when considering the rational design of a tissue engineered replacement.

2.1.1 Articular Cartilage Structure & Function

2.1.1.1 Tissue Composition

Articular cartilage is a white, dense, connective tissue, from 1 to 5 mm thick, that covering the ends of diarthrodial joints (Mow et al. 1984). It is composed of two distinct phases: a

solid organic phase consisting of cells and extracellular matrix, and an aqueous phase which fills the interstitial space of the matrix. The structure and composition of the solid phase varies in terms of cell shape and arrangement, proteoglycan concentration, and collagen fiber diameter and orientation as a function of distance from the articular surface. Close to the surface, thin collagen fibrils surround elongated chondrocytes and are oriented parallel to the surface. The proteoglycan content in this region, in low and the water content high largely due to its proximity to the synovium. Below this superficial region, exists a transitional region containing collagen fibers of a larger diameter lacking apparent organization, and chondrocytes of a more rounded morphology. Deeper still, the composition of the extracellular matrix increases in proteoglycan content, and contains a high concentration of large diameter collagen fibrils oriented perpendicularly to the articular surface. Chondrocytes in this region are typically arranged in a columnar fashion. Beyond this deep zone, there exists a region of calcified cartilage which is adjacent to the subchondral bone and characterized by small cells populating a cartilaginous matrix incorporating apatitic salts.

2.1.1.1.1 Chondrocytes

Chondrocytes are the specialized cells, derived from mesenchymal stem cells during skeletal morphogenesis, on which the formation of articular cartilage is dependent. They are the sole cell type present in mature articular cartilage and are highly sparse in distribution representing only 5% to 10% of the total cartilage volume (Hunziker et al. 2002). While metabolically active and responsive to various environmental stimuli, including soluble cytokines and changes in mechanical loading (Buckwalter 1997), they are non-migratory and non-proliferative under normal physiology and subsequently offer little regenerative capacity in the event of traumatic injury. Their primary function in their mature state is the turnover of cartilaginous matrix macromolecules in a state of dynamic

equilibrium between the cellular environment and the structure of the tissue (Lin et al. 2006).

2.1.1.1.2 Extracellular Matrix

The extracellular matrix of articular cartilage is comprised of two principal classes of macromolecules: collagens and proteoglycans (**Figure 2.2**).

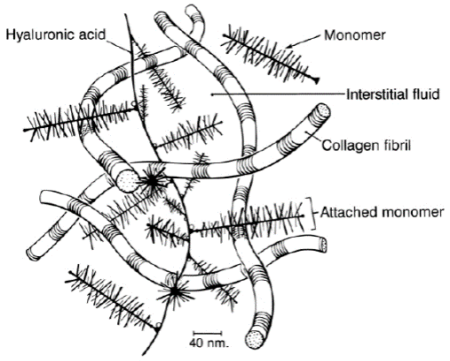

Figure 2.2: Illustration of Cartilaginous Matrix Components
The cartilaginous matrix is primarily made up of type II collagen fibrils and proteoglycans such as hyaluronic acid. Filling the interstitial space between these components is an aqueous fluid phase. Image adapted from Buckwalter, J., Mow, V., et al. (1994). "Restoration of Injured or Degenerated Articular Cartilage." Journal of the American Academy of Orthopaedic Surgeons **2**(4): 192-201.

Other biomolecules including lipids, phospholipids, and non-collagenous proteins, and make up the remaining portion of the ECM. Among collagen types II, VI, IX, X, and XI, type II collagen is the most abundant accounting for 90-95% of the collagen in hyaline cartilaginous matrix (Temenoff and Mikos 2000). The collagenous portion of the matrix generally consists of thin fibrils in a cross-linked network lacking organization with the exception of the superficial layer in which fibrils align parallel to the articular surface and in the deep zone where fibrillar arrangement perpendicular to the articulating surface promotes anchoring of the cartilage to the subchondral bone. In addition to imparting the tensile properties of the tissue, the collagen network also serves to control of the loss of fluid through the cartilage, and to encapsulate the other major constituent of the ECM, the

proteoglycans (Buckwalter and Mankin 1998; Cohen et al. 1998). Proteoglycans are complex macromolecules consisting of a protein core with covalently bound glycosaminoglycan chains. Glycosaminoglycans are long unbranched polysaccharides containing repeating carboxyl and/or sulfate groups which become ionized rendering them highly hydrophilic and promoting matrix hydration and resilience to compressive loads.

2.1.1.1.3 Water

Accounting for up to 80% of the wet weight of the tissue (Temenoff and Mikos 2000), water plays a critical role in the structure and function of articular cartilage. Water fills the intrafibrillar space of the collagenous matrix and associates with the negative charges on the glycosaminoglycan chains of the proteoglycan complexes to support the matrix under high compressive loads due to its incompressibility. The water is largely free to move through the matrix under the influence of a pressure gradient. As the water contains dissolved salts, gases, and metabolites this movement of water and exchange with the fluid of the synovium serves as the primary means of nutrient transport to the avascular tissue.

2.1.1.2 Tissue Mechanics

As previously discussed, articular cartilage is a biphasic material consisting of the solid components of the extracellular matrix and the aqueous fluid which fills its void space and it free to move through the tissue. It is this unique combination of tensile elements (collagens) and compressive strength through fluid pressurization that impart upon the tissue its viscoelastic mechanical properties and make it exceptionally wear resistant and absorbent of shocking deformations. Under compressive loading, the observed viscoelasticity is primarily due to drag as a result of interstitial flow of synovial fluid through the molecular pore space. Under shearing loads, the observed viscoelasticity is independent of fluid flow and largely due to straightening of the collagen fibers, friction between adjacent fibers, and the breaking of intermolecular bonds as is typical of most polymers.

2.1.2 Subchondral Bone Structure & Function

Subchondral bone refers to the cortical endplate and trabecular bone lying just below the calcified zone of the articular surface. Architecturally, it is composed of a branching lattice of internal beams and plates aligned along areas of mechanical stress. This region also contains a significant population blood vessels and nerves which can extend into the calcified cartilage. Physiologically, subchondral bone serves multiple functions including calcium homeostasis and housing bone marrow which serves as the production site of hematopoietic and mesenchymal precursors. Structurally, the synergy of the molecular, cellular, and tissue arrangement results in a strong yet light weight structural tissue, which serves as an anchoring and structural support for articular cartilage.

2.1.2.1 Tissue Composition

2.1.2.1.1 Bone Cells

There are three principal cell types present in bone: osteoblasts, osteocytes, and osteoclasts. Osteoblasts are the cells responsible for the formation of bone through the production of type I collagen, osteocalcin, and bone sialoprotein and other less abundant bone proteins. Osteocytes are former osteoblasts that have become encased in a mineralized matrix. Osteocytes exhibit long processes that are able to extend through the bone's canaliculi to establish cell-to-cell contact with adjacent cells. For this reason, osteocytes are believed to play a mechanosensory role in bone metabolism and calcium exchange. At the other end of the spectrum are osteoclasts, the cells responsible for the resorption of bone through production of acid phosphatases. They are derived from the same hematopoietic precursors of monocytes and macrophages.

2.1.2.1.2 Extracellular Matrix

The composition of bony matrix consists of two solid phases of which approximately 60-70% is inorganic in nature with the remainder consisting of collagen and other organic

molecules (Biltz and Pellegrino 1969; Fritsch et al. 2009; Lees 2003; Vuong and Hellmich 2011). The matrix takes on the form of an interpenetrating mesh with strength in both tension and compression due to the organic and inorganic phases respectively. The inorganic component of bone is principally composed of a calcium phosphate mineral analogous to crystalline calcium hydroxyapatite, which is deposited by osteoblasts. These deposits act as a both a reservoir for ion homeostasis and as a dopant to increase the compressive strength of the tissue. The organic phase is primarily type I collagen and plays a significant role in determining the structure and the mechanical properties of the bone. Collagen type I owes its strength to structure in the form of a triple helix of three alpha chains stabilized by hydrogen bonding. This structure makes collagen an excellent tension element, particularly when bundled. The remaining portion of the organic matrix consists osteopontin, bone sialoprotein, and growth factors responsible for maintenance of bone structure.

2.1.2.2 Tissue Mechanics

Bone is an interesting structural material in that it can modulate its properties and geometry at the microscopic level in order to accommodate changes in metabolic demand and mechanical loading at the macroscopic level. This is particularly true for trabecular bone for which large spatiotemporal variations in density are observed due to age and the amount of load a particular anatomic site typically bears. In general, the apparent modulus of trabecular bone can vary from approximately 10 MPa to 2,000 MPa, depending on the anatomic site and age (Morgan et al. 2003). These variations in trabecular density also result in significantly different behaviors under tensile loads relative to compressive loading. Under tension, the failure mode is significantly different as individual trabeculae will tend to fracture in areas of highly concentrated stress. This is important as failure under compression in not likely to have an effect at the organ level, whereas tensile failure could lead to fracture propagation across large swaths of the bone.

2.2 Intra-Articular Injury & Treatment

The average human knee experiences approximately one million cycles of loading each year. In the event that an injury compromises the function of a synovial joint, damage to the articular surface often occurs either through direct insult or as a result of incongruities and abnormal loading (Buckwalter 1992; Buckwalter 2002). This damage may take the form of fissures, flaps, and tears, which are permanent in nature due to the lack of regenerative capacity inherent in articular cartilage. Injuries which penetrate to the subchondral bone may result in filling of the defect with a suboptimal fibrocartilage resulting from the migration and differentiation of bone marrow progenitor cells. These sites subsequently result in a high reoccurrence of injury and progressive degeneration through a process coined post-traumatic osteoarthritis.

2.2.1 Post-Traumatic Osteoarthritis

If allowed to progress unabated, a degenerative condition coined post-traumatic osteoarthritis (PTOA) may become symptomatic within three months of the initial injury (Buckwalter 1992; Buckwalter and Brown 2004; James et al. 2004; Nelson et al. 2006). Because articular cartilage lacks a sufficient self-repair mechanism, the injury site becomes a nucleating center for the progressive degeneration (**Figure 2.3**) of the articular surface due to incongruities and unnatural loading regimes which if left unchecked, could lead to osteoarthritis and the associated chronic, debilitating pain and swelling (Buckwalter 1992; Buckwalter 2002; Buckwalter and Brown 2004; Buckwalter and Mankin 1998; Nelson et al. 2006).

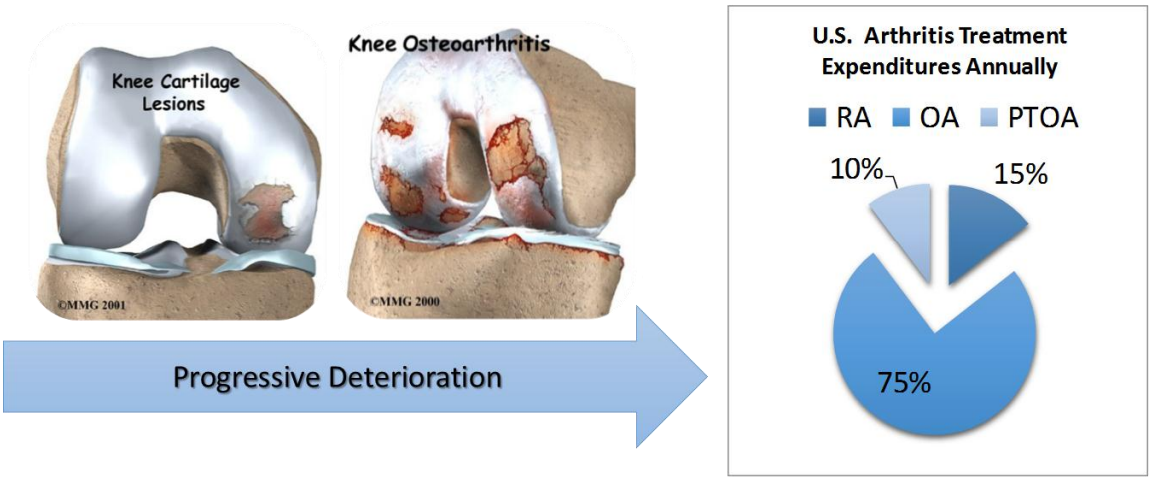

Figure 2.3: Etiology & Incidence of PTOA

PTOA arises from incongruities of the articular surface and abnormal loading conditions following traumatic injury, and results in treatment expenditures representing 10% of total arthritis related expenditures in the United States. This image was modified and adapted from www.maitrise-orthop.com.

While older patients with crippling OA often can be treated effectively with joint replacement or joint fusion, these approaches are not as acceptable or effective for the young and middle-aged adults which PTOA most commonly afflicts. For this reason, younger patients with PTOA present an especially difficult clinical problem. Thus, new therapeutic approaches aimed at regenerating the articular cartilage surface with respect to biological and mechanical function are sought, which might prevent the onset of PTOA, and mitigate the future physical and medical costs associated with end-stage osteoarthritis (OA).

2.2.2 Standard of Care

Due to the inability of intra-articular injuries to adequately self-heal, current therapies are largely focused on alleviation of symptoms and restoration of joint function rather than true regeneration. Non-surgical treatments, suitable for partial thickness defects, include pharmacological treatment of inflammation and viscosupplementation therapies based on the injection of hyaluronate based materials. The long-term efficacy of such approaches,

however, is poor. Full-thickness osteochondral defects are generally too severe for these types of treatments to have any significant benefit and generally require surgical intervention. The least invasive procedures include lavage and debridement which can be performed arthroscopically and consist of the removal of irritating debris and the contouring of the articular surfaces to minimize unnatural loading due to geometric incongruities. Like pharmacologic interventions and viscosupplementation protocols, these procedures are palliative in nature, and may still result in degenerative changes within the joint, particularly in the long-term. The first set of more efficient repair techniques consists of stimulation of the bone marrow within the subchondral bone. This is accomplished by drilling, abrasion or microfracture techniques and results in filling of the defect by migration of MSCs (Simon and Jackson 2006). This approach, however, is suboptimal as the repair tissue secreted by the MSCs exhibits fibrocartilaginous characteristics including inferior mechanical properties to the surrounding native tissue resulting in the repair site remaining a nucleating center for degeneration within 1-2 years.

The other category of reparative procedures includes the implantation of a graft. Autologous transplantation techniques require sourcing the patient's own healthy tissue for grafting material to be placed into the defect site. The mosaicplasty or OATS (osteochondral autologous transfer system) procedure is one such technique in which the defect is cleaned up through debridement and multiple individual osteochondral biopsies are harvested from an adjacent, non-load bearing region and press fit into the defect (**Figure 2.4**).

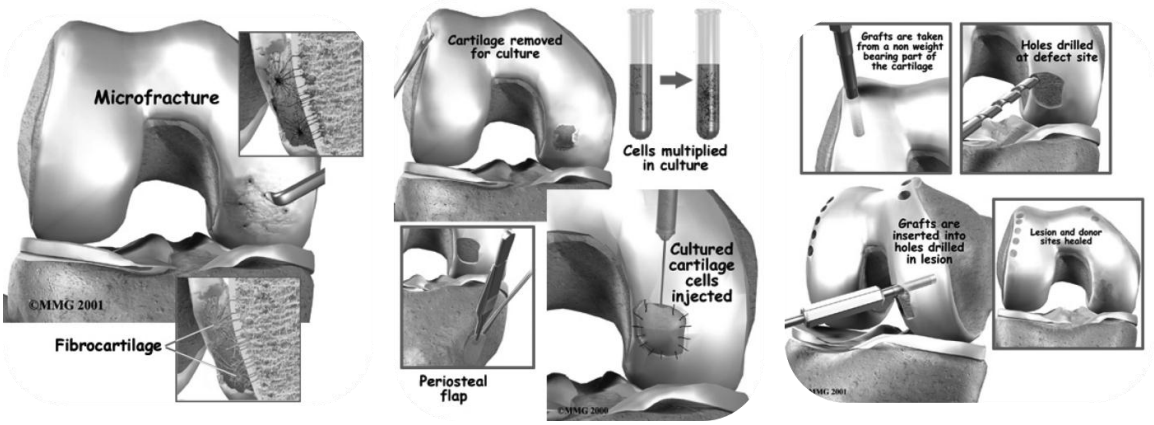

Figure 2.4: Overview of Osteochondral Repair Procedures
The mosaicplasty procedure is an autologous grafting technique used to treat osteochondral lesions through the transplantation of healthy, native tissue to the defect site from an adjacent, non-load bearing region. This image was modified and adapted from www.maitrise-orthop.com.

This technique represents a suitable reparative approach, but carries with it a high risk for donor-site morbidity. Another similar approach involves the transplantation of allogenically sourced grafts inserted into the defect in a similar manner. While this approach eliminates the donor site morbidity associated with mosaicplasty, it carries with it immunological risks that may result in transmission of disease or the rejection of the donor tissue.

Autologous Chondrocyte Implantation (ACI) is yet another similar approach to mosaicplasty in that it uses autologous material from a non-load bearing site. It differs, however, in that the biopsied tissue is digested and the patient's cells are expanded in culture before reintroduction into the defect underneath a flap fashioned from the patient's periosteum. Finally, non-biological approaches include total knee replacement via condylectomy and insertion of a metallic implant. Because this prosthesis is only typically viable for just over a decade, such a drastic procedure is reserved for patients over the age of 65, and typically not recommended for younger patients. Additionally, the materials

these implants are construct from poorly simulate the physiological and mechanical functions of native tissues, often resulting in disrupted gait.

2.3 Tissue Engineering

2.3.1 General Approach

Tissue engineering is an interdisciplinary field that draws from concepts of the traditional engineering disciplines and life sciences and is focused on the development of biological substitutes for the repair and restoration of tissue function in the event of injury or disease. Subsequently, tissue engineering & regenerative medicine as complementary fields have the potential to transform the landscape of current treatment strategies for severe physical injuries and to provide a better quality of life for the patient population. The classical approach to tissue engineering involves the incorporation of a suitable cell source into a biodegradable scaffold within which the resident cells synthesis an extracellular matrix under the influence of mechanical and chemical signals within the controlled environment of a bioreactor system. To understand tissue engineering as a field and identify areas for innovation in the case of osteochondral regeneration, it is paramount to understand the role of each of the members of this triad and how they interact to produce an osteochondral tissue construct.

2.3.1.1 Cell Sourcing

The production of an engineered tissue *in vitro* requires the use of cells to populate the tissue construct and produce neotissue through proliferation and matrix elaboration that resembles that of the native tissue in both composition and function. The most common cell sources for osteochondral tissue engineering are primary chondrocytes and osteoblasts as wells as their common progenitor, mesenchymal stem cells (Martin et al. 2007). Autologous chondrocytes must be harvested from a non-load bearing donor site, and as a result suffer from the additional clinical symptoms of donor site morbidity (Huntley et al.

2005). Additionally, the harvest procedure is generally low yield necessitating the *in vitro* expansion of the primary cells prior to incorporation into a tissue engineered graft (Brittberg et al. 1994; Huntley et al. 2005; Mats 2008). The low availability of these cells represents a significant challenge to any large scale manufacturing process of engineered constructs as a limited life span, dedifferentiation upon monolayer expansion (Darling and Athanasiou 2005), and the high cost of maintaining these cells in culture become prohibitive. With these challenges in mind, mesenchymal stem cells (MSCs), whose availability, multi-potentiality, and expanded lifespan make them commercially enticing, are seen as a promising alternative cell source for regeneration of osteochondral defects (Kuo and Tuan 2003; Merceron et al. 2010). Induction of the desired phenotype is generally accomplished through chemical induction, but may also be accomplished through manipulation of the cellular microenvironment by manipulating the attachment substrate or external forces. No matter the method or combination of methods chosen, a robust and repeatable induction protocol is necessary to achieve the desired phenotype and to avoid the development of non-desirable tissue traits.

2.3.1.2 Scaffolding

Tissue-engineering approaches typically employ exogenous scaffolds intended to recapitulate the three-dimensional extracellular matrix and provide mechanical support during the early stage growth of the engineered construct (Kim and Mooney 1998). Typically, a well-designed scaffold with be highly porous with an interconnected pore network to accommodate the transport of nutrients and wastes from the seeded cell population to allow for cell proliferation and elaboration of a tissue specific matrix. Additionally, the material should have material properties such that it is biocompatible, bioresorbable, and of appropriate stiffness to meet the functional requirements of the target tissue either on its own or in concert with the properties of accumulated neotissue following cultivation. Given that the scaffold must be both bioresorbable and mechanically function

will require careful matching of the dynamics of scaffold degradation and neotissue accumulation such that the accumulated matrix can fill both the physical space vacated by the scaffold and its role in supporting further development in vitro or intended function in vivo. In attempts to meet these criteria, a myriad of natural and synthetic polymers have been investigated as potential scaffolding materials for cartilage and osteochondral tissue engineering applications. Structurally, the materials generally take on one of several forms: woven or non-woven meshes, ordered or random open cell structures, and hydrogels (Dietmar W 2000). Among these forms, hydrogels are of particular interest due to their diffusion properties, wide availability, and capability to be homogeneously seeded by mixing a concentrated cell solution with the polymer solution prior to gelation (Vinatier et al. 2006). Further, hydrogels are highly customizable in terms of gelling mechanisms for manufacturing and incorporation of biomimetic features to permit cellular processes such as adhesion, migration, proliferation, and differentiation.

2.3.1.3 Bioreactors

Bioreactors are systems which allow for biological processes to develop under tightly controlled environmental and operating conditions (e.g. pH, temperature, pressure, nutrient supply and waste removal) (Martin et al.). Within the context of tissue engineering and *in vitro* tissue culture, bioreactors permit the cultivation of larger, better organized engineered cartilage than can be grown in static Petri dishes (Concaro et al. 2009; Darling and Athanasiou 2003; Haasper et al. 2008). This is due in large part to the flow and mixing of culture media within bioreactors that is expected to affect tissue formation in at least two ways: by enhancing mass transfer and by direct physical stimulation of the cells (Bilgen et al. 2005; Bilgen et al. 2006; Boschetti et al. 2005; Cinbiz et al. 2010; Hutmacher and Singh 2008; Kenneth A. Williams 2002; Lawrence et al. 2009; Sucosky et al. 2004; Yao and Gu 2004b). Depending on the application, several configurations of bioreactors have been well studied in the literature for the purpose of cartilage and/or osteochondral tissue

engineering (**Figure 2.5**). *In vivo*, mass transfer to chondrocytes involves diffusion and convective transport by the fluid flow that accompanies tissue loading (Albro et al. 2008; Mow et al. 1984). *In vitro*, the bioreactors achieved convective mass transport either through compressive loading intended to mimic physiological loading, direct perfusion of the tissue construct through the action of an external pump, or through mixing of the culture media around the constructs to enhance mass transport at construct surfaces. As the development of the tissue construct occurs over time, transport provided to the construct surface may become insufficient for the cells embedded deep within large tissue constructs resulting in nutrient transport becoming the key limiting factor the functionality of tissue derived from the cultivation process.

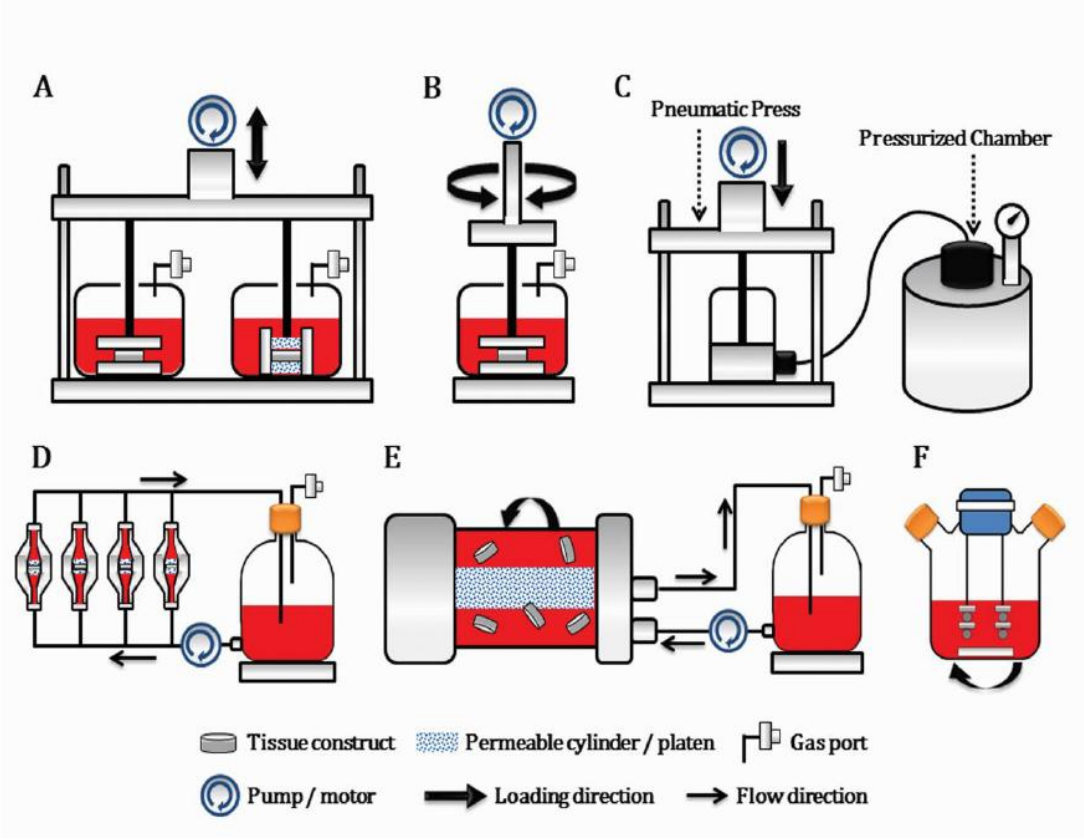

Figure 2.5: Bioreactor Configurations for Tissue Engineering
Bioreactor systems in cartilage tissue engineering. (A) Confined and unconfined compressive loading. (B) Shear deformation. (C) Hydrostatic pressure. (D) Direct perfusion. (E) Rotating vessel. (F) Spinner flask. Image adapted from Yang, Y.-H. and Barabino, G.A. (*in press*) Environmental Factors in Cartilage Tissue Engineering. *Tissue*

and Organ Regeneration: Advances in Micro and Nanotechnology. Editors: Zhang, L.G., Khademhosseini, A. and Webster T.

Although the tissue-engineering strategy is not widely implemented clinically, it presents obvious advantages when compared with traditional treatments. First, the tissue engineering paradigm in which autologous cells are utilized in the production of the construct ensures immunocompatibility and eliminates the disease transmission worries of traditional allografts. Second, bioreactor technologies allow for the optimization of the cultivation process to ensure the repair tissue is mechanically and physiologically functional. Finally, the scale-up made possible through the culture of such bioartificial substitutes solves the problem of the critical donor shortage presently limiting the application of the transplantation technique. Those benefits justify the current efforts to better control this treatment strategy and to address its challenges.

2.4 Osteochondral Tissue Engineering

Having covered the general philosophy of tissue engineering, it is also pertinent to review the literature on common approaches specific to repairing articular cartilage and the osteochondral unit. Challenges specific to this biphasic tissue include spatially varying material properties, cell types, and biochemical composition and the development of appropriate bioreactors and bioprocessing procedures for the cultivation of osteochondral grafts. Regarding cell sourcing and scaffolding selection, the literature can be grouped into three primary categories: primary chondrocytes alone (Hung et al. 2003; Kandel et al. 2006; Kreklau et al. 1999; Niederauer et al. 2000; Waldman et al. 2003a; Wang et al. 2004), spatially segregated chondrogenic and osteogenic sources (Cao et al. 2003; Schaefer et al. 2002; Schaefer et al. 2000; Schek et al. 2004), and a multipotent stem cell source having both chondrogenic and osteogenic differentiation capacity (Alhadlaq et al. 2004; Gao et al. 2001a; Tuli et al. 2004). Additionally, acellular regenerative approaches employing only a scaffold or a scaffold loaded with cellular recruitment factors have been pursued (Fukuda

et al. 2005). Of the cell-based approaches, the stem cell strategy suffers from the least tradeoffs in terms of proliferative capacity and sourcing material scarcity. These cell groups have then be seeded onto a number of scaffolding materials and architectures including: (I) scaffold-free approach for the chondrogenic region coupled with a scaffolded approach for the bony region, (II) separate scaffolding strategies for each region, and (III) a single scaffolding strategy for both regions (Martin et al. 2007). For instance, Tuli et al. utilized strategy (I) by coating polylactic acid (PLA) scaffolds with progenitor cells of mesenchymal origin to produce osteochondral grafts. One face of the grafts was seeded with cells precultured in chondrogenic media, while the other was coated with cells precultured in osteogenic media. Following seeding the constructs were cultured in a mixed-cocktail media with the goal of promoting chondrogenesis and osteogenesis simultaneously (Tuli et al. 2004). Following culture, construct exhibited hyaline cartilage overlying a bony region with an interface between the two regions resembling the tidemark of the native tissue. While the results of this study were promising, the approach was non-optimal as it required redundant cultures prior to scaffold incorporation and subjected to the construct to non-optimal maintenance media rather than media which might further promote region specific properties. As for the second scaffolding strategy, Gao et al. reported osteochondral constructs by combining precommitted MSCs into a hyaluronate-ceramic composite scaffolds (Gao et al. 2001b). Like the study by Tuli et al., these constructs also required a predifferentiation step prior to incorporation into the composite scaffolding. They also required the use of a glue to incorporate the two layers together. When implanted subcutaneously in an immunocompromised mouse model for six weeks the constructs showed evidence of non-desirable collagen type I expression within the chondral region for a more fibrocartilaginous character than that of the desired hyaline composition. Significant results using the third strategy in which a single, homogenous scaffold seeded with a common cell source include the work of Alhadlaq et al in which they separately predifferentiated progenitor cells of mesenchymal origin and incorporated

them into two integrated PEG hydrogel layers through sequential photopolymerization (Alhadlaq et al. 2004). This approach resulted in spatially separated synthesis of cartilaginous and bony matrices following 4 weeks of implantation into a mouse model. The common limitation present in each of the highlighted studies above is the reliance on a predifferentiation step prior to incorporating the mesenchymal progenitor cells into the osteochondral scaffold. This reliance on predifferentiation limits the usefulness of these approaches test beds for studying the development of tissues and makes them commercially less viable as they require longer times in culture, which increases their production cost relative to a solution in which the cells can be differentiated in situ with spatial specificity. Advancement of the production of tissue engineered medical products for osteochondral repair will require further development of enabling technologies to better control the culture of the cell source for both differentiation and promotion of region specific matrix development.

2.5 Microfluidic Scaffolding in Tissue Engineering

Microfluidic systems have gained popularity as a way to mitigate the issues of cultivating large, densely populated constructs, by combining the three pillars of the tissue engineering triad into a single highly controllable complex. The incorporation of microchannels throughout the construct allows for convective transport of nutrient and oxygen into and waste products out of the developing tissue creating the potential for the creation of function tissues and the ability to control spatiotemporal presentation of nutrients, cytokines, growth factors, and other morphogens (Huang et al. 2011). Hydrogels are an optimal target material class for the embedding of microfluidic channels due their advantageous diffusion properties, tunable mechanical properties, and ease of production. Additionally, the presence of arranged channels reduces the resistance to perfusion of hydrogel constructs effectively increasing the perfusion capacity. By incorporating multiple independent networks within a single construct, microfluidics also offers the

ability to impart spatial complexity on the tissue as networks can be differentially loaded. To date several groups have attempted to utilize the concept of microfluidic hydrogels for cell and tissue culture (Bettinger and Borenstein 2010; Borenstein et al. 2010; Golden and Tien 2007; Johann and Renaud 2007; Ling et al. 2007; Song et al. 2009), a primary focus on fabrication techniques and characterization of transport properties (**Figure 2.6**).

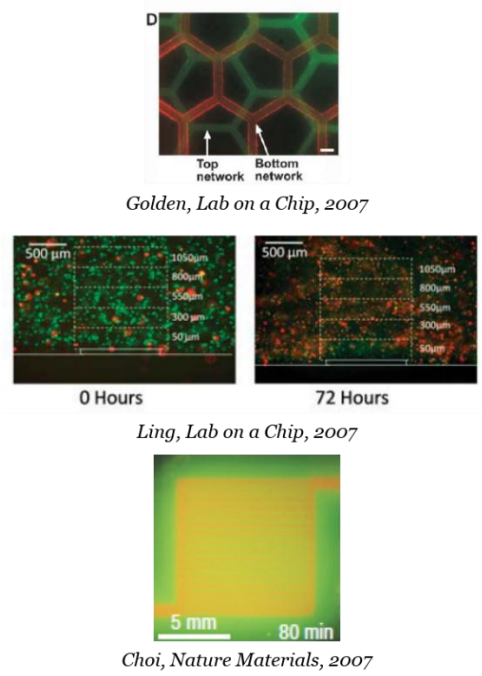

Figure 2.6: Overview of Pioneering Microfluidic Hydrogel Technologies
The pioneering work in the field of microfluidic hydrogels focused on fabrication technologies, characterization of transport properties and assessment of cell viability.

The first significant reports of microfluidic hydrogels appeared in 2007 when Ling et al., Golden et al. and Choi et al. separately reported transport characteristics and cell viability measurement in agarose, collagen, and calcium-alginate based hydrogels respectively. Choi et al. provide a particularly nice treatment of the mass transport properties by both transient measurement of FITC-labeled BSA and diffusion-reaction dynamics of a live dead stain using two independent networks spatially separated within the same plane. While Ling et al. and Choi et al. used molding techniques to produce their microfluidic networks, Golden et al. utilized a sacrificial element approach to selectively degrade the

microchannel space (Golden and Tien 2007). Subsequent studies, expanded on these works to include further optimization of transport and assessment of mechanical properties. For instance, Park et al (2010) fabricated a micro-porous cell-laden agarose hydrogel with a single microfluidic channel formed via insert molding around a capillary tube (Park et al. 2010). Additionally the porosity of the agarose was modulate via the introduction of sucrose crystal. Utilizing this system, hepatocytes were cultured for a period of 5 days. Mass Transport properties of the microfluidic hydrogel were assess via a FITC-labeled tracer and viability assessed via a live-dead stain and image analysis. Primary findings indicated that transport properties and hepatocyte viability were increased with sucrose incorporation while mechanical properties were decreased. In summary, these studies have modeled nutrient transport using one and two dimensional diffusion-uptake models (Song et al. 2009), exhibited cell viability of short culture periods (Bettinger and Borenstein 2010; Borenstein et al. 2010; Golden and Tien 2007; Ling et al. 2007; Song et al. 2009), or only studied a single channel system (Ling et al. 2007), but none have extended their analysis to three dimensional studies of nutrient transport or extended culture periods, a critical step to expanding the paradigm for widespread adaptation.

3 DEVELOPMENT AND VALIDATION OF A MICROFLUIDIC HYDROGEL FOR TISSUE ENGINEERING†

†Portions of this chapter are adapted and modified from: Stephen M. Goldman and Gilda A. Barabino. Long-Term Culture of Agarose-Based Microfluidic Hydrogel Promotes Proliferation and Development of Critically Sized Tissue Engineered Articular Cartilage Constructs, Journal of Tissue Engineering & Regenerative Medicine, Available Online 4 SEPT 2014, DOI:10.1002/term.1954.

3.1 Introduction

Tissue-engineered cartilage constructs show great promise as a future regenerative therapy for patients suffering from PTOA by offering the potential to relieve symptoms and prolong patient mobility without the inherent disadvantages of total joint arthroplasty. Even so, challenges persist and clinically relevant successes have proven difficult to achieve. Chief among these challenges is poor mass transfer and nutrient transport to the interior of large, full-thickness constructs resulting in large gradients in cell viability and matrix deposition as well as inadequate mechanical functionality (Bueno et al. 2008; Bursac et al. 1996). Various approaches have been taken to improve the influx of nutrients and efflux of wastes from the bulk of hydrogel constructs including altering the density and geometry of the inherent pore structure of hydrogel scaffolding (Annabi et al. 2010; Hollister et al. 2002; Hwang et al. 2010) and forced convection approaches in which media is perfused through the construct (Davisson et al. 2002; Porter et al. 2005). The effects of the former of these approaches are short lived as cell proliferation and matrix deposition quickly fill the void space in the nanoporous hydrogels, and the latter approach requires large pressure heads due to the low permeability of the constructs. Embedded microfluidic channels offer the potential to maximize the perfusion capacity, create spatial complexity, and allow control over the spatial and temporal presentation of hydrodynamic and chemical cues within the developing construct (Bettinger and Borenstein 2010; Bettinger et al. 2005; Borenstein et al. 2010; Choi et al. 2007b; Golden and Tien 2007; Huang et al. 2011; Johann and Renaud 2007; Khademhosseini et al. 2006; Ling et al. 2007; Song et al. 2009; Sugiura et al. 2011).

Methods for the production of the microfluidic channels include molding (Borenstein et al. 2010; Choi et al. 2007a; Ling et al. 2007), bioprinting (Boland et al. 2007; Lee et al. 2010), photopatterning (Cuchiara et al. 2010; Lee et al. 2008), and use of sacrificial elements (Golden and Tien 2007). These pioneering studies, however, have fallen short of achieving a microfluidic construct which is sufficiently thick and robust for long term culture of tissue engineered substitutes.

We designed and characterized a microfluidic agarose-based construct for articular cartilage replacements by first determining the parameters for an optimal microfluidic network in terms of the number, size and spacing of channels, as well the material properties of the agarose hydrogel, the rate of perfusion of media through channels, and the cell seeding density, factors known to impact the distribution and utilization of nutrients, wastes, and chemical signaling molecules in tissues (Devarapalli et al. 2009; Galban and Locke 1999; Huang et al. 2011; Roberts et al. 2011; Sengers et al. 2005; Song et al. 2009; Yao and Gu 2004a). Chondrocyte-seeded, agarose-based microfluidic constructs were cultivated for up to two weeks and evaluated for cell proliferation and elaboration of a cartilaginous matrix relative to solid, statically cultured controls. Specifically, we are interested in the production of Collagen II and glycosaminoglycans within the construct as these are the primary components of the cartilaginous matrix which contribute to the unique biomechanical properties of the tissue (Mow et al. 1980).

3.2 Microfluidic Construct Design

In designing our microfluidic construct, we assumed a spatially homogeneous population of bovine articular chondrocytes encapsulated within an agarose gel, and embedded with a microfluidic network of square cross section (**Figure 3.1**). An additional requirement was that, microfluidic channels within tissue constructs be distributed such that the encapsulated cells are all well-nourished. Therefore, the design parameters for the

construct include the nominal dimensions of the construct, microchannel spacing, and number of microchannels, volumetric flow rate, cell seeding density, and the solid volume fraction of the agarose gel.

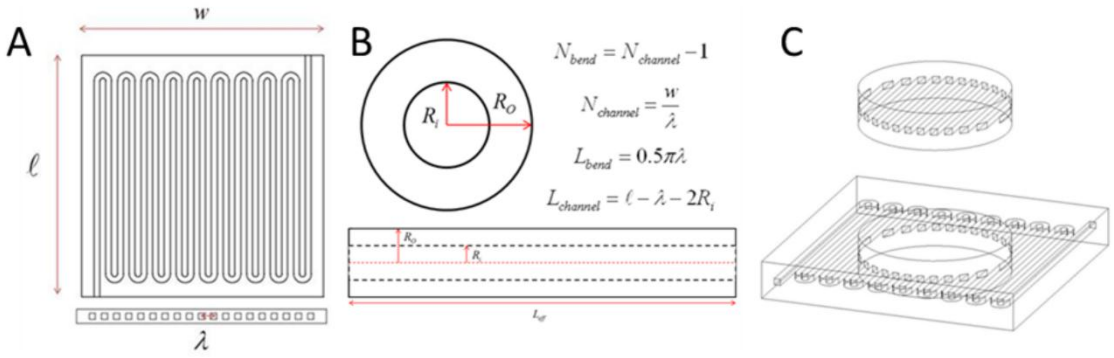

Figure 3.1: Microfluidic Construct Geometry
(A) Cross-section of microfluidic construct. (B) Approximation of construct as a tissue cylinder. The effective length of the cylinder is the total length of the microfluidic network, including bends, with construct with design equations defining the relationship between the nominal dimensions of the construct to the number and spacing of the microchannels. (C) A volume of interest was defined within the perfusion-cultured microfluidic constructs, on which all data analysis was performed to avoid edge effects and achieve geometric similarity with the static controls

To simplify the design process, the construct was modeled as a single cylindrical unit with an effective length (L_{eff}) equal to the total length of the serpentine microfluidic network as defined in Equation 3.1, where N_{bend} and $N_{channel}$ are the number of 180° bends and network passes respectively. L_{bend} and $L_{channel}$ are the equivalent length of the bend and each network pass respectively defined in terms of the construct dimensions and channel spacing.

$$L_{eff} = N_{bend}L_{bend} + N_{channel}L_{channel} \quad (3.1)$$

Appropriate spacing for the microchannels was determined based on a two-dimensional axisymmetric diffusion-consumption analysis. For the system under consideration, the Thiele modulus (φ) can be expressed in terms of the inner (R_i) and outer (R_O) radii of a single cylindrical tissue unit (**Equation 3.2**), with appropriate diffusion and kinetic parameters (**Table 1.1**).

$$\varphi = \frac{R_O^2 - R_i^2}{2R_i}\sqrt{\frac{\nu_{max}}{K_m D_{eff}}} \tag{3.2}$$

Table 1.1: Parameters for Microfluidic Construct Design

Physical Parameter	Value	Units
D_{media}	9.2e-10[#]	m^2/s
D_{eff}	7.5e-10[$]	cm^2/s
C_0	5.5	mol/m^3
ν_{max}	1.1e-16[#]	$mol \cdot cell^{-1} \cdot s^{-1}$
K_m	0.35[#]	mol/m^3
ρ_{media}	1030	kg/m^3
μ_{media}	1.00	cP
Q_{media}	0.25	cm^3/min

[#]as reported by Sengers et. al. 2005
[$]Calculated using Mackie-Mears Relationship

The outer radius of this unit represents the extent to which encapsulated cells are well nourished. With an inner radius corresponding to the fixed hydraulic radius, and an upper bound set on the Thiele modulus of 0.3 to ensure no mass transfer limitations on glucose consumption, the maximum metabolically allowable spacing (on center) between two adjacent cylindrical units, λ, can be expressed as twice the maximal outer radius (Equation 3.3).

$$\lambda = 2R_o \tag{3.3}$$

The final design parameter for the construct is the volumetric flow rate of the culture media through the microfluidic network. The calculation determining the maximal channel spacing distance is dependent on the fact that the concentration at the microchannel walls is at quasi steady state. To ensure nutrients in the channel are not appreciably diminished, it is necessary to set the flow rate at the inlet sufficiently high to provide nutrients at a rate

greater than the rate of consumption. If a constraint requiring the outlet concentration (C_{out}) be within 1% of the inlet concentration (C_0) is placed on the system (Equation 3-4), the required volumetric flow rate (Q) through the construct can be stated in terms of the construct dimensions, cell seeding density (ρ_{cell}), kinetic parameters, and nutrient concentrations (Equation 3-5).

$$C_{out} = 0.99C_0 \tag{3.4}$$

$$Q(C_0 - C_{out}) = \rho_{cell}\frac{\nu_{max}C_0}{K_m + C_0}\pi(R_O^2 - R_i^2)L_{eff} \tag{3.5}$$

These equations (3.1-3.5) when solved simultaneously for varying cell seeding density and hydrogel properties provide design parameters for the production of microfluidic articular cartilage constructs.

3.3 Parametric Study of Bioprocessing Parameters

A parametric analysis was performed to determine the maximal channel spacing and minimal flow rate criteria for transport of glucose within a construct of arbitrary dimensions. Construct dimensions were constrained to a footprint of 17.5mm x 17.5mm while the microfluidic network was defined to have a 425 μm square section to accommodate traditional machining. Cell seeding density and agarose concentration were varied across the ranges established from the literature to provide the following flow rate and channel spacing recommendations (**Figure 3.2**).

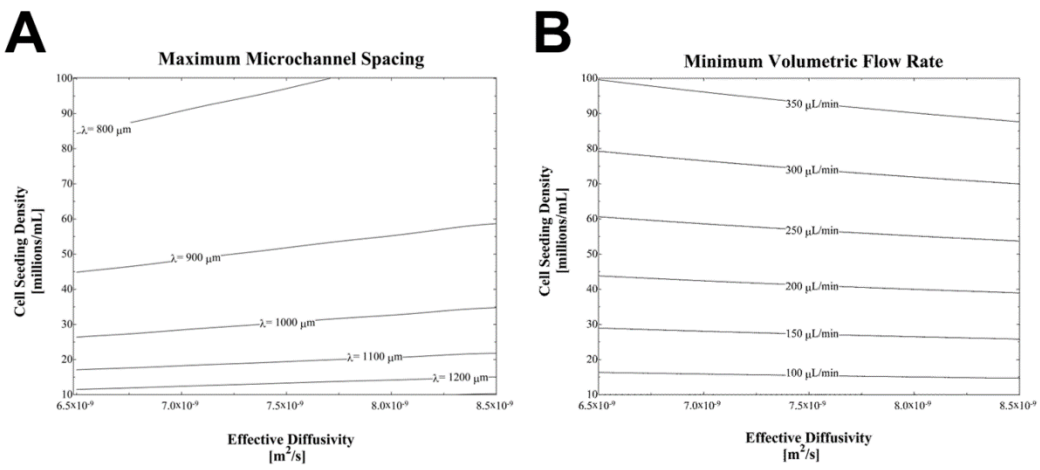

Figure 3.2: Bioprocessing Guidelines for Microfluidic Tissue Construct
Bioprocessing guidelines for the production of tissue-engineered articular cartilage, using the geometric constraints described herein. Maximum microchannel spacing (A) and minimum volumetric flow rate (B) are were found through parametric analysis and plotted as contours to provide bounding conditions for varying cell-seeding densities and hydrogel properties. The effective diffusivity (x axis) is plotted in lieu of agarose weight percentage for extension of the analysis into alternative material systems. Effective diffusivity is related to the weight percentage of agarose in the cell–prepolymer solution by the Mackie–Mears relationship. Values represent bounding conditions for the cell-seeding densities and hydrogel properties commonly observed in the cartilage tissue-engineering literature

The smallest maximum channel spacing for the range of conditions studied herein was 557 μm occurring at a seeding density of 100 million cells per milliliter and a 5% agarose solution. The greatest channel spacing recommendation was 820 μm occurring at a seeding density of 10 million cells per milliliter and a 1% agarose solution. Recommended minimal flow rates ranged from 55.95 to 248.50 μL/min at the low and high end of range of independent parameters respectively. At these flow rates the magnitude of shear stress on the microchannel walls would range from 5.39×10^{-3} dynes/cm^2 to 0.239 dynes/cm^2 according the following expression for wall shear stress in a square duct (Equation 3-6).

$$\tau_W = \frac{3\mu Q}{4R_i^3} \qquad (3\text{-}6)$$

These values are well within the estimated range of shear stresses due to interstitial fluid flow in articular cartilage *in vivo*. This is an important realization as it will allow this microfluidic hydrogel approach for future mechanobiological studies in which the wall shear stress is varied without significant impact on nutrient transport for a range of cell seeding densities and hydrogel material compositions.

3.4 Materials & Methods

3.4.1 Chondrocyte Isolation

Bovine articular cartilage explants were prepared from the femoral condyles and patellar groove of 2–4 week old calves (Research 87, Marlborough, MA) and finely minced into pieces with a characteristic length of less than 1mm. The explants were then digested in a type II collagenase solution (90% DMEM, 10% FBS and 4-5 U of enzyme/mL) and incubated (37°C, 5% CO_2) under agitation for 48 hours. Following digestion, the solution was filtered through a 40 μm mesh to remove undigested tissue and assessed for cell number and viability using an automated cell counter (Nexcelom Biosciences, Lawrence, MA) and trypan blue exclusion assay. The chondrocytes were then isolated from the resulting solution by centrifugation and suspended in a cryoprotective medium (70% DMEM, 20% FBS, 10% DMSO) at a concentration of 1 million cells/mL and stored in liquid nitrogen in 1mL aliquots.

3.4.2 Construct Fabrication

The selected construct design was that of a serpentine network with 425μm x 425μm square cross-section spaced 850μm apart on center within the recommended specifications provided by the solution of Equations 3.1-3.5 such that the acrylic casings and negative reliefs of the microfluidic network could be produced through micromachining (HAAS Automation, Inc., Oxnard, CA). Construct molds were produced by pouring Polydimethylsiloxane (PDMS) into the acrylic molds and curing the polymer at 90°C for

90 minutes following degassing under vacuum. Molds were then exposed to oxygen plasma for 30 seconds to render the surface of the molds hydrophilic, and subsequently steam sterilized. Primary chondrocyte aliquots from three animals were thawed, pooled, and mixed into a 2.5% agarose gel at a density of 25 million cells/mL. Microfluidic constructs were then produced by casting the cell-agarose solution between the acrylic casing and the PDMS mold, and allowing to gel at room temperature for 20 minutes. The molded portion was then sealed against a planar slab of the cell-agarose solution to complete the construct as depicted in **Figure 3.3**. Control constructs were produced by casting the cell-agarose solution in a cylindrical acrylic mold (d=10mm, h=2.5mm or 5.0mm).

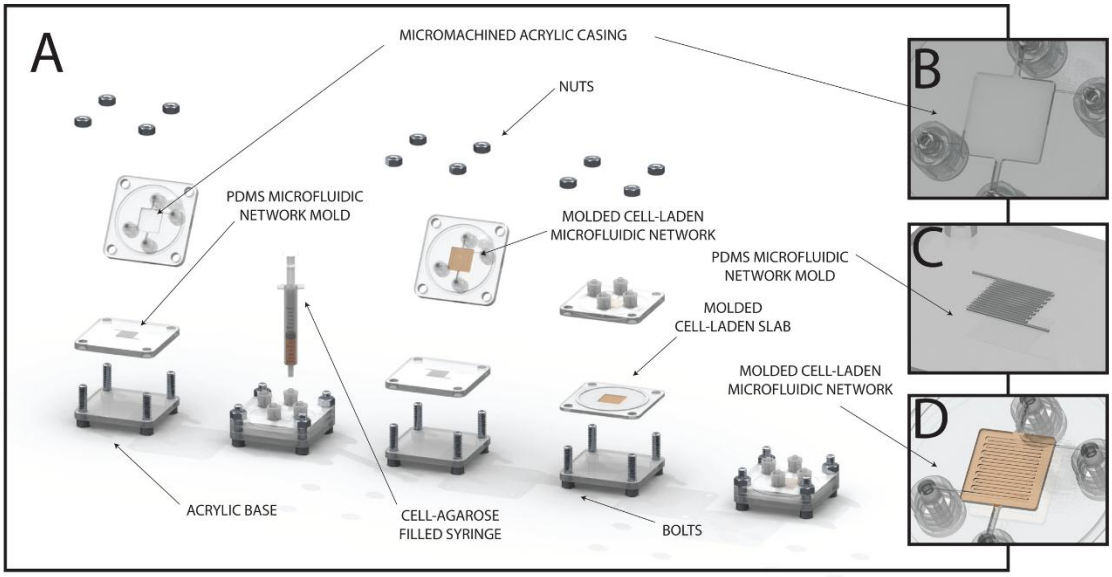

Figure 3.3: Fabrication Process for Microfluidic Constructs
The microfluidic construct fabrication is depicted in (A) from left to right. First, the PDMS mold of the microfluidic network is sandwiched between two machined acrylic casings, detailed in (B), and held together with bolts. Then, the cell–prepolymer solution is injected through the loading ports via a syringe and allowed to gel for 15 min. The PDMS mold, detailed in (C), is then removed and replaced by a planar slab of cell-laden agarose from the same prepolymer batch as the molded portion of the construct, detailed in (D). The two construct portions are secured between the two acrylic casings, and external plumbing is connected for culture medium perfusion.

3.4.3 Tissue Culture

External plumbing was connected through the acrylic casing and culture commenced under constant perfusion at a volumetric flow rate of 250 μL/min. The prescribed flow rate was selected to both fulfill the minimal flow rate requirements for the chosen design as shown in Figure 2, and to provide a uniform shear stress distribution of 1 dyne/cm^2 at the microchannel walls in the central region of interest. Constructs were connected to independent flow loops through which media was recirculated via a syringe pump equipped with dual check valves to achieve unidirectional flow. A gas exchange reservoir was connected to the flow loop and a 5% CO_2 mixture bubbled through the culture media to maintain pH. Total culture media volume was maintained at 100mL and fresh media exchanges were performed every 3-4 days through sampling ports attached to the gas exchange reservoir. Control constructs were cultured in 6-well plates supplied with 5mL of fresh media every 3-4 days.

3.4.4 Defining a Volume of Interest

As an initial proof of concept for the prototype system, tissue culture experiments were carried out to monitor the development of cartilaginous neotissue over the course of a 2-week cultivation period and developing constructs were evaluated relative to static free swelling controls. To achieve geometric similarity across experimental groups and avoid adverse concentration gradients due to edge effects, a volume of interest (VOI) was defined for analysis of the perfused microfluidic constructs. The VOI is a cylindrical region (d= 10mm, h= 2.5mm or 5.0mm) centered within the construct volume as depicted in Figure 1. Biochemical, mechanical, and histological analyses were performed on the VOI only.

3.4.5 Biochemical Analyses

Prior to biochemical analyses, constructs were weighed (wet weight), frozen, lyophilized, weighed (dry weight), and digested with papain enzyme in 0.1 M sodium acetate containing 0.05 M ethylenediaminetetraacetic acid and 0.01 M cysteine-HCl for 16 hours

at 60°C. Construct cell content was assessed from the DNA content of construct digests using a PicoGreen double stranded DNA kit. The construct glycosaminoglycan (GAG) content was assessed spectrophotometrically at 525 nm using a 1, 9-dimethylmethylene blue dye-binding assay (Farndale et al. 1982). The concentration of hydroxyproline was measured spectrophotometrically at 550 nm after acid hydrolysis and reaction with chloramine-T and 4-Dimethylaminobenzaldehyde. The total collagen content was calculated assuming a 1:10 hydroxyproline to collagen concentration ratio.

3.4.6 Mechanical Analyses

An unconfined compression testing protocol was used to measure the dynamic modulus of the constructs on an ELF3200 testing frame (Enduratec, Minnetonka, MN). The constructs were placed in the chamber and preloaded to 0.01 N to establish contact with the sample. For dynamic modulus, 5% peak-to-peak sinusoidal strains at frequencies in the range of 0.01-10 Hz were applied at a static offset strain of 10%. The dynamic modulus was calculated, at a frequency of 1 Hz, as the ratio of the measured oscillatory load normalized by the circular area of the disc to the amplitude of the applied displacement normalized by the thickness of the construct.

3.4.7 Histology & Immunofluorescence

For histological analysis, constructs were fixed in 10% buffered formalin, embedded in paraffin and sectioned into 5μm thick sections for the midsubstance of the construct. Sectioned samples were stained with safranin-O solution according to the manufacturers' instructions. For immunofluorescence, sections were incubated with a citrate buffer heated to 99°C for 30 min to retrieve antigens, and allowed to cool to room temperature. The samples were then incubated in blocking buffer for 30 minutes and primary rabbit anti-bovine Collagen II antibodies (1:100, Abcam, Cambridge, MA) at 4°C overnight. Sections were then washed three times in PBS and with DyLight®594 goat anti-rabbit secondary antibodies (1:200, Abcam, Cambridge, MA) for one hour at room temperature. Finally,

samples were washed and mounted with Vectashield with DAPI and visualized on a Nikon Ti Eclipse inverted fluorescence microscope (Nikon Instruments, Inc., Melville, NY), with representative images captured using a CoolSNAP HQ2 CCD camera (Photometrics, Tucson, AZ).

3.4.8 Statistical Analyses

Independent experiments produced construct samples for mechanical analyses (N=3 per group), histology (N=3), and biochemical analyses (N=12 for 2.5mm samples, N=3 for 5mm samples). For all image analysis of histology specimens, the minimum number of images required to accurately represent the whole section were used. Data for mechanical testing and biochemical analysis is reported as the mean ± SEM with statistically significant differences defined as $p < 0.05$ using two-way ANOVA with Bonferroni post-hoc tests for multiple comparisons.

3.5 Results

3.5.1 Biochemical Composition

DNA content increased with cultivation time for both solid, static cultures and microfluidic constructs. This effect was significantly greater in the perfused microfluidic construct relative to the solid, statically cultured construct (**Figure 3.4**).

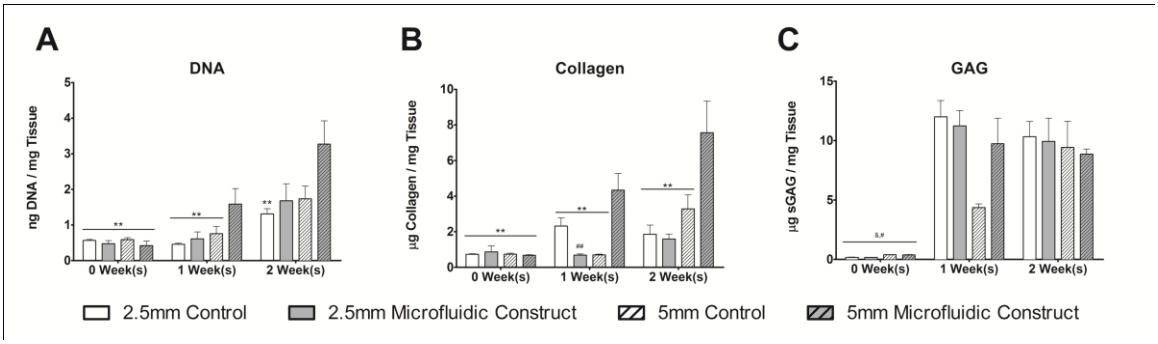

Figure 3.4: Biochemical Composition of Microfluidic Constructs
Biochemical composition of statically cultured solid constructs and perfused microfluidics constructs expressed as a mass fraction. Samples sizes for assays were n=12 for 2.5mm samples, n=3 for 5mm samples: &, && statistically significant ($p<0.05$) differences with respect to the 2.5 and 5mm control construct groups, respectively, at the 1week time point; ^, ^^ statistically significant ($p<0.05$) differences with respect to the 2.5 and 5mm control constructs groups, respectively, at the 2week time point; #, ##statistically significant ($p<0.05$) differences with respect to the 2.5 and 5mm microfluidic construct groups, respectively, at the 1 week time point; *, ** statistically significant ($p<0.05$) differences with respect to the 2.5 and 5mm microfluidic constructs groups, respectively, at the 2week time point

Additionally, collagen accumulated in each experimental group over time with the exception of the 2.5mm thick statically cultured constructs. When the construct thickness is increased to 5mm, collagen synthesis in the microfluidic geometry is significantly increased relative to both the statically cultured construct and the thinner microfluidic constructs at both time points. GAG content within each group increased significantly within the first week of culture and remained statistically unchanged thereafter for all groups with the exception of the 5.0mm thick control group, which increased significantly during the second week of culture rather than the first. There was no statistical difference in GAG concentration between any of the groups at the two week time point.

3.5.2 Mechanical Properties

The dynamic modulus of the constructs across all conditions ranged between 159.8 kPa for the 2.5mm thick, statically cultured control and 328.8 kPa for the 2.5mm thick microfluidic construct. There was no statistical difference in modulus for the different culture conditions for a given culture period. There was a significant difference in moduli for each culture condition at 2 weeks relative to the acellular control and the identical culture condition at the 1 week time point for the 2.5mm thick constructs (**Figure 3.5**).

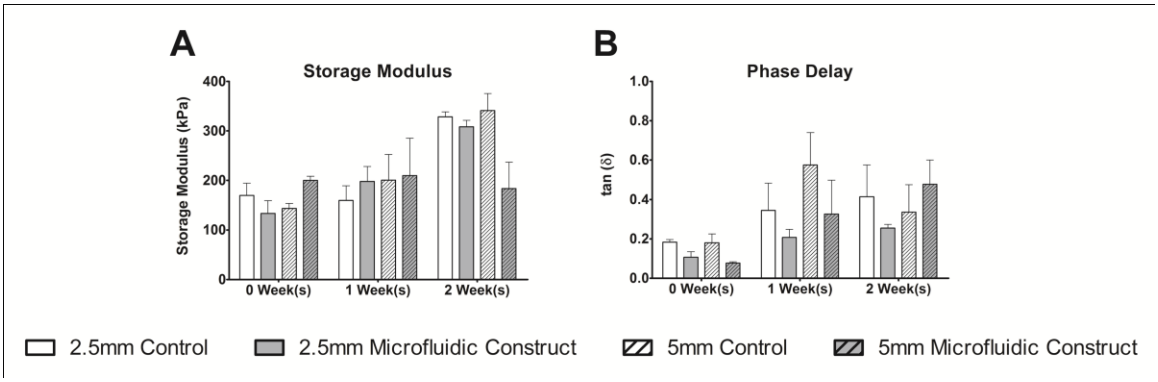

Figure 3.5: Mechanical Properties of Microfluidic Constructs
Storage modulus and phase delay for constructs of solid and microfluidic architectures for the 1 and 2week cultures, as determined through dynamic unconfined compression testing at 1Hz

Within the 5mm construct grouping, the statically cultured construct exhibited a significant increase in dynamic modulus versus the acellular control at the 2 week time point. The phase delay of the constructs varied between 8.57° for the 2.5mm microfluidic construct at 1 week and 14.46° for the 5mm static construct at 1 week. None of the conditions, however, produced differences which are considered statistically or practically significant.

3.5.3 Histological & Immunofluorescence Staining

Control constructs stained weakly and relatively homogeneously for both GAG and Collagen II for all culture periods (**Figure 3.6**). At the one week time point there was no

noticeable difference in Collagen II or GAG staining between the microfluidic and control constructs. At the two week time point, however, there is increased GAG staining in the construct space between microchannels. The staining is not homogeneous, but rather confined to the microenvironment immediately surrounding the chondrocytes.

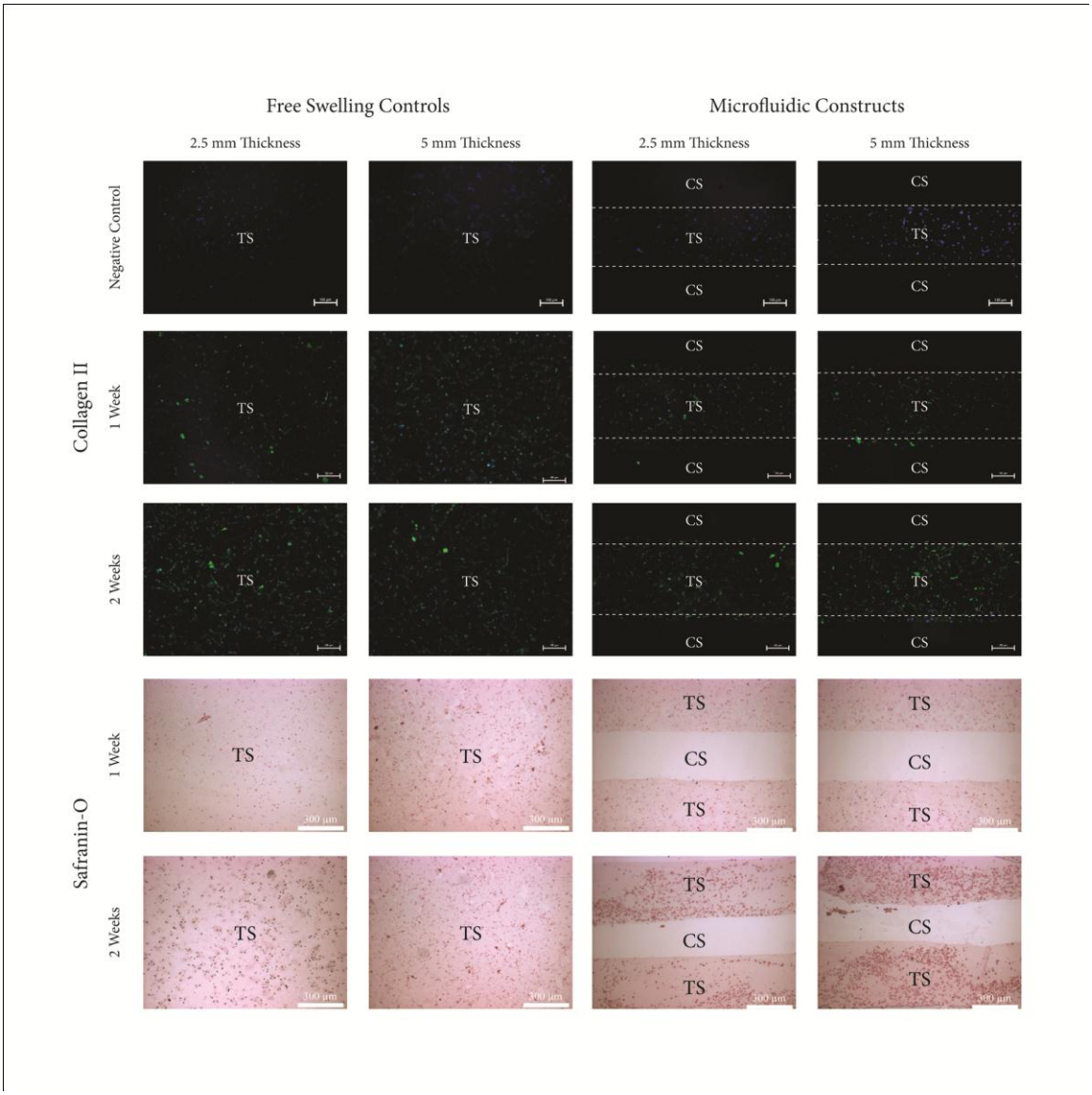

Figure 3.6: Histological Staining of Microfluidic Cartilage Constructs
Staining of Collagen II (top) by immunohistochemistry and GAGs (bottom) by safranin O. The stains suggest that the microfluidic channels provide local increases in both extracellular matrix components at both time points. For immunofluorescence, green and blue pseudo-colorings are applied for Collagen II and nuclei, respectively; the images are marked to indicate the tissue space (TS) and channel space (CS) of the constructs.

3.6 Discussion

The purpose of this study was to investigate the incorporation of microfluidic networks in cell-laden agarose gels as an approach to improve cell proliferation and biosynthesis in tissue engineered constructs of clinically relevant thicknesses. As evidenced by an increase in DNA and collagen contents with time for 2.5 mm and 5 mm thick microfluidic constructs cultivated for 2 weeks, over that for corresponding solid control constructs, our design achieved a measure of success.

Others have demonstrated the feasibility of directly perfused microfluidic channels within hydrogels, yet in these studies culture periods were short (up to three days) and constructs were limited to thicknesses less than 2mm (Choi et al. 2007a; Golden and Tien 2007; Johann and Renaud 2007; Ling et al. 2007). Buckley et al were able to produce a large microchanneled tissue construct which they cultivated under rotational culture (Buckley et al. 2009). The key difference between rotational and direct perfusion culture lies in the ability to control mass flow and shear rates to the construct interior rather than relying on convection from the external flow in rotational culture. One anticipated benefit of our construct design relative to other directly perfused microfluidic constructs was that a slightly larger microchannel cross-section would accommodate greater neotissue accumulation within the construct without resulting in flow occlusions do to tissue in growth into the microchannels over time. By extending the culture duration to two weeks, we were able to parse the role of fluid shear within the construct in regulating the synthesis of collagen by the embedded chondrocytes. The increased collagen synthesis in the thick constructs relative to the thin constructs suggests that this effect may be impacted by the increased internal surface area over which shear stress is applied due to the presence of the second microfluidic network. The presence of a second fluidic network within the thicker construct doubled the amount of surface area exposed to shear, an effect that was recapitulated in the construct collagen composition at one and two-week time points. The

lower nominal values of cartilage specific matrix molecules within the microfluidic constructs may be due to shear stimulated release of secreted macromolecules into the culture media (Grad et al. 2012). We expect that even longer culture periods are possible using our approach, as even after two weeks in culture, flow within microfluidic channels did not become occluded.

Additionally, we were able to increase the thickness of the microfluidic construct to 5mm, approaching the maximum thickness of the femoral condyle (Ateshian et al. 1991), by incorporating an independent, supplemental microfluidic network offset from the original network. While prior studies alluded to the concept of incorporation multiple networks for building construct thickness (Choi et al. 2007a; Cuchiara et al. 2010; Golden and Tien 2007; Huang et al. 2011; Johann and Renaud 2007; Ling et al. 2007; Song et al. 2009), our study extends the concept by establishing the feasibility of culturing such constructs for extended periods, and showing that this strategy results in greater cell viability relative to solid, statically cultured constructs of the same thickness.

One limitation of our design is that multiple fluidic networks may negatively impact the apparent mechanical properties of the tissue engineered construct. As expected, the modulus of the constructs increased with time concurrently with the increase in extracellular matrix components. However, no significant difference between the solid and microchanneled architectures was observed for the thinner geometry, and the incorporation of a second fluidic network resulted in a decrease in apparent properties. For successful clinical implementation, the use of multiple fluidic networks will require manipulation of additional factors such as an alternative material platform, and further investigation into the mechanics of a microchanneled construct. There was no statistical difference in the phase delay of the constructs under dynamic compression. Since the phase delay indicates a measure of the viscoelasticity of the constructs, this finding indicates that the magnitude

of any changes in the viscoelasticity of the constructs due to neotissue development are dominated by the viscoelastic properties of the agarose scaffolding for the culture periods studied.

We selected an agarose hydrogel as the material for our microfluidic constructs based on its demonstrated suitability for cultivation of chondrocytes. For these agarose-based microfluidic hydrogels, we found that the incorporation of the microfluidic network and application of shear stress due to culture media perfusion affected cell proliferation and matrix elaboration in a similar manner to other forms of mechanical environment perturbations including dynamic compressive and shear loading. The effects of dynamic loading, under compression and shear, have been repeatedly shown to increase cartilaginous matrix synthesis, chondrocyte proliferation, and construct modulus over a range of stimulation frequencies and culture durations (Buschmann et al. 1995; Mauck et al. 2000; Waldman et al. 2003b; Waldman et al. 2004). Our results are in agreement with previous reports of increased cell proliferation and collagen production, but contrast findings with respect to GAG production, as the beneficial effect of loading on GAG was not observed in our microfluidic constructs. We speculate that the presence of the microfluidic network(s) may have contributed to the loss of newly synthesized GAG to the culture medium due to the relatively high velocities within the microfluidic channels, a mechanism not present in dynamic loading studies, thus even if GAG production was stimulated in response to mechanical stimuli, losses to the media could prevent detection of an increase.

We expected that incorporating microfluidic channels and increasing construct thickness would confer improved mechanical properties, however, improvements were not observed, particularly for the thicker construct in which two fluidic networks were incorporated. In the case of the 5mm microfluidic construct, a likely explanation for the decrease in apparent

mechanical properties is reduced construct mass due to the increased void space necessary to incorporate the microfluidic network. Given that mechanical stimulation tends to have a greater effect when more *ex novo* matrix is present (Bueno et al. 2008; Buschmann et al. 1995; Mauck et al. 2000), we predict future, longer term studies in our microfluidic system may prove even more effective than static controls.

3.7 Conclusions

We have developed a microfluidic culture system designed to meet nutrient transport requirements of a large, full-thickness articular cartilage construct over a two week culture period, and shown that the incorporation of the microfluidic network and perfusion of culture media through the network resulted in significant enhancement of cell proliferation and increases in dry weight fractions of both GAG and collagen for 5mm thick constructs. Incorporation of multiple fluidic networks within the agarose construct resulted in a decrease in the apparent dynamic modulus of the construct. Our findings that approaching thicker and more robust constructs through incorporation of microfluidics in agarose-based hydrogels led to improvements in proliferation and matrix deposition to some extent, but not apparent mechanical properties suggests that for this platform to have clinical utility, future studies involving longer cultivation periods, alternative material selection, and further optimized bioprocessing parameters are needed.

4 EFFECT OF HYDRODYNAMIC LOADING ON MESENCHYMAL STEM CELL DIFFERENTIATION EFFICIENCY

4.1 Introduction

Due to their limited supply and decreased proliferative capacity, the sole use of autologous chondrocytes and osteoblasts for regenerative medicines is likely unsustainable (Mauck et al. 2006). Subsequently, mesenchymal stem cells (MSCs) have emerged as a clinically relevant cell source for regenerative medicine, due to their ease of procurement, multipotentiality, high proliferation rate, and ability to be expanded *in vitro* while maintaining a stable phenotype (Bruder et al. 1997; Caplan 2005; Pittenger et al. 1999). Directed differentiation of MSCs along various mesenchymal pathways can be achieved by manipulation of the cell culture environment including supplementation of culture media with soluble morphogens (Cheng et al. 1994; Indrawattana et al. 2004; Mackay et al. 1998; Roelen and Dijke 2003; Worster et al. 2001), modulation of culture substrate stiffness (Marklein and Burdick 2010a), and external forces (Guilak et al. 2009; Maul et al. 2011). Of particular interest are environmental approaches which might increase differentiation efficiency while reducing upstream bioprocessing costs for the purpose of large scale commercial operations.

A predominant challenge of the scaling operations required to process large numbers of cells and/or critically sized tissue constructs is the control of nutrient and waste transport from the cells/tissues during culture. To overcome these issues, a number of bioreactor concepts have been developed to provide the flow of culture media through (Porter et al. 2005), across (Saini and Wick 2003), and around the constructs (Bueno et al. 2005; Spaulding et al. 1993). As a result of the media exchange, the constructs are concurrently

nourished and exposed to hydrodynamic loading. Shear stress is known to cause varied effects on cell populations, including transmembrane ion leakage, as well as physiological and metabolic changes. The presence of fluid shear stress, therefore, is an important environmental factor which may play an important role in the stability or instability of the MSC phenotype in culture. Furthermore, if the magnitude and spatiotemporal presentation of hydrodynamic loading can be controlled, it may represent a novel approach to modulating the efficiency of directed MSC differentiation. The primary objective of this study, therefore, was to determine the effect of uniform shear stress magnitude and duration on MSC gene expression through a panel of key differentiation markers along the osteochondral differentiation pathway. These genes were selected for their importance in orthopedic tissue engineering applications and potential to provide a window into the chondrogenic and osteogenic differentiation processes.

Given the well-documented sensitivity of mature chondrocytes and osteoblasts to growth factors from the TGF-β superfamily (Roelen and Dijke 2003), a secondary objective of this study was to examine the response of MSCs to varying magnitudes of superficial hydrodynamic shear stress in cultures supplemented with varying concentrations of TGF-β3 and BMP-2. Drawing on evidence that both bone and cartilage are mechanosensitive (Papachroni et al. ; Szafranski et al. 2004) and mechanical stimuli are anabolic (Huiskes et al. 2000; Jeon et al. 2012), we hypothesized that hydrodynamic loading would increase the efficiency of MSC differentiation down the desired pathways as revealed through systematic changes in phenotypic markers. The scope of the study was limited to a range of hydrodynamic conditions within the reported interstitial flow regime of bone (Fritton and Weinbaum 2009) and cartilage (Mow et al. 1984) with a view to determining an optimum for lineage specific differentiation. Additionally, the growth factor concentrations were varied by one order of magnitude in either direction from the most

ubiquitous supplementation protocols found in the literature concurrently to determine how hydrodynamic culture might minimize their necessity.

4.2 Materials & Methods

4.2.1 MSC Isolation

Bovine bone marrow aspirates were harvested from within the subchondral trabecular bone of the femoral condyles of 2–4 week old calves (Research 87, Marlborough, MA). Isolated marrow was mixed with expansion medium (high glucose Dulbecco's Modified Eagle Medium [DMEM] supplemented with 10% certified fetal bovine serum [FBS] and 1× penicillin-streptomycin-fungizone [PSF]) supplemented with 300 U/ml heparin), vortexed to remove any undesirable fat and bone fragments from the marrow, passed through a 60μm cell strainer, and centrifuged to collect cell pellets. Cells were resuspended in the expansion medium and plated onto T-75 flasks (Corning, Inc., Corning, NY). After an initial period of 24 hours, nonadherent cells were removed from the flasks, whereas adherent cells were cultured in expansion medium for an additional 7–10 days until cultures reached confluence. Subsequent subculturing was carried out to Passage 3 at a splitting ratio of 1:3. Following Passage 3, MSCs that were suspended in a cryoprotective medium (70% DMEM, 20% FBS, 10% dimethylsulfoxide, 1X PSF) at a concentration of 1 million cells/mL and stored in liquid nitrogen in 1mL aliquots.

4.2.2 Assays for Multipotentiality

Following Passage 1, a portion of MSCs were fixed, treated with a nonspecific blocking agent for 30 minutes, and split into six tubes. Four of the six populations were then incubated with one of the following fluorescently tagged antibodies: fluorescein isothiocyanate [FITC]-conjugated mouse anti-human antibodies against each of CD166, CD271, and CD45, or R-phycoerythrin [RPE]-conjugated mouse anti-bovine CD44 antibodies for 1 hour. The remaining two populations were incubated with FITC and RPE

conjugated antibodies against mouse IgG as the negative isotype controls. Flow cytometry was performed in a FACScan (BD Biosciences, San Jose, CA). Forward scatter and side scatter parameters were used to evaluate the size and granularity of cells, respectively. Surface marker analysis was performed following Passage I and then verified again following Passage III to insure that spontaneous differentiation had not taken place.

Following confirmation of a consistent set of multipotent cell surface markers, MSCs were plated in a 12 well plate at a seeding density of 100,000 cell/well in one of four culture media preparations: expansion media (EM), osteogenic media (OM), adipogenic media (AM), and chondrogenic media (CM). Osteogenic media consisted of high glucose DMEM supplemented with 10% FBS, 1X PSF, 100 nM dexamethasone, 10 mM sodium β-glycerophosphate, 0.05 mM ascorbic acid. Adipogenic Media consisted of high glucose DMEM supplemented with 10% FBS, 1X PSF, 1 μM dexamethasone, 0.5 mM indomethacin, 10 μg/ml insulin, 100 mM 3-isobutyl-1-methylxantine. Chondrogenic Media consisted of high glucose DMEM supplemented with 1× PSF, 0.1 μM dexamethasone, 50 μg/mL ascorbate 2-phosphate, 40 μg/mL l-proline, 100 μg/mL sodium pyruvate, 1X insulin–transferrin–selenium [ITS], and 10 ng/mL TGF-β3. Following 21 days of culture, the monolayers were fixed and assessed for successful induction. Osteogenesis was determined by fixing monolayers in isopropanol and staining with Alizarin Red for mineralized matrix. Adipogenesis was assessed by fixing with paraformaldehyde and staining with freshly prepared Oil Red O to visualize lipid droplets. Chondrogenesis was determined by fixing monolayers with 10% formalin and staining with Toluidine Blue for an abundance of proteoglycans.

4.2.3 Experimental Design

To elucidate the role of hydrodynamic loading in MSC differentiation towards the osteochondral lineages, we selected three magnitudes of fluid shear stress (0 dynes/cm^2, 1 dyne/cm^2, 10 dynes/cm^2) to be applied in the presence of four levels of growth factor stimulation (0 ng/mL, 1 ng/mL, 10ng/mL, 100ng/mL) for two different growth factors (BMP-2, TGF-β3) resulting in 18 experimental groups which received some level of both stimuli, 3 groups which received only TGF-β3 stimulation of varying degrees, 3 groups which received only BMP-2 stimulation of varying degrees, and 3 unsupplemented groups which received only hydrodynamic stimulation of varying degrees. Samples from each experimental group were collected on a weekly basis for 2 weeks. Additional samples for each group were generated at the start of tissue culture (Week 0), but never subjected to any of the stated experimental conditions in order to generate a baseline for downstream analysis.

Table 4.2: **Experimental Design Matrix**

Supplementation	Concentration	Wall Shear Conditions	Durations
TGF-β3	100 ng/mL	0, 1, 10 dynes/cm^2	0, 1, 2 Weeks
	10 ng/mL	0, 1, 10 dynes/cm^2	0, 1, 2 Weeks
	1 ng/mL	0, 1, 10 dynes/cm^2	0, 1, 2 Weeks
Unsupplemented		0, 1, 10 dynes/cm^2	0, 1, 2 Weeks
BMP-2	1 ng/mL	0, 1, 10 dynes/cm^2	0, 1, 2 Weeks
	10 ng/mL	0, 1, 10 dynes/cm^2	0, 1, 2 Weeks
	100 ng/mL	0, 1, 10 dynes/cm^2	0, 1, 2 Weeks

4.2.4 Tissue Culture

MSCs from three different animals were mixed with sterile agarose solution such that the final concentration of MSCs in 2.5% w/w agarose solution was 25 million cells/mL. Constructs were then cast into a polydimethylsiloxane [PDMS] mold and cultured either statically (0 dyne/cm^2) or loaded in a custom flow chamber (**Figure 4.1**) for dynamic culture at one of two wall shear stress (WSS) conditions: low shear (1 dyne/cm^2) or high shear (10 dynes/cm^2). To achieve the variation in shear stress at the wall (τ_{wall}), the channel height (h) was varied between two different chamber designs while the kinematic viscosity (μ), Volumetric Flow Rate, and the channel width (b) were held constant. This approach allowed multiple flow loops from different experimental groups to be driven simultaneously by a single, multi-channel peristaltic pump (Masterflex, Cole Parmer, Vernon Hills, IL).

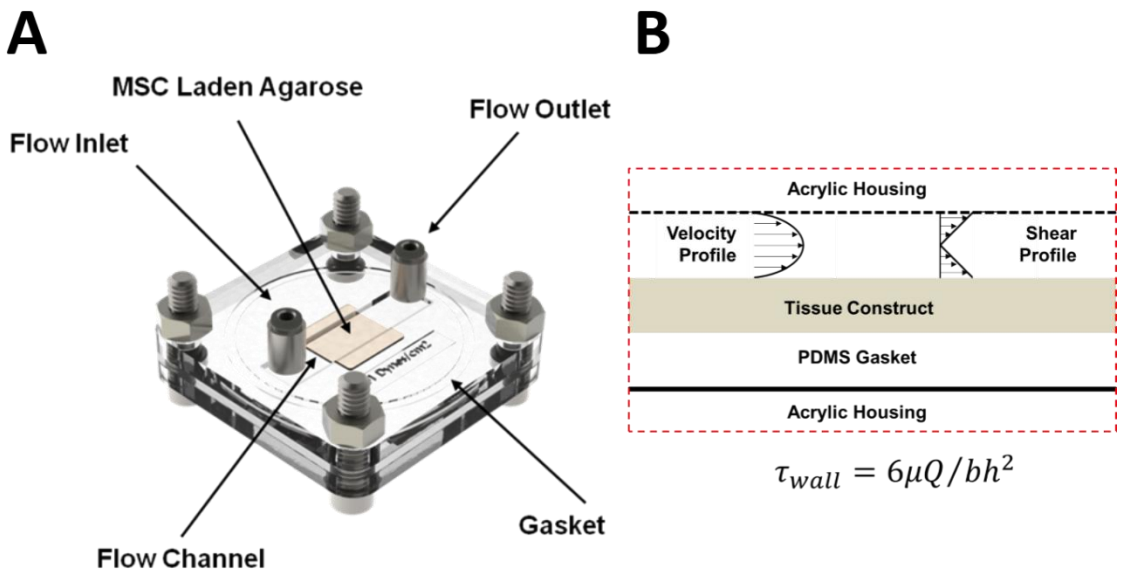

Figure 4.1: Illustration of Custom Parallel-Plate Culture System
Tissue constructs were cultivated utilizing a custom built laminar flow chamber (left). Two separate devices with varying channel heights were produced such that parallel cultures of different hydrodynamic loading magnitudes could be simultaneously driven by a single peristaltic pump.

4.2.5 Gene Expression

Real-time polymerase chain reaction (qRT-PCR) was used to quantify gene expression in harvested monolayer cells. Cells were fixed in TRIzol, and RNA was isolated from the homogenized cell lysate through a series of rinse, elution, and centrifugation. The RNA samples were then reverse transcribed into cDNA using a QuantiTech Rev Transcription kit (Qiagen, Hilden, German) according to the manufacturer's protocol. Gene expression for target mesenchymal lineage markers was assessed using custom-designed primers (Table 1) with quantitative PCR amplification performed on a StepOnePlus™ Real-Time PCR System (Applied Biosystems) in the presence of SYBR Green/ROX master mix (Applied Biosystems). GAPDH and β-actin were both used as endogenous controls for normalization through geometric averaging. Relative expression (n=3 per condition and time point) of each target gene was calculated according to Equations 4-1 and 4-2 using LinReg-PCR, where $N_{0,i}$ represents the initial concentration of the target gene, $N_{q,i}$ represents the concentration of the target gene at the threshold, E_i represents the amplification efficiency of the polymerase chain reaction, and C_q is the selected threshold value.

$$N_{0,i} = N_{q,i}/E_i^{C_q} \tag{4-1}$$

$$Fold\ Change = \left(\frac{N_{0,i}}{\sqrt{N_{0,GAPDH}N_{0,ACTB}}}\right)_{sample} \Bigg/ \left(\frac{N_{0,i}}{\sqrt{N_{0,GAPDH}N_{0,ACTB}}}\right)_{control} \tag{4-2}$$

Endogenous controls were evaluated for each experimental group to ensure that their expression levels were not significantly altered across time or culture conditions.

Table 4.3: Parameters for Microfluidic Construct Design

Function	Gene	Primer Nucleotide Sequence
Housekeeping Genes	ACTB	Forward 5'GAGCGGGAAATCGTCCGTGAC 3' Reverse 5' GTGTTGGCGTAGAGGTCCTTGC 3'
	GAPDH	Forward 5' CCTTCATTGACCTTCACTACATGGTCTA 3' Reverse 5' TGGAAGATGGTGATGGCCTTTCCATTG 3'
Chondrogenic Markers	sox9	Forward 5' CATGAAGATGACCGACGAG 3' Reverse 5' CGTCTTCTCCGTGTCGGA 3'
	aggrecan	Forward 5' CACTGTTACCGCCACTTCCC 3' Reverse 5' GACATCGTTCCACTCGCCCT 3'
	col2α1	Forward 5' ATCCATTGCAAACCCAAAGG 3' Reverse 5' CCAGTTCAGGTCTCTTAGAG 3'
Hypertrophic Marker	colXα1	Forward 5' CATGCTGCCACAAACAGC 3' Reverse 5' TGGATGGTGGGCCTTTTA 3'
Osteogenic Markers	runx2	Forward 5' TTA CAG ACC CCA GGC AGG CAC A 3' Reverse 5' TCC ATC AGC GTC AAC ACC ATC A 3'
	osteocalcin	Forward 5' TGACAGACACACCATGAGAACCC 3' Reverse 5' AGCTCTAGACTGGGCCGTAGAAG 3'
	col1α1	Forward 5' TGCTGGCCAACCATGCCTCT 3' Reverse 5' CGACATCATTGGATCCTTGCA G 3'

4.2.6 Histological Analyses

For histological analysis, constructs were fixed in 10% buffered formalin, embedded in paraffin and sectioned into 8μm thick sections for the midsubstance of the construct. Sectioned samples were stained with Toluidine Blue and Alizarin Red per established protocols. For immunofluorescence, sections were incubated with a citrate buffer heated to 99°C for 30 min to retrieve antigens, and allowed to cool to room temperature. The samples were then incubated in blocking buffer for 30 minutes and primary rabbit anti-bovine antibodies (1:100, Abcam, Cambridge, MA) for Collagen I, II, and X at 4°C overnight. Sections were then washed three times in PBS and with DyLight®594 goat anti-rabbit secondary antibodies (1:200, Abcam, Cambridge, MA) for one hour at room temperature. Finally, samples were washed and mounted with Vectashield with DAPI and visualized on a Nikon Ti Eclipse inverted fluorescence microscope (Nikon Instruments, Inc., Melville,

NY), with representative images captured using a CoolSNAP HQ2 CCD camera (Photometrics, Tucson, AZ).

4.2.7 Statistical Analyses

Independent experiments produced construct samples for RT-qPCR and immunohistochemistry (N=3 per group). For all image analysis of histology specimens, the minimum number of images required to accurately represent the whole section were used. Gene expression is presented as the mean fold change ± SEM with statistically significant differences defined as $p < 0.05$ using two-way ANOVA with Bonferroni post-hoc tests for multiple comparisons.

4.3 Results

4.3.1 MSC Characterization

Flow cytometric analysis showed a consistent expression of MSC surface markers (CD166, CD271, CD44) while being negative for CD45, a key hematopoietic stem cell marker (**Figure 4.2**), for each of the cell population utilized prior to pooling for experiment.

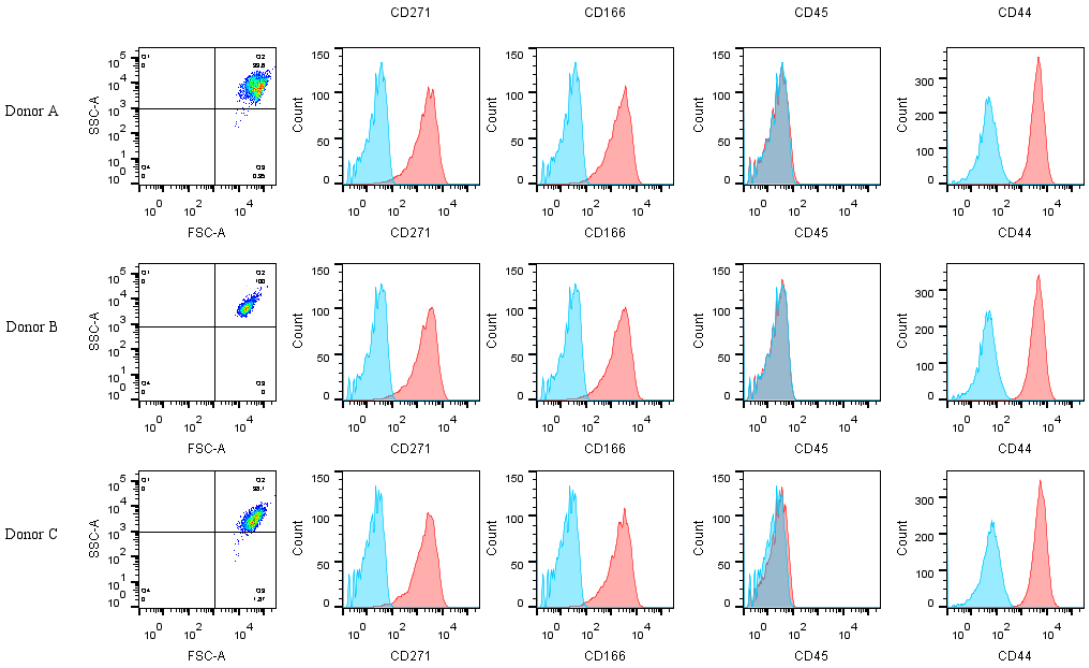

Figure 4.2: Expression of MSC Surface Markers
Adherent cells were lifted from culture after one passaging and test for the presence of bovine MSC surface markers consisting of CD271, CD166, and CD44. Additionally, cells were tested for the absence of hematopoietic surface marker CD45.

When these MSCs were subsequently cultured in the presence of inductive media for 3 weeks, populations cultured in adipogenic, osteogenic, and chondrogenic media deposited fat droplets, mineralized matrix, and an abundance of proteoglycans respectively (**Figure 4.3**). These results, taken together, indicate that the population of cells used in this study fit the definition of a multipotent mesenchymal stem cells at the onset of tissue culture.

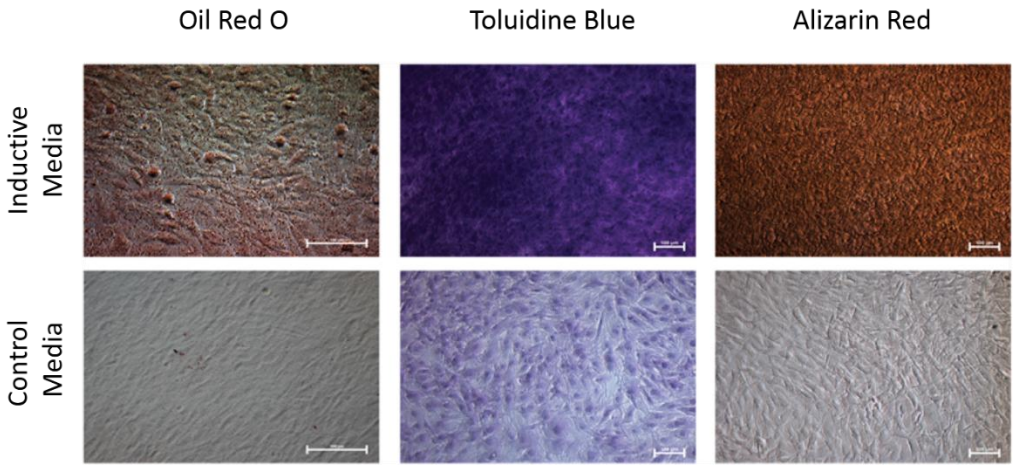

Figure 4.3: MSC Trilineage Induction
Following confirmation of MSC biomarkers via flow cytometry, MSCs from the bone marrow of three calves were pooled, plated, cultured and assessed for tri-lineage differentiation potential. From left to right MSCs culture in inductive media (top) and growth media (bottom row) were stained with Oil Red O, Toluidine Blue, and Alizarin Red to confirm evidence of adipogenesis, chondrogenesis, and osteogenesis respectively.

4.3.2 Transcriptome Stability of Unsupplemented Cultures

In order to control for the effect of hydrodynamic loading on the gene expression profile of MSCs, a round of control experiments was performed to assess the stability of the MSC transcriptome in unsupplemented, static, three dimensional culture over the course of two weeks of cultivation (**Figure 4.4**). None of the genes measured exhibited significant regulation over the time course of the experiment with respect to the initial expression profile, indicating three dimensional culture in isolation of other factors was not a significant contributor to differentiation of the MSCs toward the desired lineages and that this culture format represents a suitable control for differentiation studies. This was an important realization, as there is evidence in the literature that subtle changes in culture conditions, such as the transition from monolayer to three-dimensional culture represented here can induce phenotypic changes in stem cell populations (Marklein and Burdick 2010a; Marklein and Burdick 2010b; Maul et al. 2011), particularly as a significant contributor to chondrogenesis (Bosnakovski et al. 2004).

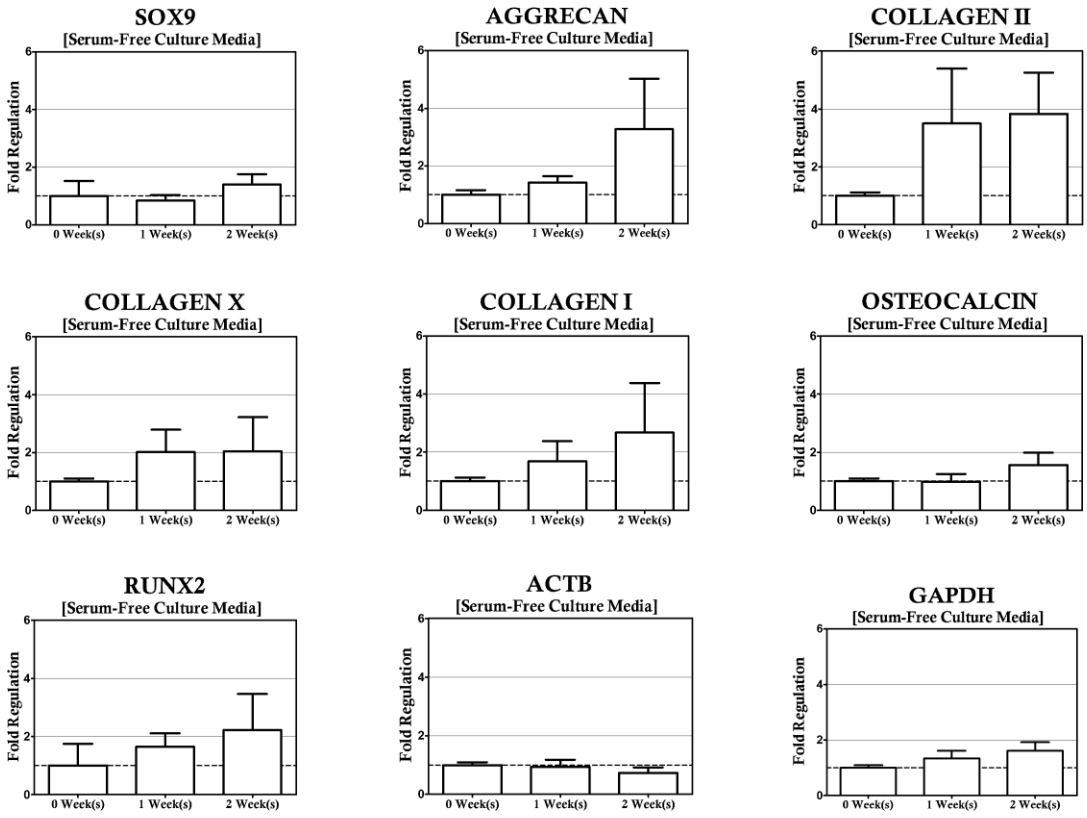

Figure 4.4: Gene Expression of Unsupplemented Static Cultures
Gene Expression profiles were determined for unsupplemented, static cultures via RT-qPCR. No statistically significant regulation of the genes in the panel was observed.

It is important to note, however, that many of the protocols from the prior art depend on pellet culture whereas this study is dependent on the encapsulation of the MSCs in a three dimensional agarose hydrogel. The introduction of the hydrogel material provides additional barriers to communication by cell to cell contact, a factor known to play a role in chondrogenesis (Tuli et al. 2003), and the deviation of the observations produced between these different systems may exist due to the relative differences in cell density between the two culture types. It is also noteworthy that the seeding density of the constructs was not varied in this study. It is possible seeding density may also play a role in this observation, as prior literature indicates seeding density can have an impact on ECM deposition in MSC-based tissue constructs (Huang et al. 2009; Hui et al. 2008).

Nevertheless, this observation confirmed the utility of this culture condition as a suitable control for our subsequent hydrodynamic culture studies aiming to determine the effect of exogenous growth factor supplementation on the mRNA expression profiles of this MSC population.

4.3.3 Effect of Hydrodynamic Loading on Unsupplemented Cultures

With a suitable control group established, the first step in addressing the potential of hydrodynamic loading as a differentiation tool was to culture MSC based tissue constructs under laminar flow profiles with nominal shear stress magnitudes of 1 dyne/cm^2 and 10 dynes/cm^2 and to compare the expression of a panel of genes spanning the phenotypic diversity of cells along the endochondral ossification pathway to the previously discussed static controls. When hydrodynamic culture was introduced as a variable to the three-dimensional, serum-free cultures (**Figure 4.5**), no significant regulation of the chondrogenic gene panel was observed, significant upregulation of the osteogenic transcription factor (*RUNX2*), and two of the three collagens investigated (*COL1A1* and *COLXA1*) occurred under high shear conditions. *RUNX2* and *COLXA1* were both upregulated early in cultivation (1-week) and remained elevated relative to both the time matched static controls and the low shear treatment.

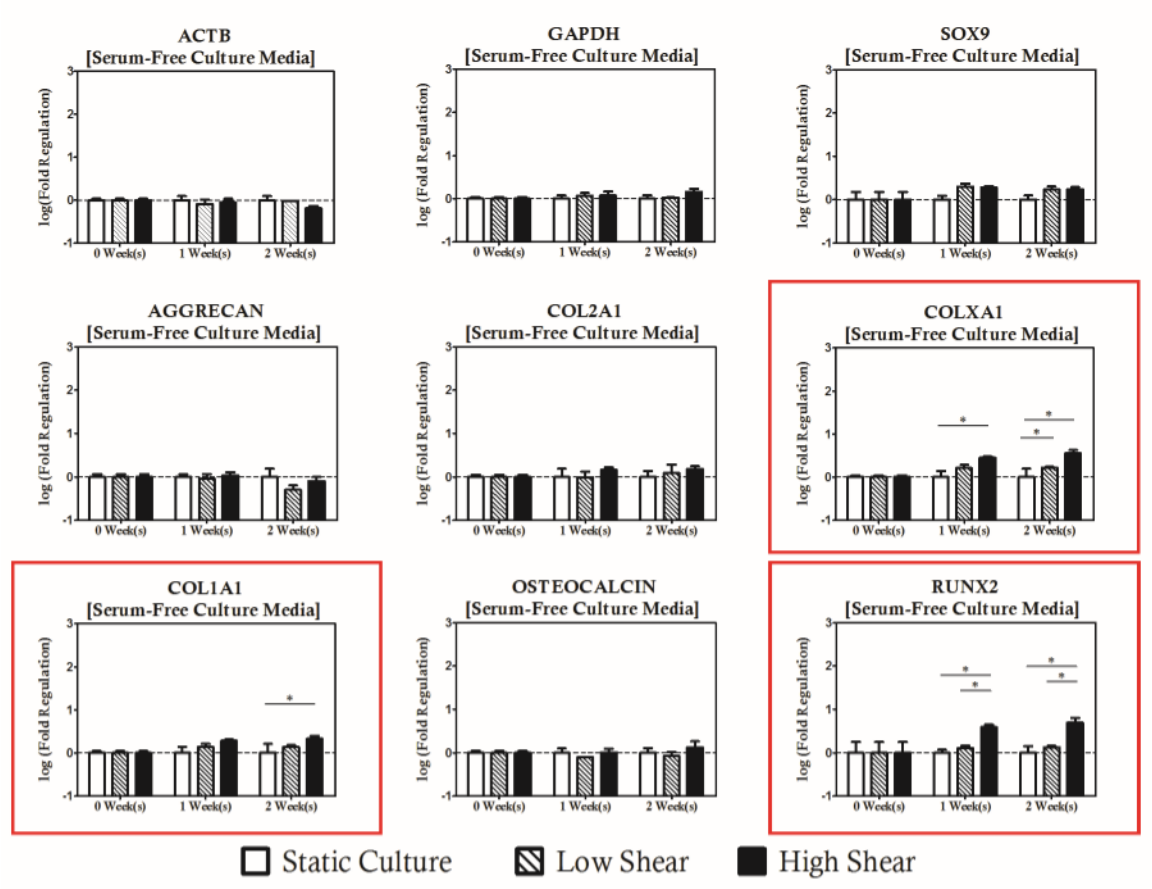

Figure 4.5: Gene Expression of Unsupplemented Hydrodynamic Cultures
Hydrodynamic loading induced changes in gene expression of several osteochondral markers even in the absence of exogenous growth factor supplementation. Genes with statistically significant regulation are highlighted with a red box. Statistically significance is indicated by asterisks.

At the 2-week time point, upregulation of *COL1A1* was considered significant relative to the static cultures. Interestingly, no significant difference in gene expression was observed with lower magnitude hydrodynamic loading, indicating that magnitude of shear in the absence in exogenous growth factor supplementation is not inconsequential. While these changes are considered statistically significant, the nominal change in expression of these genes was of less than one order of magnitude from the expression profile measured in the cell source population. When compared to the magnitude of impact of growth factor supplementation on gene expression when controlled for culture duration (>2 orders of magnitude difference), this effect is not likely to be useful as a tool for directed

differentiation. At the same time, however, this finding suggests that great care should be taken to minimize the hydrodynamic loading applied to MSC expansion cultures in upstream bioprocessing procedures to prevent non-specific induction of undesirable phenotypes.

4.3.4 Effect of Cytokine Supplementation on Differentiation Markers

While hydrodynamic loading in isolation of exogenous supplementation is not sufficiently potent to control differentiation in a selective manner, the results of our initial studies in unsupplemented, serum-free cultures suggested that hydrodynamic loading may be useful as when presented in concert with morphogens with a known inductive capacity. To investigate this possibility, we analyzed the expression profiles of statically cultured constructs which received either TGF-β3 or BMP-2 supplementation at a concentration of 1 ng/mL, 10 ng/mL, or 100 ng/mL for the purpose of inducing a chondrogenic or osteogenic phenotype, respectively. The resident MSCs tend towards expression of chondrogenic markers as function of time in culture and concentration of exogenous growth factor supplementation for both BMP-2 and TGF-β3 supplementation.

For TGF-β3 supplemented cultures, the expression of all three chondrogenic markers increased significantly relative to the unsupplemented control group for culture durations of at least 2 weeks provided the culture media was supplemented with TGF-β3 at a concentration of at least 10 ng/mL while differences in expression of the chondrogenic markers for cultures supplemented at concentrations lower than 10 ng/mL were not considered significant (**Figure 4.6**).

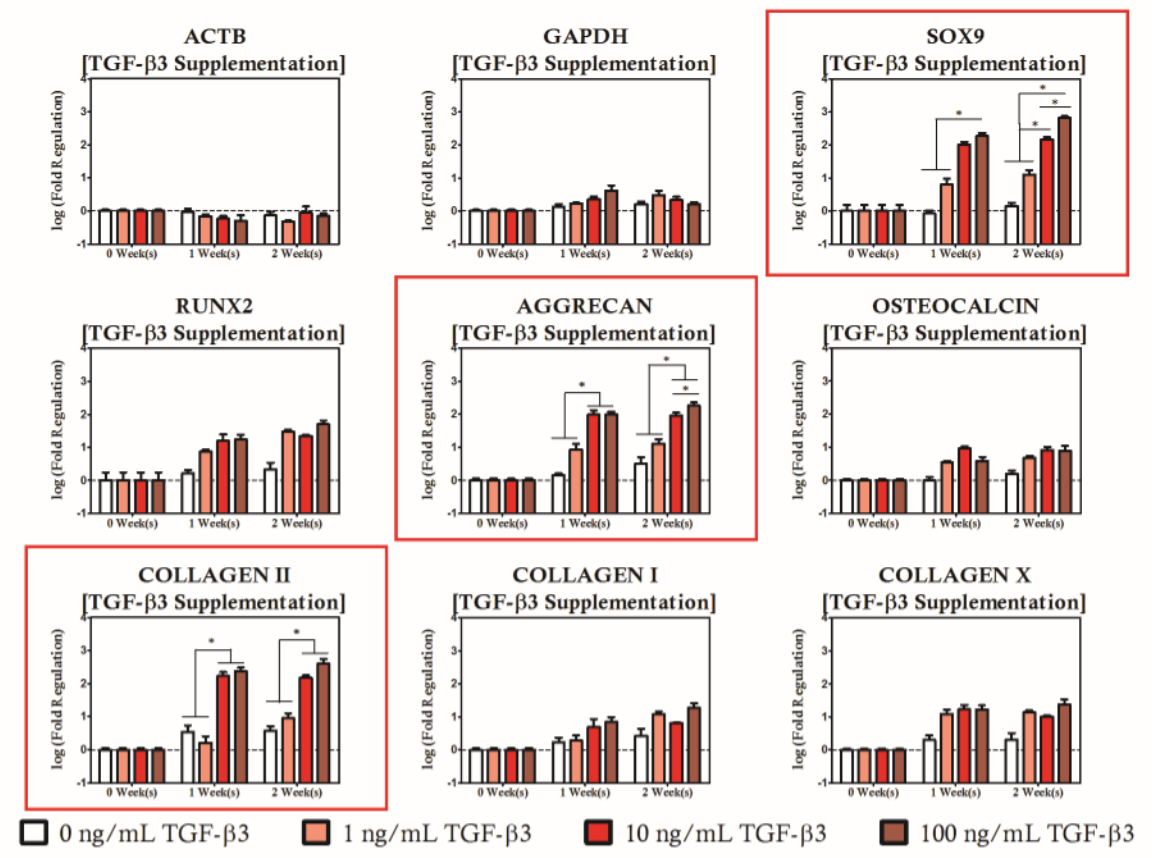

Figure 4.6: Gene Expression of TGF-β3 Supplemented Static Cultures
TGF-β3 supplementation modulates expression of chondrogenic markers without significantly altering the expression profile of the osteogenic panel. Genes with statistically significant regulation are highlighted with a red box. Statistically significance is indicated by asterisks.

After two weeks of culture, *SOX9* was expressed in a concentration dependent manner as the greatest change in expression relative to the source cell population occurred in the 100 ng/mL supplementation group (667 fold) which was significantly higher than the 10 ng/mL supplementation group (145 fold), which in turn was significantly greater than the 1 ng/mL supplementation group (12.7 fold). A similar trend in *AGGRECAN* and *COL2A1* expression was observed as increases in *AGGRECAN* expression relative to the source cell population was highest in the 100 ng/mL supplementation group (181 fold), which was statistically indeterminate from the 10 ng/mL supplementation protocol, but significantly higher than 1 ng/mL or lower concentration supplementation protocols. Likewise,

COL2A1 expression reached a maximum among the static cultures when TGF-β3 supplementation was provided at a concentration of 100 ng/mL (403 fold) for a period of two weeks. Considering the expression of undesirable hypertrophic and osteogenic genes, we found comparable mRNA levels among all TGF-β3 supplementation protocols. Additionally, the expression level of the hypertrophic and osteogenic markers are statistically indeterminate from the unsupplemented controls.

For BMP-2 supplemented cultures, upregulation of genes from both the chondrogenic and osteogenic panels at high growth factor concentrations was evident (**Figure 4.7**).

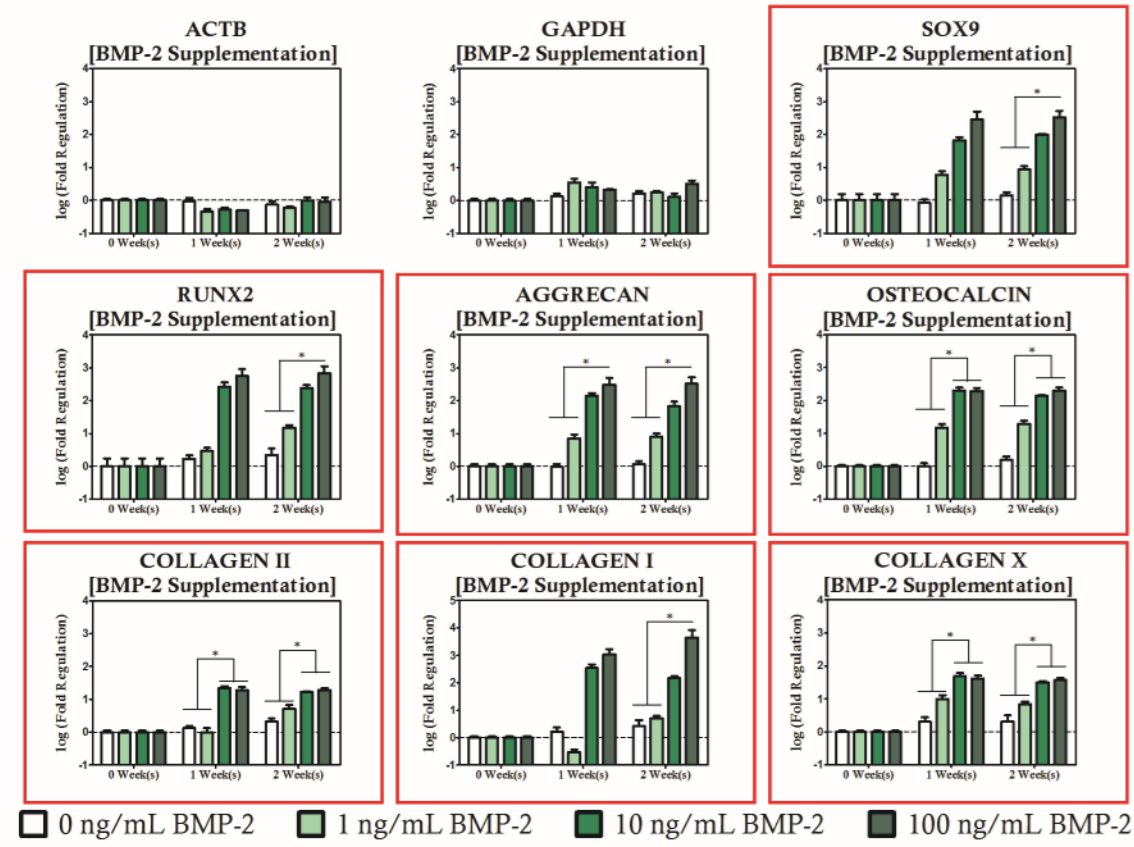

Figure 4.7: Gene Expression of BMP-2 Supplemented Static Cultures
BMP-2 supplementation modulates expression of both chondrogenic and osteogenic markers. Genes with statistically significant regulation are highlighted with a red box. Statistically significance is indicated by asterisks.

When the culture media was supplemented with BMP-2 in concentrations in excess of 10 ng/mL, the entire chondrogenic gene panel (*SOX9*, *AGGRECAN*, and *COL2A1*) was upregulated relative to duration matched cultures receiving BMP-2 supplementation at a concentration of 1 ng/mL or less. Hypertrophic marker *COLXA1* also showed increases with respect to duration matched unsupplemented controls as BMP-2 concentration was increased. Regarding the osteogenic gene panel, *OSTEOCALCIN* was upregulated in cultures supplemented at 10 ng/mL or greater relative to duration matched cultures receiving 1 ng/mL or less for each culture period studied. *RUNX2* and *COL1A1* were also upregulated relative to the low supplementation groups (0 ng/mL and 1 ng/mL), but only when BMP-2 supplementation was provided at a concentration of at least 100 ng/mL for a period of two weeks.

4.3.5 Effect of Hydrodynamic Loading on Cytokine Supplemented Cultures

Both BMP-2 and TGF-β3 produced strong differentiation of the MSC population utilizing the static culture platform, and provided a baseline for normalization of the hydrodynamically loaded cultures to control for the independent effect of the growth factors so that we might investigate whether stimulation via hydrodynamic loading can induce a synergistic effect on the gene expression profile of the differentiating cell population.

BMP-2 supplemented cultures exhibited a strong shear coupling with respect to expression of *SOX9*, *RUNX2*, and all of the collagens studied, and was strongly biased towards high magnitude loading protocols (**Figures 4.8-4.10**). It is apparent that *RUNX2* was strongly upregulated for all BMP-2 supplementation protocols with concurrent high magnitude hydrodynamic loading as evidenced by significant increases relative to time-matched static controls at each time point investigated as well as significantly high expression relative to the low magnitude loading when BMP-2 concentration was at least 10 ng/mL. In addition

to changes in expression of *RUNX2*, it was also observed that *COL1A1* was upregulated for the high shear condition groups. For the 1 ng/mL BMP-2 group, *COL1A1* expression was significantly higher in the high shear group compared to the static controls at two weeks of culture (**Figure 4.8**).

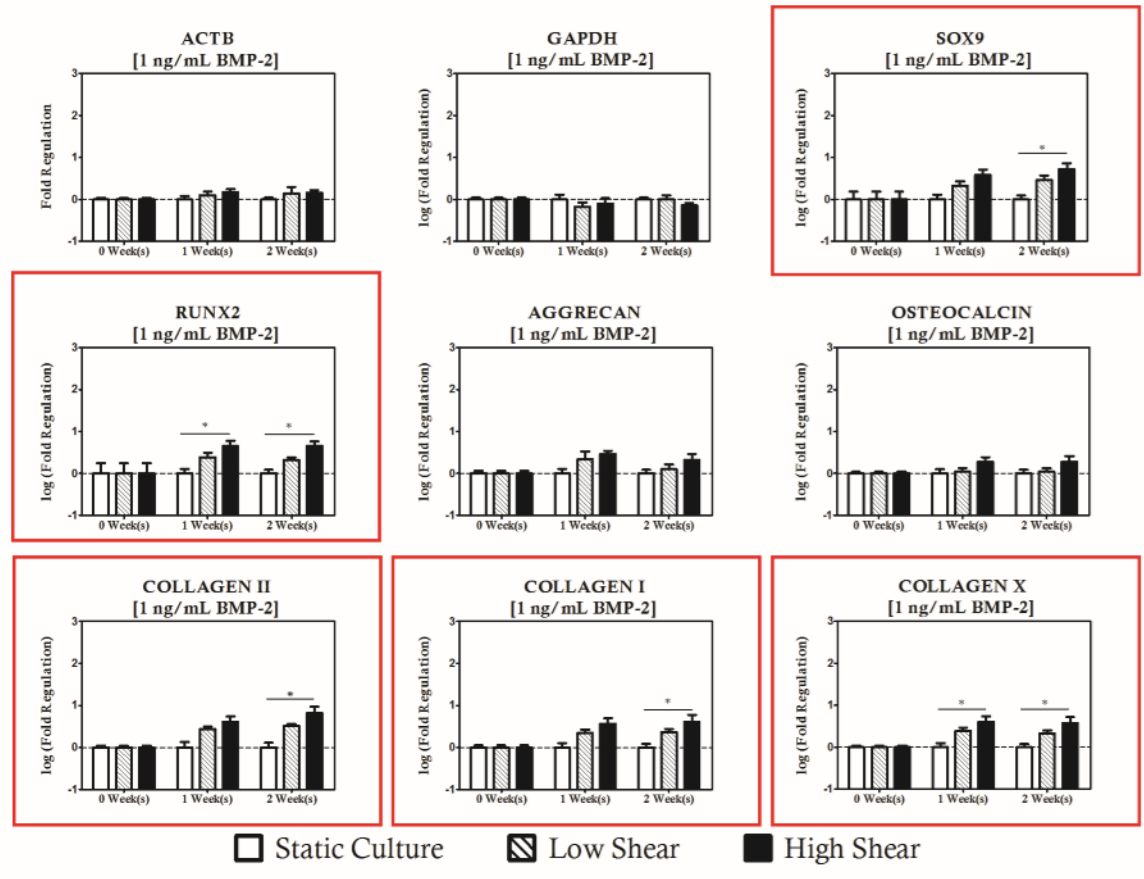

Figure 4.8: 1 ng/mL BMP-2 Supplemented Hydrodynamic Cultures
Even at low levels of BMP-2 supplementation, significant regulation of collagens and osteochondral transcription factors is observed. Genes with statistically significant regulation are highlighted with a red box. Statistically significance is indicated by asterisks.

When the concentration was raised to 10 ng/mL it was observed that the behavior was sustained in addition to being significantly higher than the low magnitude loading group as well (**Figure 4.9**). When BMP-2 supplementation was provided at a concentration of 10 ng/mL or lower, there was no significant difference in expression between the static and low magnitude hydrodynamic groups for either *RUNX2* or *COL1A1*.

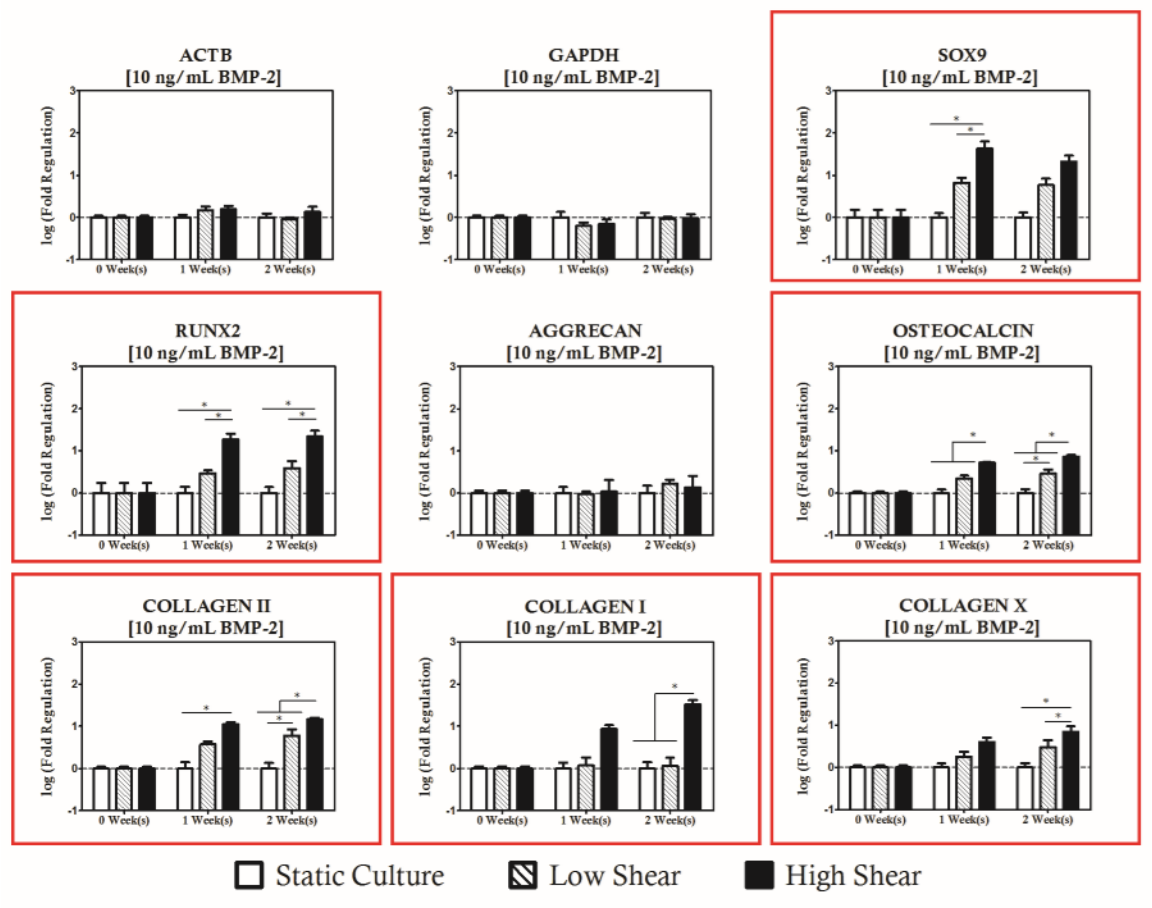

Figure 4.9: 10 ng/mL BMP-2 Supplemented Hydrodynamic Cultures
Transcription factors and collagen modulation is maintained in cultures supplemented with 10 ng/mL. Osteocalcin regulation is also observed under high shear conditions, suggesting a commitment to the osteogenic differentiation pathway. Genes with statistically significant regulation are highlighted with a red box. Statistically significance is indicated by asterisks.

When BMP-2 supplementation was increased to 100 ng/mL, however, it was observed that *COL1A1* was significantly upregulated in the low magnitude loading group relative to the static control after two weeks of culture (**Figure 4.10**). Additionally, hydrodynamic modulation of *OSTEOCALCIN* expression was observed for the first time in these studies in the high magnitude loading group relative to the static control after two weeks of culture in cultures receiving at least 10 ng/mL of BMP-2.

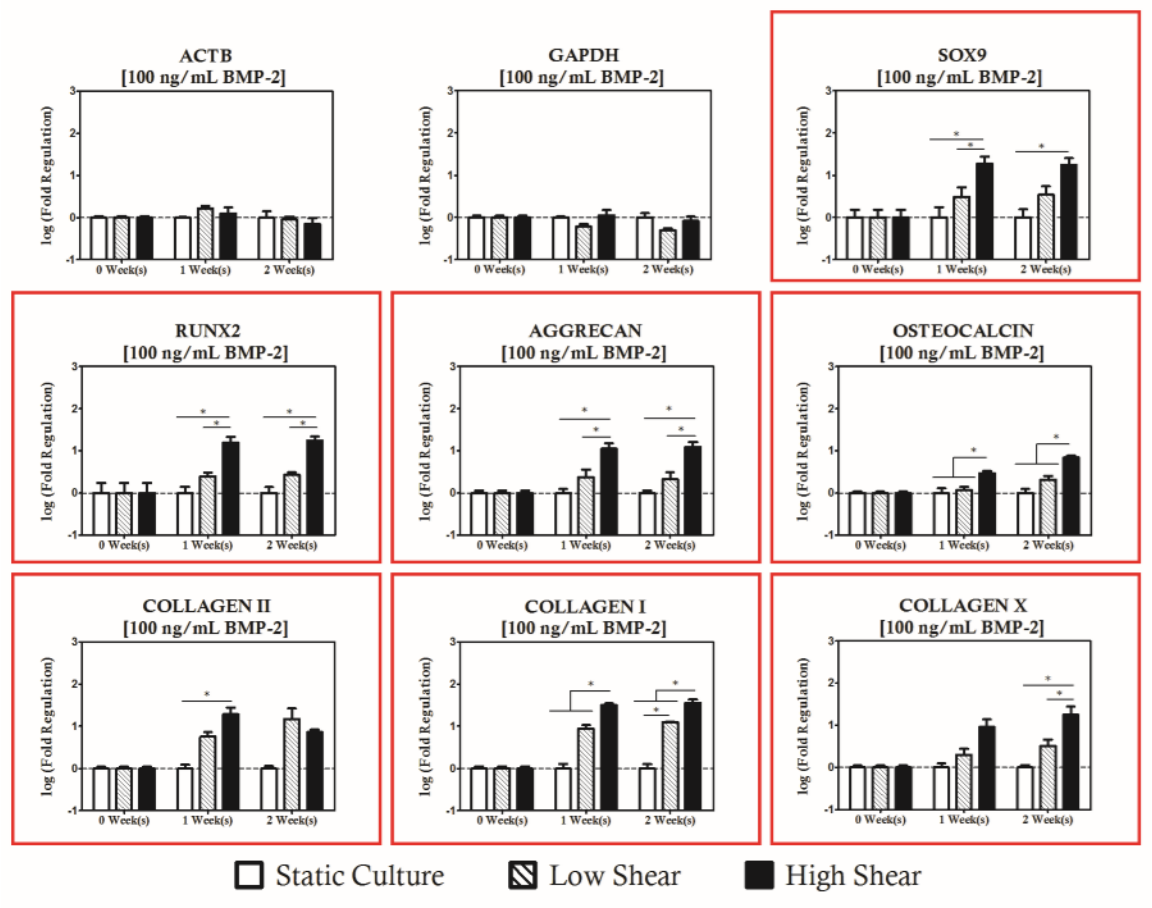

Figure 4.10: 100 ng/mL BMP-2 Supplemented Hydrodynamic Cultures
When BMP-2 is supplemented at a high level (100 ng/mL) shear stress is a significant modulator of all chondrogenic and osteogenic markers studied. Genes with statistically significant regulation are highlighted with a red box. Statistically significance is indicated by asterisks.

Regarding the chondrogenic markers, *SOX9* was upregulated in high magnitude loading culture relative to the static control for all BMP-2 supplementation groups, but interestingly this effect was only considered significant at the 1-week time point. *COL2A1* expression was observed to increase in high magnitude hydrodynamic cultures as well, as evidenced by significant increases relative to static controls at the 2-week time point for cultures receiving 1 ng/mL of BMP-2 and at both time points for culture receiving at least 10 ng/mL of BMP-2. This effect also appears to be sensitive the magnitude of hydrodynamic loading as significant difference were observed between the static cultures and low magnitude

cultures as well as between the low and high magnitude cultures. Differences in *AGGRECAN* expression were only considered significant under high shear and high supplementation. It is also worth noting that expression of hypertrophic marker *COLXA1* was significantly increased in the high magnitude loading group after two weeks of culture for all BMP-2 supplementation protocols relative to the static control for the low concentrations (1 ng/mL) and to both low magnitude and static cultures at elevated concentrations of BMP-2 (10 ng/mL and 100 ng/mL).

These results are not terribly surprising in light of the results from unsupplemented, hydrodynamically loaded construct group as two osteoinductive agents, hydrodynamic loading and BMP-2 supplementation, are at work simultaneously in these protocols. While the slight chondrogenic character of these cultures is not desirable, it is worth noting that modulation of chondrogenic markers (*SOX9*, COL2A1) at high shear was of less than an order of magnitude and the order of the baseline control expression of these genes being considerably lower than their osteogenic counterparts. *COLXA1* expression increased by an order of magnitude over culture period and supplementation matched static controls for both low and high shear conditions at two weeks when cultures were supplemented with 100 ng/mL of BMP-2. While the inductive impact of hydrodynamic loading is not as great in magnitude as that of BMP-2 supplementation at high levels (1 order of magnitude change vs 3 orders of magnitude) it none the less is an important modulator of osteogenic induction as no significant difference was observed between static cultures supplemented at 100 ng/mL and cultures supplemented at 10 ng/mL that were also subjected to high magnitude hydrodynamic loading in terms of total gene expression relative to the initial MSC population.

When hydrodynamic stimulation was introduced in concert with TGF-β3 supplementation, it was observed that *COL2A1* was upregulated relative to duration and supplementation

group matched controls when the hydrodynamic loading condition was high (10 dynes/cm^2) and TGF-B3 concentrations were low indicating a mild synergistic effect on the chondrogenic induction of the resident cell population (**Figure 4.11**).

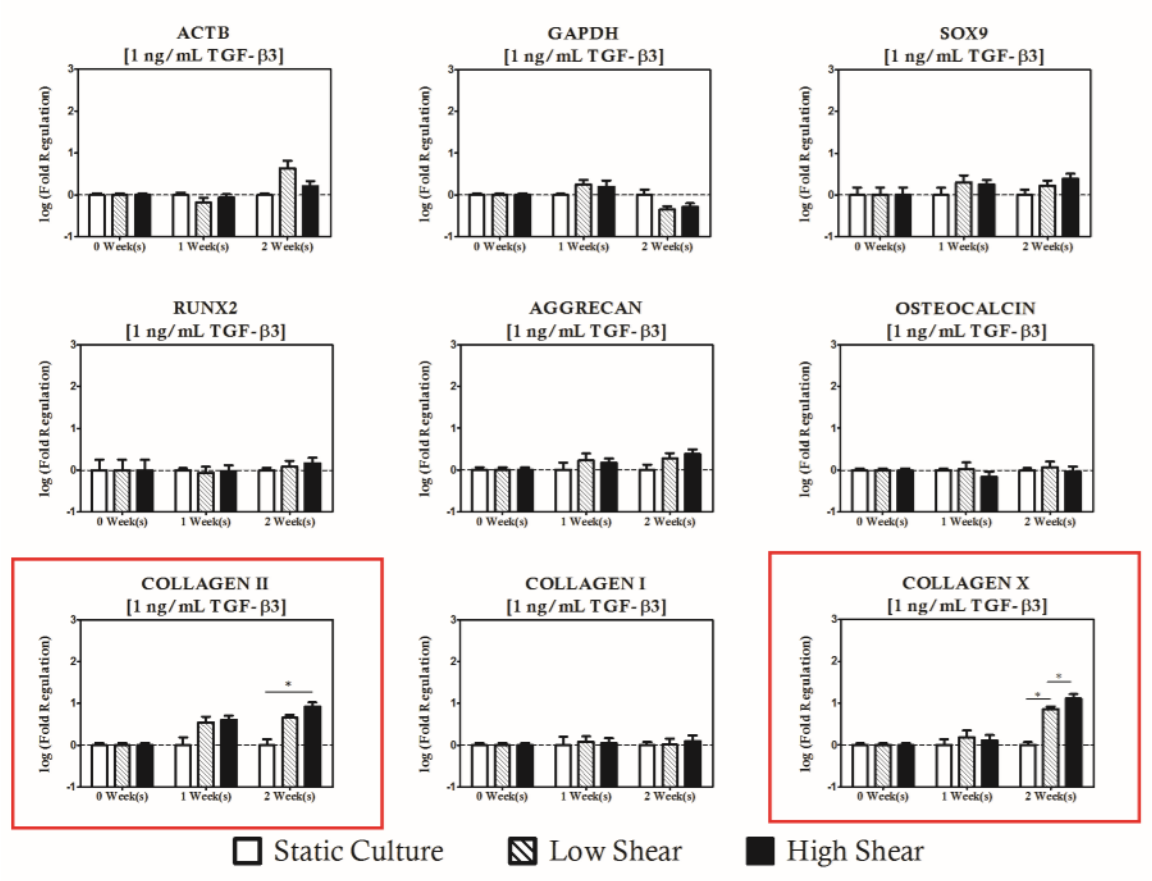

Figure 4.11: 1 ng/mL TGF-β3 Supplemented Hydrodynamic Cultures
Hydrodynamic loading has limited impact on MSC based constructs with cultivated with low concentrations of TGF-β3 (1 ng/mL). Modulation of COL2A1 was considered significant with high magnitude hydrodynamic loading after two weeks of culture relative to time and concentration matched controls. Noticeably, the regulation of osteogenic genes with shear observed in unsupplemented controls disappears. Genes with statistically significant regulation are highlighted with a red box. Statistically significance is indicated by asterisks.

When the supplementation protocol was increased to 10 ng/mL, high shear cultures resulted in upregulation of both *SOX9* and *COL2A1*. No regulation of hypertrophic or

osteogenic markers was observed at this supplementation level, and interestingly there was no effect on chondrogenic markers in low magnitude hydrodynamic cultures (**Figure 4.12**).

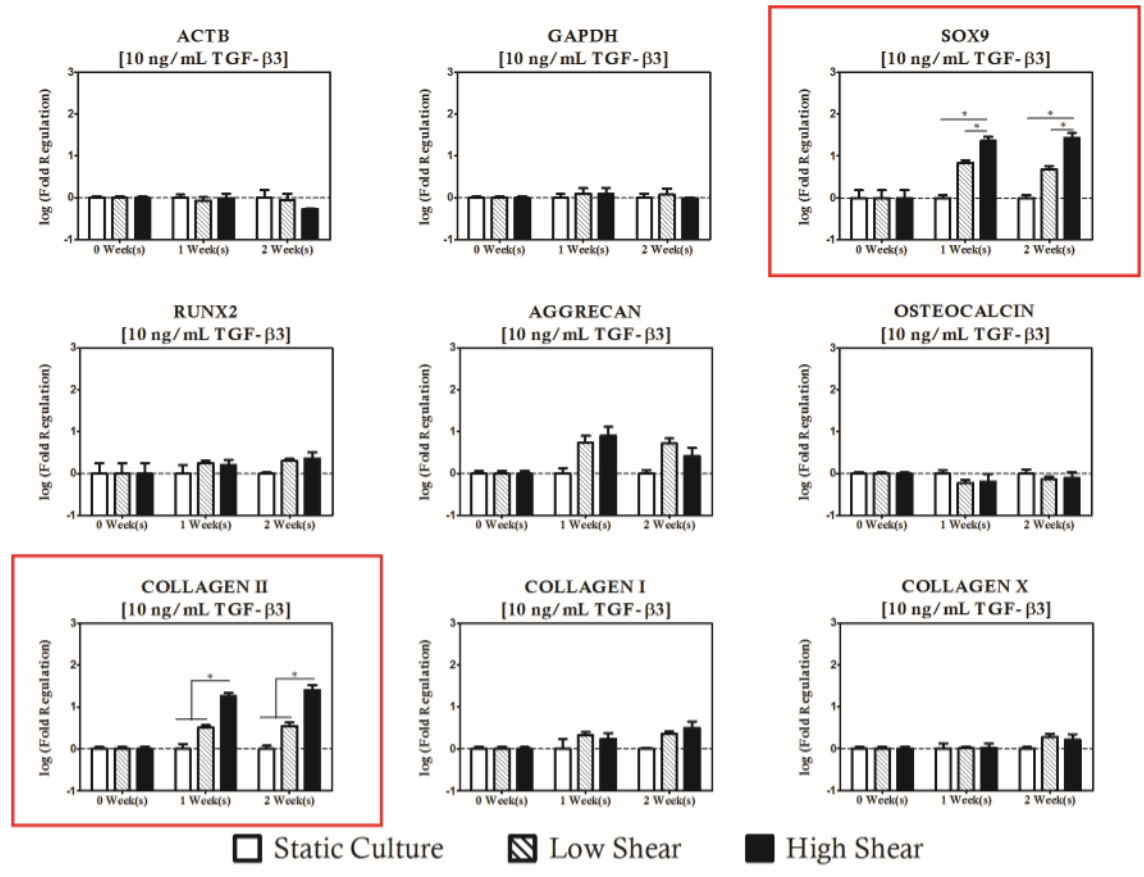

Figure 4.12: 10 ng/mL Supplemented Hydrodynamic Cultures
TGF-β3 supplementation of 10 ng/mL is the most ubiquitous supplementation protocol for chondrogenic cultures found in the literature. When hydrodynamic loading is introduced in concert at these levels of exogenous supplementation, SOX9 and COL2A1 are modulated in high shear environments. Osteogenic markers remain at levels comparable to static controls. Genes with statistically significant regulation are highlighted with a red box. Statistically significance is indicated by asterisks.

Upon increasing the TGF-β3 protocol to 100 ng/mL, shear magnitude dependent modulation of all three chondrogenic genes studied was observed. The chondrogenic panel was upregulated under high magnitude shear conditions relative to static controls after one week of culture and maintained significantly high for subsequent culture durations (**Figure 4.13**). There was no statistical difference between low and high shear conditions for

COL2A1 and *AGGRECAN* expression, but there was a shear magnitude dependency observed for *SOX9*.

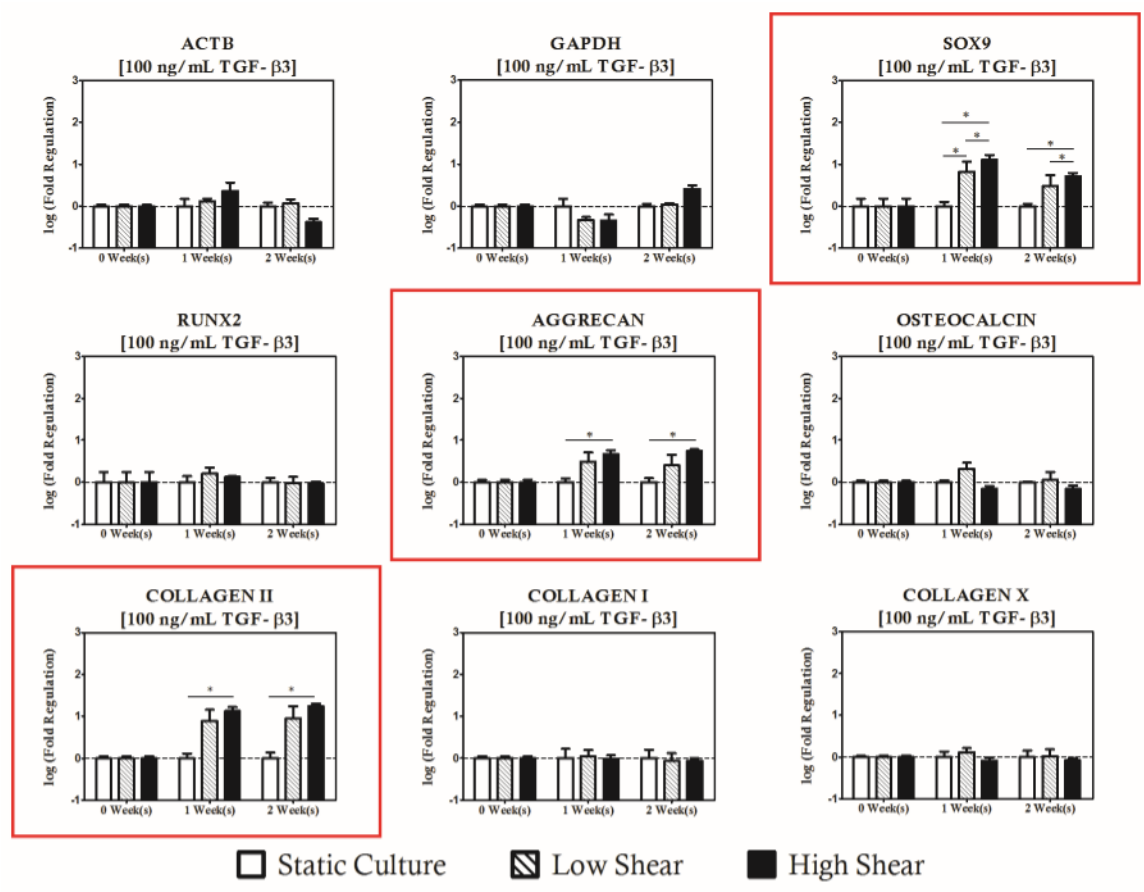

Figure 4.13: 100 ng/mL Supplemented Hydrodynamic Cultures
High levels of TGF-β3 supplementation results in strong upregulation of chondrogenic genes in the presence of hydrodynamic loading. Genes with statistically significant regulation are highlighted with a red box. Statistically significance is indicated by asterisks.

Interestingly, changes in expression of the osteogenic gene panel were not considered significant for any of the hydrodynamic regimes studied. Expression of COLXA1, however, was upregulated relative to concentration matched static controls when conditions were such that high shear magnitudes (10 dynes/cm^2) were paired with low (1 ng/mL) concentrations of TGF-β3 for a period of at least two weeks. No significant changes in COLXA1 were observed with moderate or high TGF-β3 supplementation.

These observations hint at two potentially useful characteristics of this approach. First, chondrogenic differentiation is clearly positively influenced by the presence of hydrodynamic loading when presented in concert with at least 10 ng/mL of TGF-β3, and that TGF-β3 signaling appears to have an inhibitory effect the on the osteoinductive role of high magnitude hydrodynamic loading observed with the other supplementation protocols studied herein.

4.3.6 Histology & Immunofluorescence

Histological staining and immunofluorescence of two-week culture samples qualitatively supports the gene expression profiles observed through PCR (**Figures 4.14-4.16**). Toluidine Blue staining indicates increasing expression of sulfated glycosaminoglycans with increases in both BMP-2 and TGF-β3 supplementation, while Alizarin Red staining shows greater staining with increased BMP-2 supplementation. Alizarin Red staining was relatively uniform for TGF-β3 supplemented cultures for all hydrodynamic and supplementation protocols tested. Immunofluorescence indicates increasing Collagen type I and Collagen type II expression in the BMP-2 and TGF-β3 supplemented cultures of increasing concentration respectively. Trends in collagen expression between shear conditions are less clear, but there appears to be more total collagen in BMP-2 supplemented cultures on the whole, and total collagen expression appears to increase with hydrodynamic loading.

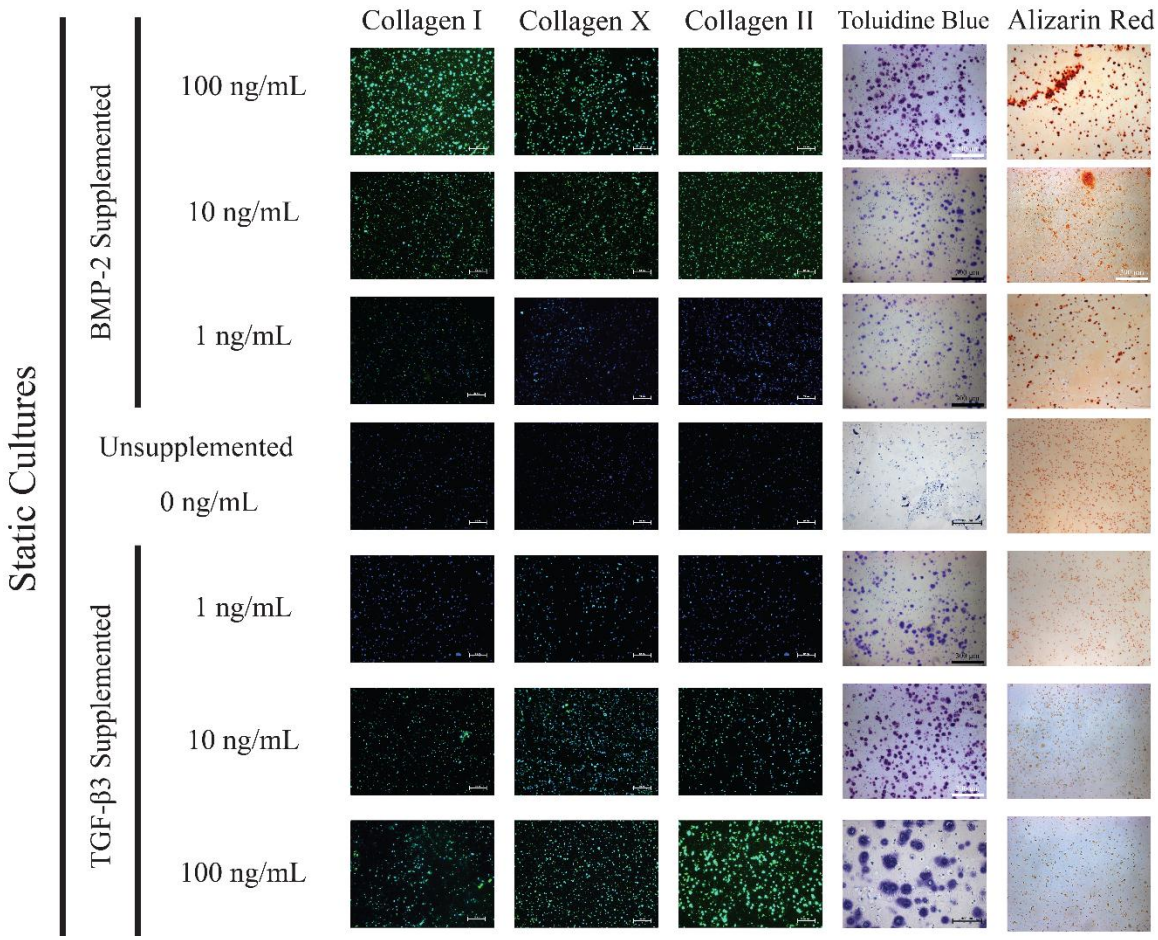

Figure 4.14: Histologic & Immunofluorescence Staining of Static Cultures
Histological and Immunofluorescence analyses of static cultures suggest increasing osteogenic character with BMP-2 supplementation and increasing chondrogenic character with TGF-B3 supplementation.

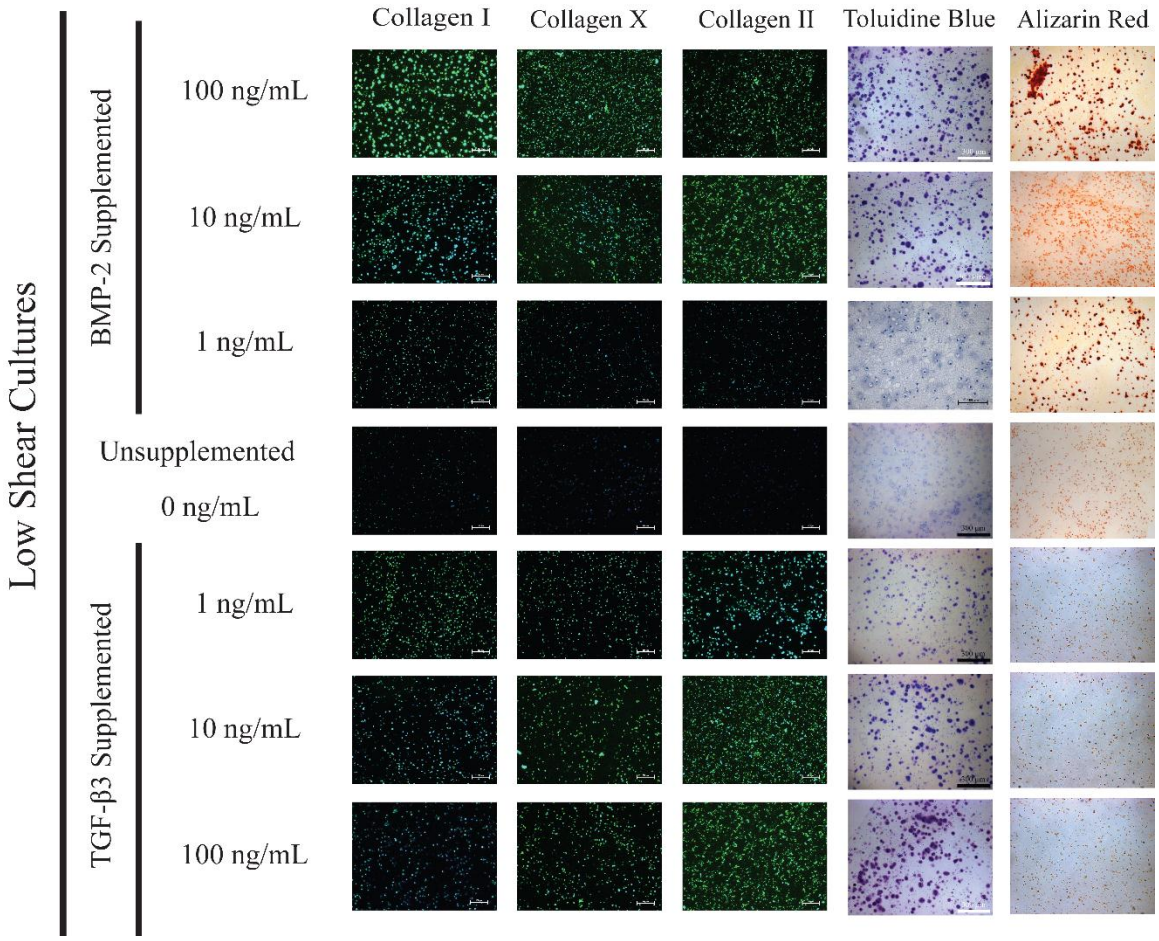

Figure 4.15: Histologic Staining of Low Shear Cultures
Histological and Immunofluorescence analyses of low shear cultures suggest increasing osteogenic character with BMP-2 supplementation and increasing chondrogenic character with TGF-B3 supplementation.

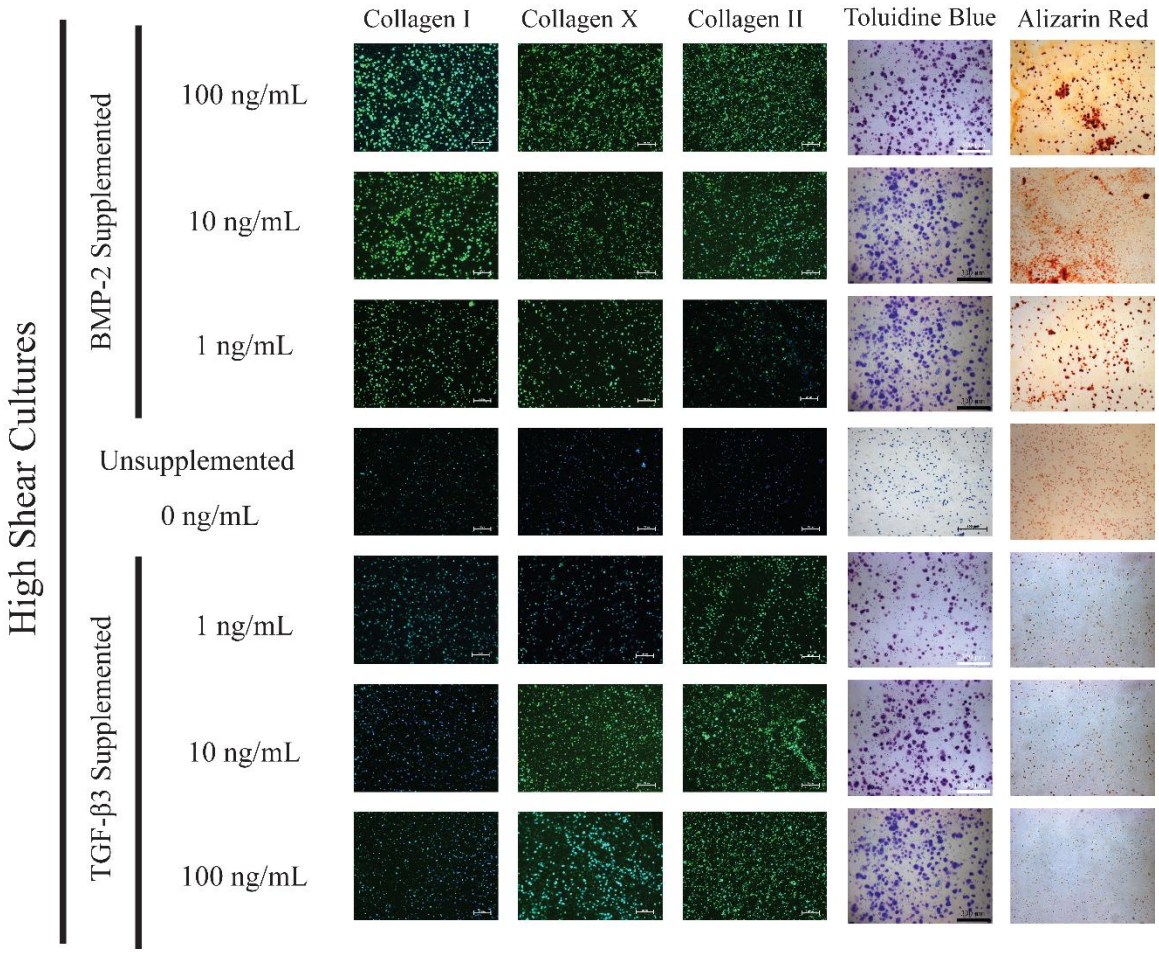

Figure 4.16: Histologic Staining of High Shear Cultures
Histological and Immunofluorescence analyses of high shear cultures suggest increasing osteogenic character with BMP-2 supplementation and increasing chondrogenic character with TGF-B3 supplementation.

4.4 Discussion

As the predominate source of cells for tissue engineered constructs has shifted from terminally differentiated primary cells towards progenitor cells of various differentiation potentials, the ability to spatiotemporally exert epigenetic control over the differentiation of stem cells within a tissue engineered construct has become desirable as a means to better reproduce native tissue complexity and reduce cultivation costs associated with traditional differentiation protocols. Subsequently, we decided to focus herein on the impact of the hydrodynamic environment on MSC differentiation due to its essential role in nutrient exchange during *in vitro* cultivation. Because of this dependency, hydrodynamic loading will be an obligate component of any commercial bioprocessing scheme. The purpose of this study was to investigate how modulation of hydrodynamic loading affects the stability of the MSC phenotype during serum-free tissue culture and how this approach might enhance differentiation efficiency in the presence of growth factors known to be either osteoinductive or chondrogenic in nature. Our primary findings were that hydrodynamic loading, in the absence of exogenous supplementation, promotes expression of hypertrophic and osteogenic genes. This observation was sustained for low levels of exogeneous supplementation irrespective of the cytokine provided. Lineage specific upregulation towards chondrogenic and osteogenic phenotypes was observed under high magnitude shear conditions when hydrodynamic loading was presented in concert with high levels of TGF-β3 and BMP-2 supplementation respectively. Generally, the observed impact of hydrodynamic loading on the desired phenotypes was greater in longer term cultures, and in cultures receiving higher concentrations of exogenous cytokines.

These findings are in agreement with prior mechanobiological studies in other osteochondral lineage cell sources. In studies based on osteoblastic cell lines, multiple studies have shown that hydrodynamic loading is osteopromotive (Bancroft et al. 2002; Datta et al. 2006; Grayson et al. 2008; Sikavitsas et al. 2003; Yu et al. 2004), and often

results in increases in type I collagen production and matrix mineralization. Hydrodynamic studies on MSCs from various donor species have also been previously shown to be osteoinductive (Grellier et al. 2009; Kapur et al. 2003; Kreke et al. 2005) Additionally, multiple studies on primary chondrocytes have shown that in addition to increases in type II collagen (Bueno et al. 2008; Gemmiti and Guldberg 2006). Exposure to high shear environments can result in development of a fibrous layer rich in non-hyaline type I collagen at shear exposed surfaces (Vunjak-Novakovic et al. 2002), particularly when cultured with serum supplemented media (Yang and Barabino 2011) versus serum free preparations. If we compare the extent of the impact of hydrodynamic loading on unsupplemented cultures in our study to that of other environmental induction schemes for MSCs, we find that the effect on gene expression is on the same order of magnitude as manipulations of scaffolding stiffness for osteoinduction (Engler et al. 2006) and both hydrostatic pressure (Miyanishi et al. 2006) and dynamic unconfined compressive loading (Huang et al. 2010; Huang et al. 2004) for chondrogenic induction . Unlike these prior studies, however, we found the impact of exogenous supplementation on gene expression to be considerably greater than the environmental stimulus applied. Our results converge again, however, when the mechanical stimuli were presented concurrently with TGF-β supplementation (Huang et al. 2004; Miyanishi et al. 2006). As in our study utilizing hydrodynamic loading, dynamic compression and intermittent hydrostatic loading both resulted in additional increases in chondrogenic gene expression when presented in cultures supplemented with at least 10 ng/mL. The order of magnitude of the change, however, is considerably greater in our hydrodynamic study (>100 fold change) than either of the prior studies utilizing compressive (<10 fold change) and hydrostatic (<10 fold change) loading.

Conversely, other studies have shown compressive loading to have a negative impact on glycosaminoglycan accumulation within the construct at the protein level (Campbell et al. 2006). It is unclear, however, if this effect is due to decreased synthesis or loss of

glycosaminoglycans to the culture media. Interestingly, the same study (Campbell et al. 2006), also showed that dynamic compressive loading resulted in increases in *COLXA1* in the absence of TGF-β supplementation, a result that mirrors our findings of both a hypertrophic influence of unsupplemented hydrodynamic loading and of the chondroprotective character of TGF-β3 supplementation. Our findings, herein, seem to indicate a comparable role of hydrodynamic loading to that of other environmental factors, particularly dynamic compression. Considering finite element analyses have shown interstitial fluid flow to be an effect of dynamic loading in biphasic materials such as those referenced herein, it is not surprising that these two loading conditions produce similar responses in MSC based tissue constructs.

Our finding that high magnitude hydrodynamic loading promotes osteogenic gene expression in unsupplemented cultures is instructive and suggests that MSCs cultures intended for chondral therapies not be subjected to high shear hydrodynamic loading conditions during processing and cultivation. It is our recommendation that the nutrient utilization of chondrogenic cultures be carefully considered such that fluid loading not be applied in excess of magnitudes needed to meet the convective transport demands of the tissue. Conversely, our findings also suggest hydrodynamic loading of osteogenic cultures can potentially be a means of either reducing culture dependence on exogenous cytokines or promoting increased matrix deposition provided the magnitude of loading is increased such that impacts cell viability in a negative manner (Chisti 2001).

4.5 Conclusions

The findings of this study bring forth a number of interesting ideas regarding hydrodynamic culture of MSC based constructs for tissue engineering applications. As evidenced by results from all growth factor supplementation groups, including serum-free expansion medium culture, it is clear that MSCs are tuned to their local mechanical loading

environment, and that prolonged exposure to high magnitude fluid shear stresses induces a hypertrophic phenotype amongst the resident MSCs ultimately resulting in expression of osteogenic markers. For the purpose of chondrogenic cultures, therefore, our results suggest minimizing the fluid shear stress imposed on the developing construct without reducing the transport of nutrients to all regions of the tissue construct. Furthermore, this phenomenon presents an interesting paradigm for the production of osteochondral tissue constructs through differential loading of the construct, both chemically and hydrodynamically, by varying the microenvironment appropriately in spatially separated regions of the tissue construct. While to overall goal of the current study of a single media source with differential loading to induce phenotypic changes in the MSC population was not achieved, there is evidence that loading will play a significant role in bioprocessing protocols of osteochondral constructs moving forward as technologies such as microfluidic hydrogels (Choi et al. 2007b; Huang et al. 2011; Johann and Renaud 2007; Khademhosseini et al. 2006) provide the means to differentially apply chemical and environmental cues within an integrated construct of a single cell type to spatially engineer osteochondral tissues for intra-articular injury repair and preclinical models for pharmacological studies against osteoarthritis.

5 SPATIAL ENGINEERING OF OSTEOCHONDRAL TISSUE CONSTRUCTS THROUGH MICROFLUIDICALLY DIRECTED DIFFERENTIATION OF BOVINE MESENCHYMAL STEM CELLS

5.1 Introduction

The development of engineered tissue grafts has emerged as a promising therapeutic alternative for the repair and replacement of organs. A number of approaches, employing a diverse spectrum of scaffolds, cell populations, and bioprocessing conditions have been pursued for the production of such grafts, and most of these efforts have focused on engineering homogenous tissues with bulk properties similar to their native counterpart. Some tissues, however, are heterogeneous both structurally and functionally, and possess spatially-varying biochemical compositions and mechanical properties for which the use of a single scaffolding material, cell source, or bioreactor chamber may be inappropriate. A classic example of this is the osteochondral unit, consisting of a hyaline cartilage layer and the integrated subchondral bone. Osteochondral defects resulting from traumatic injury are typically treated through a grafting technique termed mosaicplasty. One of the primary shortcomings of mosaicplasty is the reliance on autologous graft sourcing from a healthy, non-load bearing site that is both limited in its availability and potentially inappropriate for repair due to advanced osteoarthritic degeneration. To address this supply issue, a number or approaches have been pursued to create a suitable replacement for the autologous grafts. Common approaches to recapitulate the unique heterogeneity of the osteochondral unit include the production of homogeneous and composite scaffoldings loaded with one or more cell sources having chondrogenic and/or osteogenic potential, and cultivating them utilizing both commercially available and custom built bioreactor systems. Constructs produced in this manner, however, are still non-optimal as they suffer

from a number of shortcomings. Arguably the most pertinent shortcoming of these approaches are their reliance on terminally differentiated cells (osteoblasts and chondrocytes) isolated from patient specific biopsies and expanded *in vitro*. Use of these cells is plagued by the same dependency on an available autologous donor site as well as low proliferation rates and potential degradation of functionality should *in vitro* expansion be necessary to sufficiently populate the tissue engineered construct.

Mitigation of this particular shortcoming may be accomplished by utilizing an undifferentiated, multipotent mesenchymal stem cells as a single autologous cell source for repair of osteochondral defects. MSCs are well known progenitor cells for both the chondrocyte and osteoblast lineages which have been used to generate osteochondral constructs using single-component or composite scaffolds across a range of compositions and material properties (Bal et al. 2010; Bi et al. 2011; Cui et al. 2011; Gao et al. 2001b; Ghosh et al. 2008; Haasper et al. 2008; Hung 2003; Lima et al. 2004; Martin et al. 2007; Scotti et al. 2007; Sherwood et al. 2002; Swieszkowski et al. 2007; Taguchi et al. 2004). The primary challenge to MSC based constructs, arises from the need to either utilize costly predifferentiation operations prior to the seeding of the construct or simultaneously modulate differentiation down to distinct lineages in a unified culture solution. Using conventional bioreactor systems, the popular approach of supplementing the culture media with lineage specific signaling molecules to achieve directed differentiation of MSC is untenable for biphasic constructs without some means of spatially directed delivery to prevent dominance of one desired phenotype throughout the construct.

Based on these realities, we hypothesized that the spatially confined presentation of optimized differentiation cues would result in tissue-specific biological environments for the regeneration of both bone and cartilage tissues using a model universal donor cell source in an integrated tissue construct. To test this hypothesis, we utilized a microfluidic

hydrogel platform previously developed in our lab to stimulate region specific induction of osteoblastic and chondrogenic phenotypes through parallel, independent microfluidic networks, and evaluated the constructs after two weeks of culture for the presence of gradients in gene expression and matrix composition.

5.2 Materials & Methods

Unless specified otherwise, supplies and reagents were purchased from VWR International (West Chester, PA), Sigma (St. Louis, MO) or Invitrogen (Carlsbad, CA). Antibodies were from AbD Serotec (Raleigh, NC) or Abcam (Cambridge, MA). ELISA kits for Collagens I and II were purchased from Chondrex, Inc. (Redmond, WA) and for Collagen X from MyBioSource, Inc. (San Diego, CA).

5.2.1 MSC Isolation & Characterization

Bovine bone marrow aspirates from 2–4 week old calves (Research 87, Marlborough, MA) was isolated and mixed with expansion medium (high glucose Dulbecco's Modified Eagle Medium [DMEM] supplemented with 10% certified fetal bovine serum [FBS] and 1× penicillin-streptomycin-fungizone [PSF]) supplemented with 300 U/ml heparin), subjected to vortexing and straining processes to remove any undesirable tissues prior to cell pelleting and collection via centrifugation. Following centrifugation, cells were resuspended in fresh expansion medium and plated onto T-75 flasks (Corning, Inc., Corning, NY). Nonadherent cells were removed from the flasks during media change after 24 hours, whereas adherent cells were cultured with the EM for an additional 7–10 days until confluence. Subsequent subculturing was carried out to Passage 3 at a splitting ration of 1:3. Following Passage 3, MSCs that were suspended in a cryoprotective medium (70% DMEM, 20% FBS, 10% Dimethylsulfoxide [DMSO]) at a concentration of 1 million cells/mL and stored in liquid nitrogen in 1mL aliquots.

MSCs from Passages 1-4 were plated in a 12 well plate at a seeding density of 100,000 cell/well in one of four culture media preparations: expansion media (EM), osteogenic media (OM), adipogenic media (AM), and chondrogenic media (CM). Osteogenic media consisted of high glucose DMEM supplemented with 10% FBS, 1X PSF, 100 nM dexamethasone, 10 mM sodium β-glycerophosphate, 0.05 mM ascorbic acid. Adipogenic Media consisted of high glucose DMEM supplemented with 10% FBS, 1X PSF, 1 μM dexamethasone, 0.5 mM indomethacin, 10 μg/ml insulin, 100 mM 3-isobutyl-1-methylxantine. Chondrogenic Media consisted of high glucose DMEM supplemented with 1× PSF, 0.1 μM dexamethasone, 50 μg/mL ascorbate 2-phosphate, 40 μg/mL l-proline, 100 μg/mL sodium pyruvate, 1X insulin–transferrin–selenium [ITS], and 10 ng/mL TGF-β3. Following 21 days of culture, the monolayers were fixed and assessed for successful induction. Osteogenesis was determined by fixing monolayers in isopropanol and staining with Alizarin Red for mineralized matrix. Adipogenesis was assessed by fixing with paraformaldehyde and staining with freshly prepared Oil Red O to visualize lipid droplets. Chondrogenesis was determined by fixing monolayers with 10% formalin and staining with Toluidine Blue for an abundance of proteoglycans.

MSCs from Passages 1-4 were fixed, treated with a nonspecific blocking agent for 30 minutes, and split into six tubes. Four of the six populations were then incubated with one of the following fluorescently tagged antibodies: fluorescein isothiocyanate [FITC]-conjugated mouse anti-human antibodies against each of CD166, CD271, and CD45, or R-phycoerythrin [RPE]-conjugated mouse anti-bovine CD44 antibodies for 1 hour. The remaining two populations were incubated with FITC and RPE conjugated antibodies against mouse IgG as the negative isotype controls. Flow cytometry was performed in a FACScan (BD Biosciences, San Jose, CA). Forward scatter and side scatter parameters were used to evaluate the size and granularity of cells, respectively.

5.2.2 Tissue Culture

Microfluidic constructs were prepared as described previously. Briefly, construct molds were produced by casting polydimethylsiloxane (PDMS) against micromachined acrylic molds and curing the polymer at 90°C for 90 minutes following degassing under vacuum. On Day 0 of tissue culture, the surface of the PDMS molds were rendered hydrophilic via oxygen plasma and autoclaved before construct fabrication by casting a 25 million cell/mL, 2.5% agarose solution, between the acrylic casings and the PDMS molds (**Figure 5.1**). A planar slab of the cell-agarose solution was then sealed between the two molded portions to complete the construct as depicted in **Figure 5.1**.

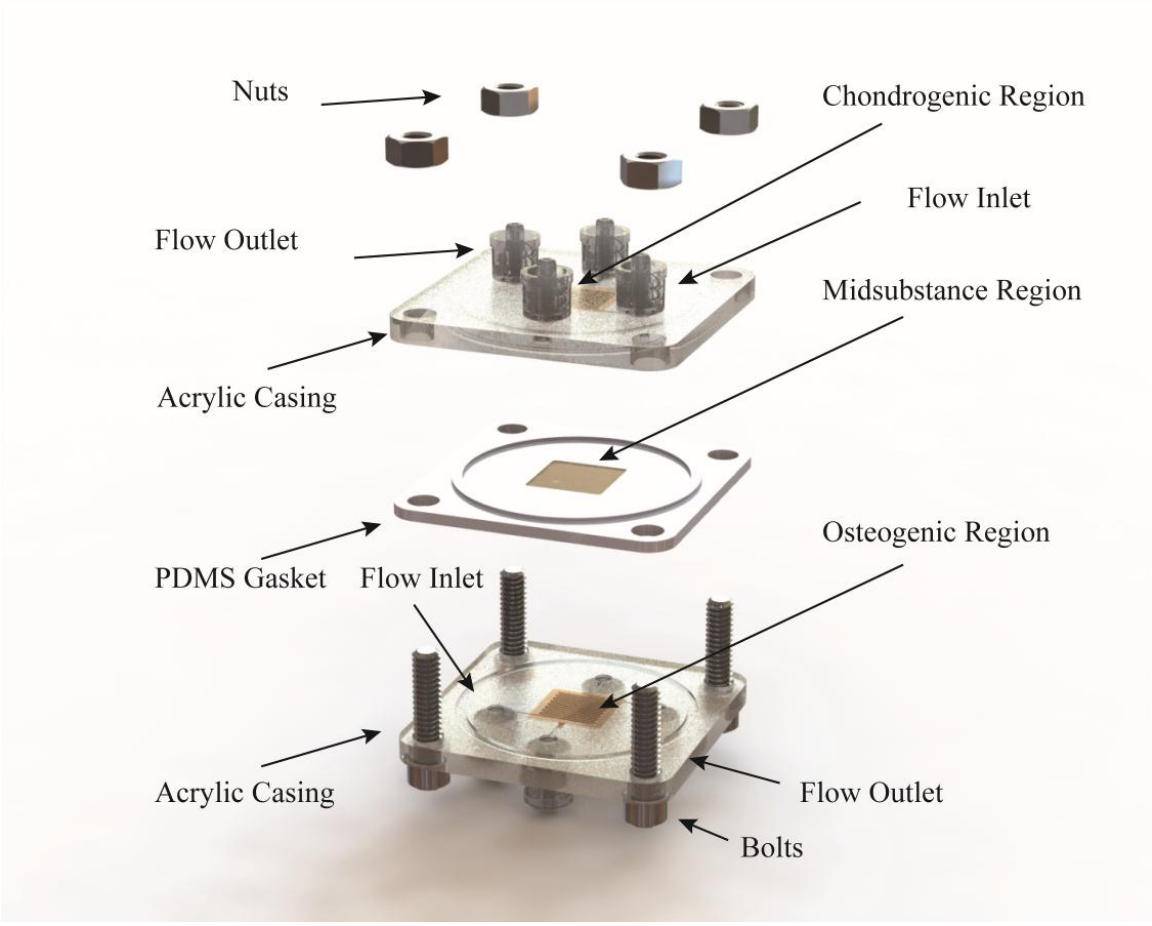

Figure 5.1: Assembly of Microfluidic Osteochondral Constructs
Construction process of the microfluidic osteochondral graft. Each target region is independently cast and controlled via ports in the acrylic casing. The chondrogenic and

osteogenic regions are separated by a planar midsubstance region molded directly into a PDMS gasket which ensures unidirectional flow through the microfluidic networks.

Constructs were connected to independent flow loops through which media was recirculated via a syringe pump equipped with dual check valves to achieve unidirectional flow and culture commenced under regionally specific bioprocessing conditions. Within the control group, EM was supplied to both microfluidic networks of the construct at constant perfusion at a volumetric flow rate of 250 μL/min. The prescribed flow rate was selected to both fulfill the minimal flow rate requirements for the nutrient demands of the resident cell population as previously determined, and to provide a uniform shear stress distribution of 1 dyne/cm2 at the microchannel walls in the central region of interest. Constructs from the experimental group received two different sets of bioprocessing conditions. The osteogenic region was provided with EM supplemented with 10 ng/mL BMP-2 at a constant perfusion rate of 2.5 mL/min such that the shear stress distribution at the microchannel walls was a uniform 10 dyne/cm^2. The chondrogenic region was supplied with EM supplemented with 10 ng/mL TGF-β3 at a the same flow rate as the control group so as to produce a uniform 1 dyne/cm^2 shear stress distribution at the microchannel wall. A gas exchange reservoir was connected to the flow loop and a 5% CO2 mixture bubbled through the culture media to maintain pH. Total culture media volume was maintained at 100mL with fresh media exchanges were performed every 3-4 days through sampling ports attached to the gas exchange reservoir.

5.2.3 Gene Expression Analysis

Real-time polymerase chain reaction (qRT-PCR) was used to quantify region specific gene expression within the constructs. Constructs were fixed in TRIzol, and RNA was isolated from the homogenized cell lysate through a series of rinse, elution, and centrifugation processes. The RNA samples were then reverse transcribed into cDNA using a QuantiTech Rev Transcription kit (Qiagen, Hilden, German) according to the manufacturer's protocol.

Gene expression for target mesenchymal lineage markers using custom-designed primers (Table 1) with quantitative PCR amplification performed on a StepOnePlus™ Real-Time PCR System (Applied Biosystems) in the presence of SYBR Green/ROX master mix (Applied Biosystems). GAPDH and β-actin were both used as endogenous controls for normalization through geometric averaging.

5.2.4 Biochemical Analysis

To determine the biochemical composition of the construct layers, assays were performed to determine the proteoglycan, DNA, and collagen content. Samples were first weighed wet and digested for 16 h in papain at 60ºC. Aliquots were analyzed for sulfated glycosaminoglycan (sGAG) content using the 1,9-dimethylmethylene blue dye-binding assay, for DNA content using the PicoGreen dsDNA Quantification kit (Molecular Probes, Eugene, OR), and for collagen types I, II, and X by ELISA.

5.2.5 Histological Analysis

For histological analysis, constructs were fixed in 10% buffered formalin, embedded in paraffin and sectioned into 8μm thick sections for the midsubstance of the construct. For immunofluorescence, sections were incubated with a citrate buffer heated to 99°C for 30 min to retrieve antigens, and allowed to cool to room temperature. The samples were then incubated in blocking buffer for 30 minutes and primary rabbit anti-bovine antibodies (1:100, Abcam, Cambridge, MA) against collagens type I, II, X at 4°C overnight. Sections were then washed three times in PBS and treated with DyLight®594 goat anti-rabbit secondary antibodies (1:200, Abcam, Cambridge, MA) for one hour at room temperature. Finally, samples were washed and mounted with Vectashield with DAPI and visualized on a Nikon Ti Eclipse inverted fluorescence microscope (Nikon Instruments, Inc., Melville, NY), with representative images captured using a CoolSNAP HQ2 CCD camera (Photometrics, Tucson, AZ).

5.2.6 Statistical Analysis

Sample sizes for RT-qPCR and Immunohistochemistry were N=3 each. Sample Sizes for biochemical analyses were N=5 each. For all image analysis of histology specimens, the minimum number of images required to accurately represent the whole section were used. Bar graphs are presented as the mean ± SEM with statistically significant differences defined as $p < 0.05$ using two-way ANOVA with Bonferroni post-hoc tests for multiple comparisons.

5.3 Results

5.3.1 Cell Proliferation

As depicted in Figure 5.2, there was no significant difference in DNA content between the osteogenic and chondrogenic regions of either the control group or experimental group osteochondral tissue constructs.

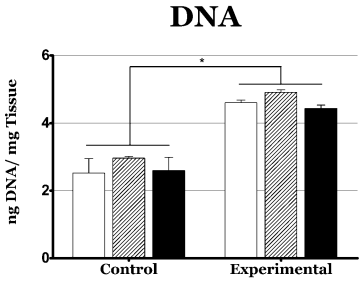

Figure 5.2: DNA Content of Microfluidic Osteochondral Constructs

After two weeks of culture DNA content was significantly higher in the experimental group which received cytokine supplementation relative to the unsupplemented control group. There were no significant differences between the various regions of the experimental cultures.

Additionally, the midsubstance region between the two microfluidic networks was not found to be significantly different from either of the target regions for either the control or experimental groups. There was, however, a statistically significant difference in DNA content between the control and experimental groups across all phenotypic regions of the tissue constructs after two weeks of culture.

5.3.2 Differential Expression of Osteochondral Genes

Looking first at the control group, there is no difference in the osteogenic (*RUNX2, OSTEOCALCIN,* and *COL1A1*), hypertrophic (*COLXA1*), or chondrogenic (*SOX9, AGGRECAN,* and *COL2A1*) gene expression profiles between the various regions of the tissue constructs. Within the experimental group, however, differential expression of both the osteogenic and chondrogenic gene expression profiles with respect to the opposing construct region was observed.

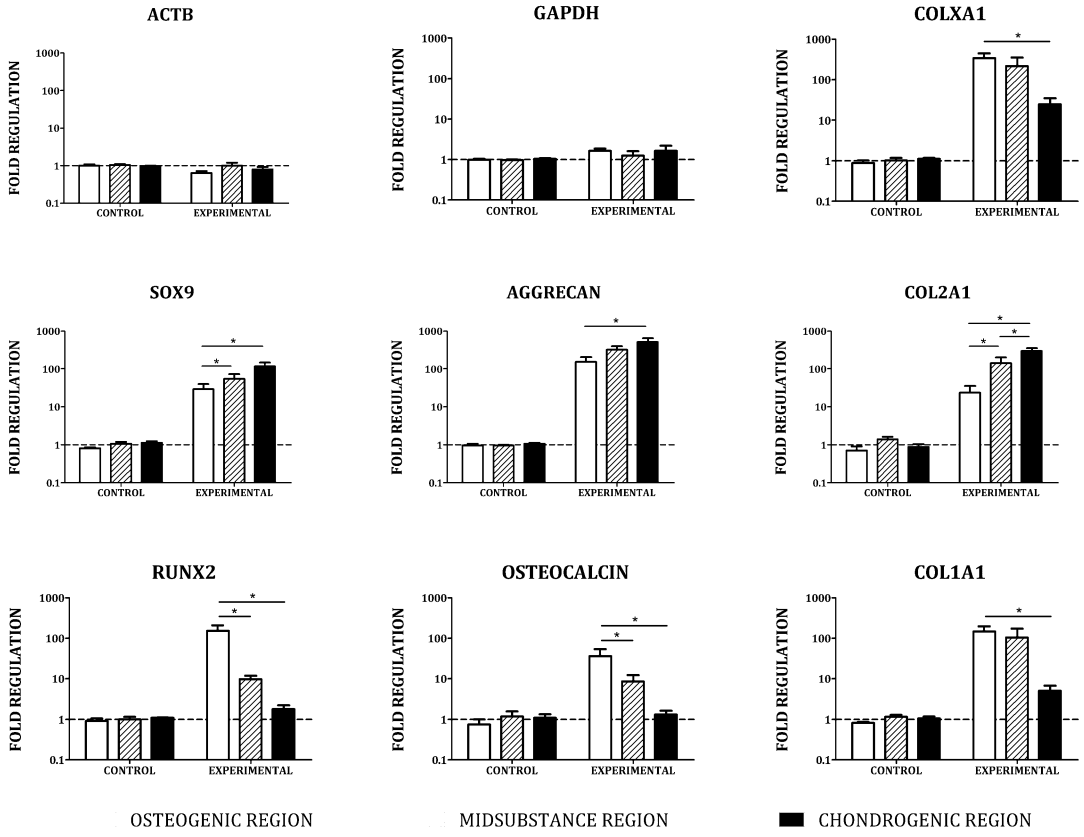

Figure 5.3: Differential Gene Expression of Osteochondral Constructs

Differential loading of an osteochondral tissue construct results in gene expression gradients of both osteogenic and chondrogenic genes

Considering first the osteogenic target region, a statistically significant upregulation of *RUNX2* and *COL1A1* was observed within the osteogenic target region relative to the chondrogenic target region. Regulation of the osteogenic gene panel was also greater than

that of the chondrogenic panel with the exception of aggrecan, but not in a statistically significant manner. With regard to the chondrogenic gene panel, a statistically significant regulation of the entire chondrogenic gene panel (*SOX9*, *AGGRECAN*, and *COL2A1*) within the chondrogenic region relative to the osteogenic target region of the construct. Additionally, *COLXA1* expression was observed to increase across the construct from the chondrogenic regions to the osteogenic region, with a statistically significant difference in expression occurring between the chondrogenic and osteogenic regions, but no with such difference occurring between the midsubstance and osteogenic regions.

5.3.3 Glycosaminoglycan Content

As evidenced by the results of the DMMB assay, glycosaminoglycan content was significantly higher in the experimental group relative to the control group (**Figure 5.4**).

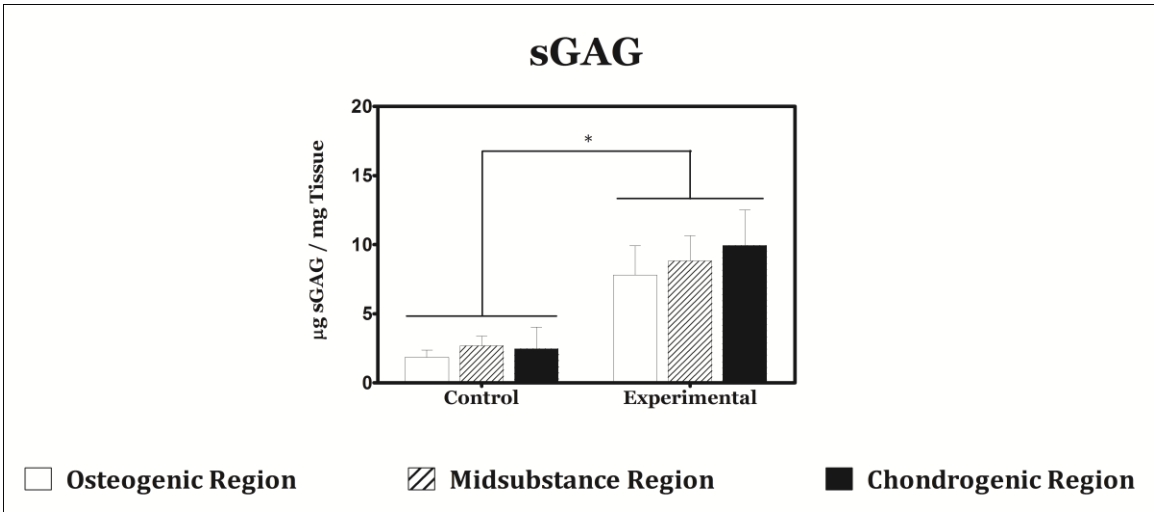

Figure 5.4: sGAG Content of Osteochondral Constructs

Measurement of sulfated glycosaminoglycan content within the various regions of the osteochondral constructs by DMMB assay reveals significantly higher sGAG accumulation in the experimental group irrespective of the construct region relative the control group. Within the experimental group, however, no statistically significant difference was observed.

Within the experimental group, however, no statistically significant regulation of sGAG was observed although the maximum value was observed within the chondrogenic region while the minimum value was observed within the osteogenic region.

5.3.4 Graded Collagen Composition

ELISA was performed for expression of collagens Type I, II, and X. As depicted in Figure 5.5, all three collagen types exhibited graded expression across the construct, with types I and X exhibiting their maximum concentration in the osteogenic target region of the construct and type II exhibiting a maximum concentration in the chondrogenic region of the construct. It is worth noting that the magnitude of collagen types II is considerably greater than that of type I, even in the osteogenic region of the experimental constructs. Within the control group, collagen content is significantly lower with no gradations of note.

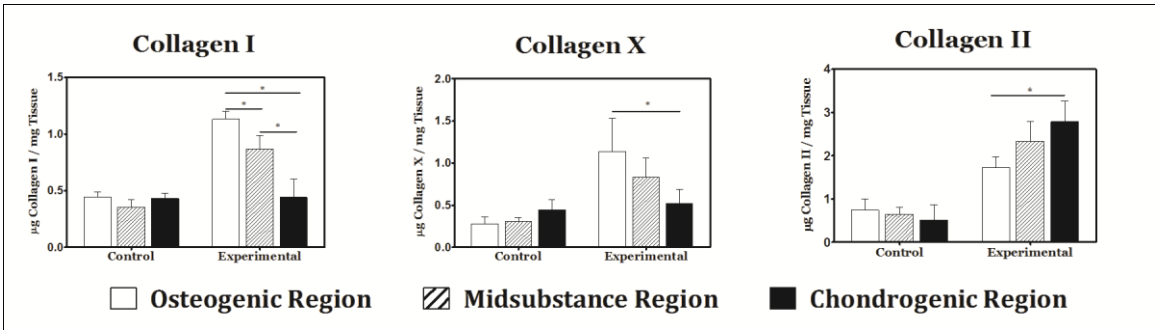

Figure 5.5: Differential Collagen Content of Osteochondral Constructs

ELISA reveals gradients in Collagen type I across the osteochondral constructs, and differential expression of collagen types II and X between the osteogenic and chondrogenic regions of the experimental group.

5.3.5 Histology & Immunofluorescence

Control constructs stained weakly and relatively homogeneously for both histological stains and for all collagens tested following two weeks of culture. The experimental group, however, exhibited much stronger staining across all regions. Within the experimental group, Toluidine Blue staining revealed no discernible difference in proteoglycan content between the various regions of the osteochondral constructs. Alizarin Red staining

revealed a slight gradient in mineralization with a region of high concentration within the osteogenic layer and a region of low concentration in the chondrogenic layer. Collagen staining revealed a mild gradient in both type I and type II collagen with the highest concentration of each located within the osteogenic and chondrogenic layers respectively. Collagen X staining results were inconclusive.

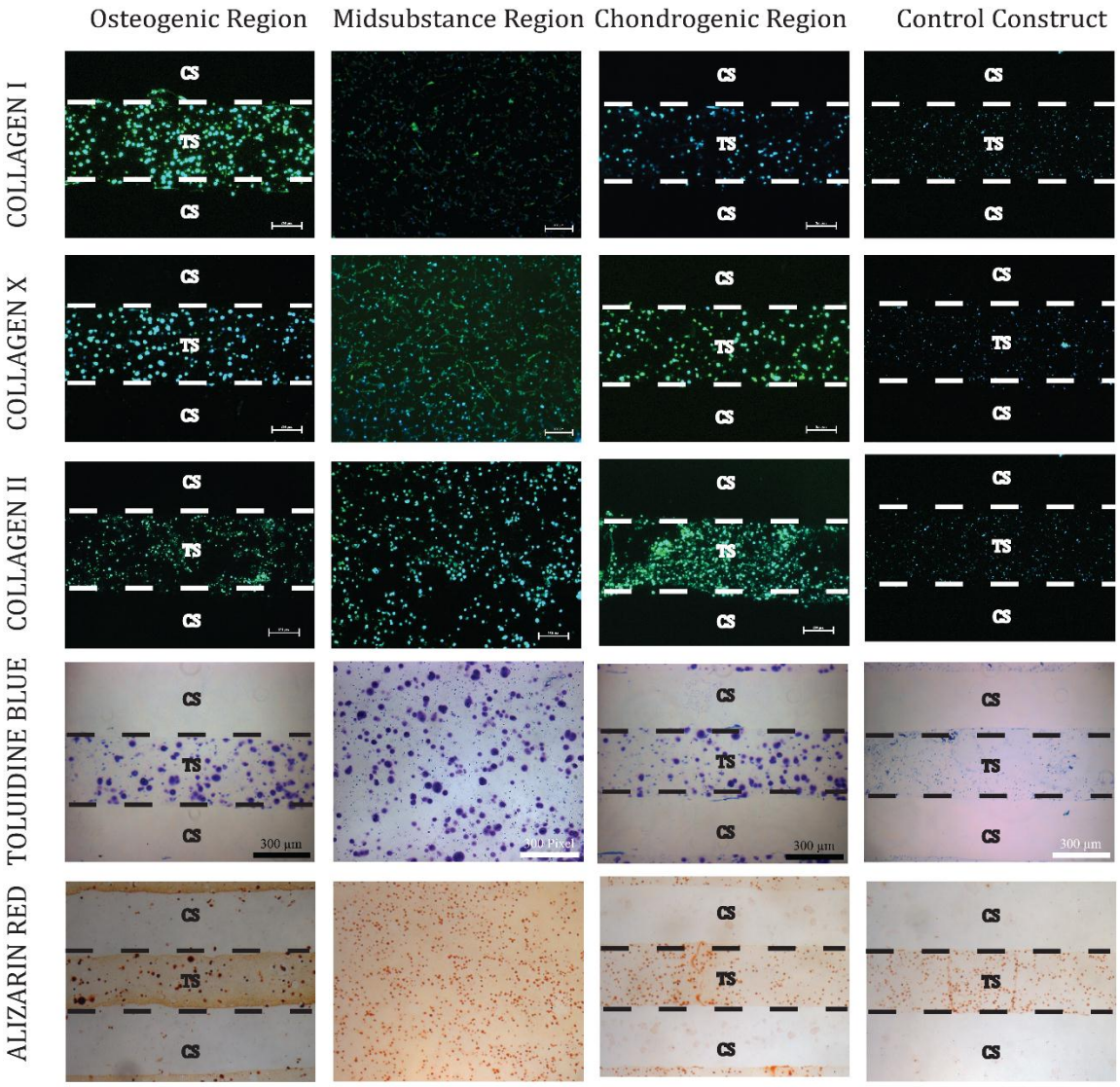

Figure 5.6: Histology & Immunofluorescence of Osteochondral Constructs
Immunofluorescence staining shows gradients in collagen types I and II. Alizarin Red staining also indicates increased mineralization within the osteogenic region relative to the chondrogenic region.

5.4 Discussion

The purpose of the study described herein was to evaluate microfluidic hydrogels as a platform for the production of osteochondral tissue constructs through the spatially directed differentiation of bovine mesenchymal stem cells. The ability of the mechano-chemical inductive cues provided through the microfluidic networks to direct zone-specific differentiation was evaluated through gene expression analysis, biochemical composition, and histological staining. Relative to our non-inductive control cultures, the spatially defined presentation of inductive factors and bioprocessing conditions had a clear impact in proliferation of the resident cell population and elaboration of a spatially discrete osteochondral matrix within our experimental group. On a whole construct basis, differences between the control and experimental constructs included significant increases in both DNA content and total osteochondral matrix elaboration. These findings are in agreement with the prior literature on the effects of the TGF-β superfamily proteins provided to these cultures (Massague 1990; Wozney 1992) as well as to previous findings from our group on the synergistic effects of hydrodynamic loading on MSC differentiation efficiency in the presence of these factors. Within the experimental group, there was evidence of spatial differences in matrix composition reminiscent of the osteochondral junction. The chondrogenic target region of the construct showed a local maximum of glycosaminoglycan content and significantly higher expression of Collagen II relative to the osteogenic target region, while significantly higher expression of Collagen I and X was observed in addition to a minimum in glycosaminoglycan content in the osteogenically targeted region of the constructs. Additionally, Alizarin Red staining showed an increase in mineralization within the osteogenic region. The dual presence of sGAG and mineralization within the osteogenic region indicates the concurrent formation of both cartilage and bone, and may represent an intermediate differentiation step along the endochondral ossification pathway for the culture period studied herein, rather than a terminal bone phenotype. While suboptimal, we believe this result to be an acceptable for

the culture durations studied and hypothesize that cultivation for longer durations would replacement of the cartilaginous portion of the matrix with higher quality bone formation (Wang et al. 1990; Wozney 1992). This is further supported by the relatively lower presence of both Collagen I and mineralization in the chondrogenic region indicating this endochondral bone formation is concentrated near the BMP-2 supply network and that the cartilage formation in the chondrogenic region is hyaline in character.

For the purpose of benchmarking our technology, there are various reports utilizing dual culture control systems for osteochondral tissue engineering are present in the literature that warrant discussion. Chang et al cultured a gelatin infused sinbone block to generate osteochondral constructs in a dual-chambered bioreactor approach that validated their scaffolding system for the production of hyaline cartilage within the gelatin portion of the composite scaffolding (Chang et al. 2004). The bony portion of this scaffold however acellular in nature. Mahmoudifar and Doran used a similar dual chambered bioreactor to that implemented by Chang et al for the production of osteochondral tissue constructs from two sutured together polyglycolic acid meshes seeded with adipose derived stem cells (Mahmoudifar and Doran 2013). This approach mirrored our results after two weeks of culture with respect to statistically indeterminate differences in glycosaminoglycan content between the layers, but did not find differential expression of collagen II as we report herein. Compared to these studies our constructs are not only cellularized in both the osteogenic and chondrogenic regions as was also show by Mahmoudifar and Doran, but our system was also shown to suppress osteogenic character within the chondrogenic layer. While the characteristics of the cell type seeded in each of these systems may also play a role in the improvement shown with respect to this metric, we believe the improvement is due to improved controlled of the microenvironment provided by the presence of the microfluidic network within the tissue construct versus the superficial delivery of inductive cues characteristic of the dual chambered bioreactor. While more challenging to

implement than the simple elegance of the dual chambered bioreactor, the paradigm proposed by our system also offers the capability to produce thicker constructs as necessary and even greater optimization of culture conditions by the incorporation of more independent microfluidic networks into the construct.

5.5 Conclusions

In this study, we have established a paradigm for the production of biphasic tissue constructs through microfluidically directed differentiation of mesenchymal stem cells using the osteochondral unit as a model tissue. While there is evidence in the literature of other approaches to spatially engineer the composition of an osteochondral construct, this study is the first of its kind to utilize microfluidic networks to successfully engineer a biphasic tissue of clinically relevant thickness with measurable differences in biochemical composition between the bony and cartilaginous regions. The results presented herein highlight how optimized mechano-chemical microenvironment can affect the production of tissue specific extracellular matrix of the resident cell population seeded in the various regions of a hydrodynamically loaded osteochondral construct compared to control constructs produced through a non-inductive bioprocessing scheme. Based on our results, we believe that this approach may have significant potential for the production of a number of interfacial tissues including tendon, ligament, and of course the osteochondral unit for use in regenerative capacities. We would be remise, however, if we did not address the dependency of the ultimate utility of this approach on the further development of enabling material and biofabrication technologies to help achieve cost effective production and processing of well-defined, robust tissue products. In light of this the need for future research in these areas, we believe these results of this study represent an important first step in the rational design of engineered osteochondral units through establishment of a platform for the future optimization of scaffolding formulations and bioprocessing

parameters towards the production of commercially viable osteochondral tissue products using microfluidic scaffolding strategies.

6 FUTURE DIRECTIONS

The work described herein represents a significant advancement of microfluidic scaffolding platforms for the production of engineered tissue grafts. As a result, these findings also warrant further development of the technology for clinical translation, and the development of engineered tissues as models for preclinical pharmacology studies. The microfluidic platform developed herein is perfectly situated as a scaffold-bioreactor hybrid to fulfill any or all of these potential purposes due to its flexibility in terms of customization with a few strategic improvements to weaknesses in its current implementation.

6.1.1 Further Investigation of Fluid Shear Effects in Scaffolding Material

The shear stresses reported in these studies refer only to the expected shear stress at the construct surface (Chapter 4) or the microchannel wall (Chapters 3 and 5). Within the porous scaffolding material, however, a boundary layer will develop in which pore-level flow exists, but the magnitude of the shear stress experienced by the embedded cells is heterogeneous and likely considerable lower than the nominal values reported herein. Additionally, the magnitude of the shear experienced will decrease with distance from the hydrodynamically loaded surface. Additional studies in which detailed measurements of these shear values as a function of distance from the tissue surface would provide valuable insight into the role of hydrodynamic loading on the biological processes occurring in the tissue constructs developed herein.

6.1.2 Longer Term Culture Periods

While the extension of cultivation of microfluidic based tissue constructs to two weeks is one of the many achievements accomplished in these studies, there would be great value in extended the cultivation period even further to reach the order of months. Longer cultivation times would likely result in better approximation of the native mechanical properties due to increased matrix elaboration in both the chondral and osteochondral tissue

constructs and increased calcification of the bony portion of the osteochondral constructs. Further, longer cultivation periods would better approximate the time period necessary to produce a functional tissue product, and thus provide greater insight into how to best optimize the construct for commercial implementation.

6.1.3 Further Optimization of Cellular Microenvironment

6.1.3.1 Cell Seeding Density

While the impact of cell seeding density was studied from a mathematical standpoint with respect to nutrient utilization within a microfluidic tissue construct, *in vitro* evaluation of microfluidic construct development was only carried out at one cell seeding density. It is well established that the cells which constitute a tissue communicate with each other through both physical contact and paracrine delivery of chemical signals. At low cell seeding densities, it is likely that the increased distance between neighboring cells will have an impact on the physiology of the cells involved due to reduced communication and increased or otherwise disrupted timing of paracrine signaling. At increased cell seeding densities is likely that increased cell-to-cell contact will result in increased communication between cells that would likely have a measurable impact on cellular metabolism and/or differentiation. A study which modulates the seeding density within the microfluidic scaffolding system described herein could potential provide valuable information for the further optimization of the microfluidic constructs for the production of tissue engineered cartilage or osteochondral grafts. Such a study would be easy to implement using the bioprocessing guidelines suggested in Chapter 3 of this dissertation, and potentially offers the opportunity to investigate the role of cellular communication at densities much higher than previously reported for tissue engineering applications due to the mass transport advantages offered by the presence of the microfluidic network.

6.1.3.2 Cellular Substrate Stiffness

It is well established that the stiffness of the substrate to which a cell is attached can have an impact on cellular processes including metabolism, proliferation, migration, and differentiation. In the studies described herein the stiffness was not addressed as a variable for differentiation, providing an opportunity for further optimization of MSC laden microfluidic hydrogel systems. Following the approach of Tse and Engler (2010) the stiffness of cellular substrate stiffness can be controlled by modulating the cross-linking density of polymeric substrates (Tse and Engler 2001). Utilizing this approach, Engler et al. varied the elasticity of a polyacrylamide substrate from 0.1 to 40 kPa and showed differentiation of MSCs toward neural, myogenic, and osteogenic lineages, with neural expression occurring at the lowest substrate stiffness and osteogenic differentiation occurring on the most stiff substrates (Engler et al. 2006). Further, Park et al. showed that substrate stiffness in combination with TGF-β supplementation was capable of modulating differentiation of MSCs between smooth muscle cell and chondrogenic phenotypes.(Park et al. 2011) with chondrogenic phenotypes occurring at lower substrate stiffnesses than that of the smooth muscle cell. These findings together indicate that spatially varying the stiffness of the hydrogel within our microfluidic platform between a lower value in the chondrogenic region and a higher value in the osteogenic region may provide an additional induction signal to further optimize differentiation efficiency within our osteochondral grafts. Implementing such a study in our current, agarose based system would require increasing the weight fraction of the agarose gel, and adjusting the microchannel spacing and culture media flow rates accordingly as defined in Chapter 3 of this dissertation. Greater control over substrate elasticity, however, would be achieved in a synthetic hydrogel material, so it might be more advantageous to pursue a change of material system prior to pursuing such studies.

6.1.3.3 Presentation of Biomimetic Features

While naturally occurring polymers are often used as scaffolding materials for tissue engineering, synthetic polymers lack inherent biological functionality. They may facilitate protein absorption, but such non-specific interactions occur spontaneously and are not controllable. Subsequently, the tethering of molecules to influence cellular processes such as adhesion, migration, or signaling represents an additional design space for the optimization of the cellular microenvironment. This approach relies on the choice of highly functional monomers that exhibit at least one site for the conjugation of a protein, peptide, or drug in addition to the polymerization groups. Additionally, the permanence or release profile of the conjugated bioactive molecule can be tailored to the intended purpose (i.e. adhesion, signaling, etc.). Utilizing this approach it may be possible to further increase the induction efficiency of MSCs within a microfluidic construct. For instance, both TGF-β and dexamethasone have been conjugated to PEG based tissue constructs for the purpose of inducing chondrogenesis (McCall et al. 2012) and osteogenesis (Nuttelman et al. 2006) respectively. Particularly in the case of dexamethasone, it may be beneficial to increase the concentration within the osteogenic region through conjugation rather than media supplementation as it is a smaller molecule than TGF-β3 and BMP-2 studied herein, and would likely diffuse more readily across the midsubstance region. Additionally, molecules such as the RGD peptide are commonly utilized in synthetic scaffolds to provide attachment sites and cell signaling via integrins, both of which would have been shown to enhance chondrogenic and osteogenic differentiation (Re'em et al. 2010; Yang et al. 2005).

6.1.3.4 Use of Oxygen Tension as a Chondrogenic Differentiation Cue

Hypoxic Environments are well established as a chondrogenic differentiation cue in the literature. As such, control of oxygen tension within the independent microfluidic networks of the osteochondral constructs represents an additional variable that may be manipulated within the system developed herein to drive chondrogenesis and osteogenesis

in a differential manner. The expected outcome of such studies would be presentation of low levels of dissolved oxygen within the chondrogenic region relative to the osteogenic region would result in additional gains in chondrogenic gene expression and improved cartilaginous matrix deposition in the chondrogenic region relative to the osteogenic region. Impact on the osteogenic region in such a setup is expected to be minimal.

6.1.4 Improvements to Fabrication Processes

Perhaps the greatest weakness of the microfluidic scaffolding strategy presented herein is related to the technical, time consuming nature of its fabrication and reliance on a skilled operator. The fabrication is both time sensitive and susceptible to failure due to misalignment and delamination leading to material waste. Recent advances in the field of additive manufacturing offer a potential solution to this problem. As additive processes produce geometries by building up three-dimensional structures based on thin layers of two dimensional patterns they are well suited for building microfluidic networks into hydrogels in a robust and highly reproducible manner. Ideally, the scaffolding material should permit application of novel additive manufacturing technologies, so that a microfluidic construct with any desired 3-D geometry can be designed and fabricated using various medical imaging modalities. Additive manufacturing technologies produce parts by manipulating source materials in several possible ways: thermal, chemical, mechanical and/or optical (Melchels et al. 2012). Among the state of the art additive manufacturing modalities most suitable for hydrogel systems, thermal and chemical setting methods are most commonly utilized in mechanical rastering systems, while optical methods are more commonly utilized in large area methodologies. Optical methodologies typically offer advantages with respect to spatial resolution and production time over other methods, particularly those which utilize a digital mirror device to expose entire layers at once. Further, thermal and chemical methods may be inappropriate for the purpose of cell encapsulation if glass

transition temperatures, pH levels, or free radical concentrations drastically exceed physiological levels.

The encapsulation of cells during a layered manufacturing build that is based on optical methods is also non-trivial as localized heating and free radicals produced during photopolymerization can result in cell death. For UV based approaches, UV exposure is known to have a direct negative impact on cell viability. Further, given the layer-by-layer nature of additive manufacturing technologies, the encapsulated cell population is expected to experience repeated UV doses in a depth dependent fashion. Therefore, it is paramount to minimize these effects and often by optimizing exposure times and photoinitiator concentrations.

Ultimately, any practical implementation of microfluidic scaffolding technologies with require an additive manufacturing approach to limit the weaknesses of the platform developed in this dissertation. Further, the automated nature of these tissue assembly technologies makes them more scalable, reproducible, and controllable which will make tissue production cheaper, more customizable, and less dependent on the technical capabilities of the operator.

6.1.5 Incorporation of Features to Promote Integration

Even the most structurally, mechanically, and biochemically optimized tissue engineered construct will fail to function in vivo if the construct fails to integrate with the host tissue defect. Immobilization of the construct within full thickness chondral defects can be enhanced by incorporation of subchondral bone into the construct. The relatively rapid remodeling of subchondral surrounding the construct and ultimate integration with the host tissue provides quicker fixation of the construct within the defect (Khan et al. 2008). Subsequently, lateral integration of the slower remodeling cartilage tissue may therefore be enhanced in the vertically constrained construct. With respect to osteochondral grafts,

it has been postulated that the incorporation of the subchondral bone layer helps serve to improve vertical integration *in vivo* due to the increased remodeling rates present in bone relative to cartilage. Lateral integration of the graft with the native chondral tissue, however, is often neglected from a construct design perspective. As the scope of this dissertation was limited to the *in vitro* development and validation of the technology, innovative construct fixation features were not implemented herein, and represent an opportunity for further development. One logical approach to address lateral integration would be in add an integration lattice to outer surface of the tissue construct, that would provide increased access for infiltration of the surrounding tissue, and increased surface area for cell attachment and the introduction of frictional forces associated with neotissue elaboration. This approach will require improvements in the fabrication processes as previously discussed and special attention to detail near the fluidic ports to ensure the absence of leaks.

6.1.6 Assessment of *In Vivo* Performance

Within this dissertation, great consideration has been taken to carefully engineer tissue constructs with the goal of achieving comparable functional properties relative to the native tissue. This technology, however, cannot be fully evaluated without analysis of the graft function *in vivo*. Further to be commercially viable, the tissue engineered graft must not simply repair the articular surface, it must also produce better long-term joint function than would be expected if the injury was treated utilizing standard of care. For case of osteochondral grafts such as those developed herein, the most accessible load bearing animal model is that of the New Zealand White Rabbit. Using this model, experimental chondral and/or osteochondral grafts are press fit into a surgically produced full thickness defect and allowed to integrate with the native tissue for a predetermined period of time. Surgical control treatments can be introduced on the contralateral limb so that direct comparisons within the same individual can be made with respect to integration, viability,

and function. Assessing microfluidic osteochondral constructs, produced either as described herein or with one or more of the suggested improvements described above, using the New Zealand rabbit model is the logical next step in assessing microfluidic hydrogel technologies for clinical translation.

6.1.7 Microfluidic Constructs for Pharmacological Studies

While the use of the microfluidic constructs developed in this dissertation for therapeutic purposes is still far from clinical implementation, use of this system for the development of model tissues for preclinical pharmacological studies is another route that may be more tractable in terms of making an impact on treatment strategies for intra-articular injuries in the near term. Traditionally, drug discovery has been carried out in monolayer cultures which do not mimic the extracellular environment and cell-cell communication engineered tissue models can provide. Further, these 2D cultures are also carried out statically, which greatly limits the ability of the investigator to study physiological responses to gradients or dynamic presentation of the investigational drug. The microfluidic platform developed in this dissertation, however, is capable of achieving both of these key factors, and may provide more robust data to support fast tracking key compounds for clinical studies. Further, most human pharmacokinetic response data is predicted using expensive animal models. If this costly step in drug development could be reduced or eliminated by utilizing human tissue models, the total cost to market of future drugs could be drastically reduced. Finally, the ability to connect multiple units in series allows for the study of multiple organ system models to be included in the model to detect how an osteoarthritis drug candidate may impact other critical systems such as the liver. I believe this application for microfluidic tissue engineering strategies will continue to experience increased interest in the coming years and represents another great opportunity for further development of microfluidic tissue constructs.

7 FINAL THOUGHTS

Tissue engineering has the potential to eliminate the supply and demand, donor matching, and disease transmission issues associated with standard osteochondral allografts by providing highly characterized functional grafts upon demand. To achieve this lofty goal, the tissue engineering community will have to continue to develop more sophisticated tools for robust construct fabrication and manufacture. My particular approach, in spite of its inherent weaknesses, provides an excellent model for the rational design of tissue constructs of moderate spatial complexity and for studying their development over the course of weeks.

In addition to laying out the framework for the design of microfluidic tissue constructs and developing the bioprocessing methods for their cultivation, these studies advance our understanding of the *in vitro* hydrodynamic conditions of the cellular microenvironment and how they interact with the chemical environment to bring about changes in construct composition. The findings that high magnitude hydrodynamic loading of MSC-laden tissue constructs both enhances the expression of tissue specific genes in inductive cultures and osteogenic gene expression in non-inductive cultures are both important for the future translation of tissue engineered technologies. As hydrodynamic loading is ubiquitous in protocols requiring convective transport, these findings will be key for developing bioprocesses which reduce waste, minimize media supplementation costs, and achieve consistent results necessary to meet the quality standards for commercial success.

Finally, achieving functional tissue constructs will require recapitulating and controlling their spatial complexity. Our studies in Chapter 5 represent one approach towards this end. By differentially loading our microfluidic constructs both physically and chemically, I was able to modulate matrix composition in a spatially defined manner from a single progenitor

cell type. As alluded to in Chapter 6, there are a myriad of other mechanisms by which the differentiation efficiency of MSCs can be positively influenced. Achieving further increases in functional properties of osteochondral tissue constructs, or any other spatially complex tissue, such that they adequately replicate those of the native tissue will require expansion of the insights gained through this work regarding the tightly controlled presentation of inductive clues and the further development of enabling technologies in additive manufacturing and biomaterial science necessary to achieve such goals.

APPENDIX A: MASS TRANSPORT PROPERTIES OF AGAROSE

A.1.1.1. Literature Review of Solute Diffusion Coefficients in Agarose

When developing an immobilized cell system, such as the agarose based tissue constructs utilized in this dissertation, it is important to understand the transport properties of the scaffolding material for the types of solutes intended to interact with the cells contained within. In the studies described in this dissertation, the primary solutes of interest are glucose, bone morphogenic protein 2 (MW= 16 kDA), and transforming growth factor beta 3 (MW=25kDA). Therefore, we review herein the literature describing the experimentally determined diffusion coefficients of a range of biomolecules within tissue engineered constructs which might approximate the transport characteristics of our system.

Table A.1: Solute Diffusivities in Cell-Free Agarose Systems

Matrix	Solute	Molecular Mass (kDa)	Diffusion Coefficient [cm2/s]	Source
2.9% Agarose	Glucose	0.18	6.70E-06	Mignot 1990
2.0% Agarose	Dextran (10kDa)	10	8.50E-07	Albro 2009
2.0% Agarose	Lactalbumin	14.2	1.14E-06	Saltzman 1994
2.0% Agarose	Ovalbumin	45	7.80E-07	Saltzman 1994
2.0% Agarose	BSA	66.5	6.40E-07	Saltzman 1994
2.0% Agarose	Dextran (70kDa)	70	2.60E-07	Albro 2009

Table A.2: **Solute Diffusivities in Cell-Seeded Agarose Systems**

Matrix	Seeding Density [millions/mL]	Days in Culture	Culture Media	Solute	Molecular Mass (kDa)	Diffusion Coefficient [cm2/s]	Source
2% Agarose	10	1	Control	Dextran (3kDa)	3	1.35E-05	Leddy 2004
				Dextran (40kDa)	40	4.52E-06	
				Dextran (70kDa)	70	1.49E-06	
				Dextran (500kDa)	500	3.90E-07	
			Chondrogenic	Dextran (3kDa)	3	9.45E-06	
				Dextran (40kDa)	40	5.55E-06	
				Dextran (70kDa)	70	4.04E-06	
				Dextran (500kDa)	500	8.10E-07	
		28	Control	Dextran (3kDa)	3	1.16E-05	
				Dextran (40kDa)	40	2.41E-06	
				Dextran (70kDa)	70	1.25E-06	
				Dextran (500kDa)	500	4.90E-07	
			Chondrogenic	Dextran (3kDa)	3	9.10E-06	
				Dextran (40kDa)	40	2.59E-06	
				Dextran (70kDa)	70	2.09E-06	
				Dextran (500kDa)	500	5.20E-07	

Table A.3: **Solute Diffusivities in Articular Cartilage**

Matrix	Solute	Molecular Mass (kDa)	Diffusion Coefficient [cm2/s]	Source
Articular Cartilage	Dextran (3kDa)	3	7.80E-07	Leddy 2004
	Dextran (40kDa)	40	5.80E-07	
	Dextran (70kDa)	70	3.50E-07	
	Dextran (500kDa)	500	6.00E-08	

As is evident in **Tables A.1-A.3** above, the diffusivity of solutes in both agarose based tissue construct and articular cartilage tends to decrease with solute molecular mass and the presence of cells and extracellular matrix. Also based on the studies in cell-free agarose, there does not appear to be a considerable difference in diffusivity between linear and globular macromolecules. As TGF-β3 (25 kDa) is the largest molecule studied herein, it represents the case for which the static constructs will most slowly reach equilibrium with the surrounding culture media. Based on the studies referenced in the tables above, the diffusivities of BMP-2 and TGF-β3 in the 2.5% agarose gels utilized in this dissertation are likely between 10^{-5} and 10^{-7} cm^2/s. Perhaps the most relevant values are provided in **Table A.2** for the MSC seeded agarose systems under chondrogenic cultures. The data from these specific cultures were fit to a power law relationship of the form $y=Ax^{-B}$ with diffusivity on the y-axis and molecular mass on the x-axis to provide a best estimate for the diffusivities of BMP-2 and TGF-β3 of 4.3e-6 cm^2/s and 3.4e-6 cm^2/s respectively. Incorporating these values into the solution for the time constant of 1-D diffusion into a semi-infinite body (**Equation A.1)** along with the characteristic length of diffusion in our constructs (L=425 μm) provides estimated diffusion constants of 1.8 and 2.2 minutes for BMP-2 and TGF-β3, respectively.

$$\tau_{diffusion} = \frac{L^2}{4D} \tag{A.1}$$

Provided that changes in gene expression were measured on a weekly basis, or approximately 4500 times longer than the time required for the solutes to reach equilibrium in the static cultures, it is likely that the changes in gene expression measured in Specific Aim II are in fact the result of constant hydrodynamic loading through culture and not due to convective transport.

A.1.1.2. Experimental Validation of Modeling Parameters

A.1.1.2.1. Theoretical Basis

For the system described herein, the microfluidic channel spacing was designed for the conservative case of interstitial transport via diffusion alone. I assume, however, that the effect of fluid shear stress at the nominal boundary of the microfluidic channel is 'felt' by the cells encapsulated within the hydrogel scaffolding. To validate this assumption, the concentration of a fluorescent tracer within was monitored using a microscope and image grabber for a period of time. The intensity of the resulting images was averaged across the height of the region of interest and fit an analytical solution of the 1-D advection diffusion equation (Equation A1).

$$\frac{\partial C}{\partial t} + u\frac{\partial C}{\partial x} = D_x\frac{\partial^2 C}{\partial x^2} \tag{A1}$$

To match the experimental conditions, the initial condition of zero concentration everywhere is applied:

$$C(x,0) = 0$$

After time t=0, the concentration at x=0 is set to a constant concentration (C_0) equal to the concentration in the source fluid. Given these conditions, the solution for x>0 is given (Equation A2):

$$C(x,t) = \frac{C_0}{2}\left[erfc\left(\frac{x-ut}{\sqrt{4D_x t}}\right) + erfc\left(\frac{x+ut}{\sqrt{4D_x t}}\right)\exp\left(\frac{ux}{D_x}\right)\right] \tag{A2}$$

Using this solution, we are able to determine an effective diffusivity for two separate experimental conditions: static (diffusion-only) and dynamic (Poiseuille flow in the microchannel). When compared to each other the experimental value for the effective diffusivity under dynamic conditions should be lower than the static condition due to the presence of convective transport. If the experimentally determined diffusivity is entered

as a constant in Equation 2 when evaluating the images for the dynamic experiments, it is possible to determine a pore-level velocity for each discrete value of x. Using these values and a simple open pore hydrodynamic model, we can estimate the pore-level fluid shear stress magnitude experienced by the encapsulated cells.

A.1.1.2.2. Experimental Setup

To experimentally determine the validity of our assumptions regarding mass transport and fluid flow within the agarose based constructs utilized in this dissertation, a FITC labeled 70 kDa dextran was introduced at a concentration of X mg/mL into a single microfluidic channel of 425 µm x 425 µm square cross section sealed against a microscope slide. Upon introduction of the tracer into the , a series of images was captured once every minute for a period of one hour using an inverted microscope and a CoolSNAP HQ2 CCD camera (Photometrics, Tucson, AZ). Images were then analyzed for fluorescence intensity as a function of distance from the edge of the microchannel and time using a custom algorithm implemented in MATLAB.

A.1.1.2.3. Image Processing Algorithm

The Image Processing Algorithm utilized in this analysis is summarized in the flow chart presented in Figure A.1 below:

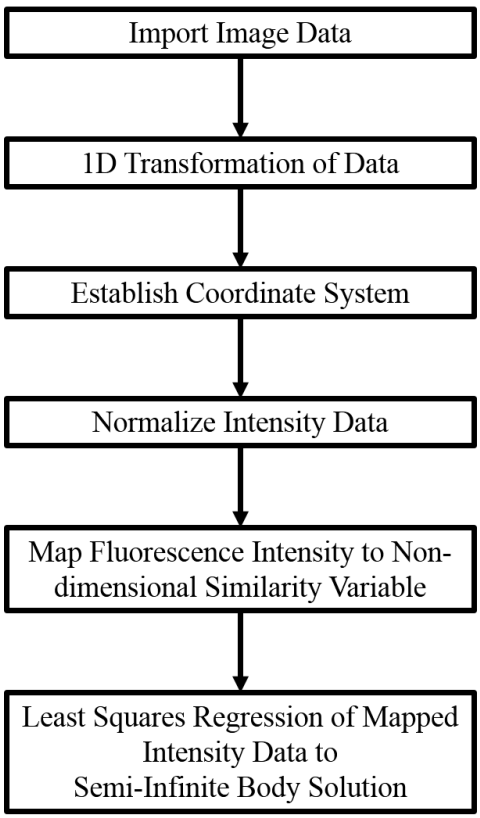

Figure A.1: Image Processing Algorithm for Mass Transport Measurements

To reduce the complexity of the analysis, the experimental system was intended to mimic one dimension transport into a semi-infinite planar body. To transform the two dimensional nature of the experimental system, each image was first imported into the MATLAB workspace as an M x N matrix of intensity values representing each pixel. The intensity data was then passed through an averaging process in which the column values were averaged to produce a 1 x N vector representing the one-dimensional transport for each frame of the time series. Once each frame was reduced to a 1xN vector, the data from the first frame captured after introduction of the tracer was placed through a thresholding process to establish the edge of the channel as the origin of a one-dimensional coordinate system based on prior calibration of the microscope objective. Intensity Values were then normalized to the average fluorescence intensity within the microchannel, and mapped to

a similarity variable of the form $\eta = x/2\sqrt{t}$ where x is the distance from the edge of the microchannel and t is the time elapsed between introduction of the tracer and the time of image capture. A least squares regression of the mapped intensity values were fit to the solution for one-dimensional mass transport into a semi-infinite planar body (Equation A2). As the velocity and diffusivity values are yet determined, the diffusion only (u=0) studies were fit to determine an estimate of the diffusivity. The dynamic studies were then analyzed using regression analysis to receive an estimate of the interstitial flow velocity.

A.1.1.2.4. Results

Model constructs were filled with 50 ng/mL of 70kDA FITC-labeled dextran, and filmed either under perfusion or hydrostatically. A truncated time series of the tracer is illustrated in Figure A.2 below:

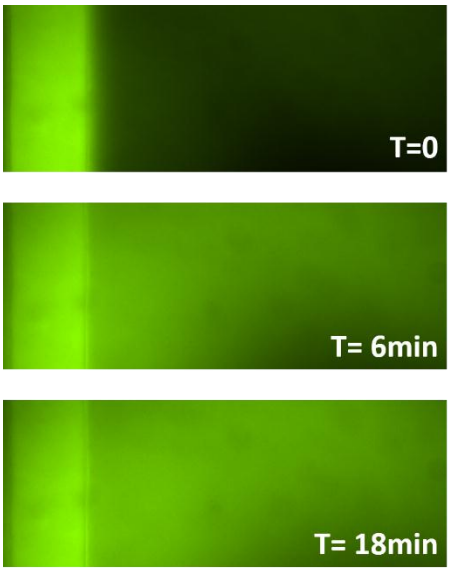

Figure A.2: Sample Time Series of Dispersion Measurements

Dispersion of the tracer was analyzed as described above, and the dispersion coefficients, determined as the average of three separately prepared measurements are given in Figure A.3 below:

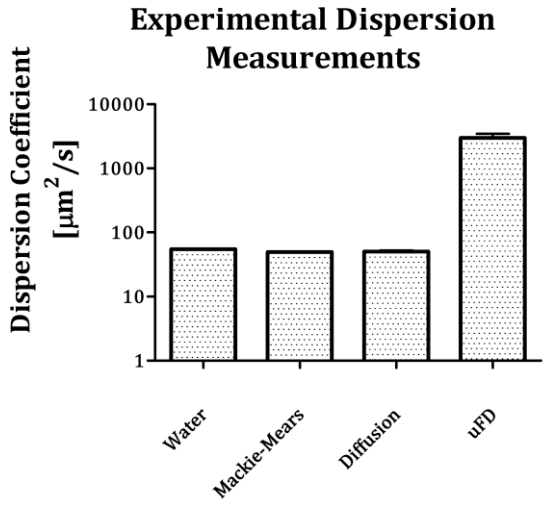

Figure A.3: Experimentally Determined Dispersion Coefficients

Prominent finding from these studies include the observation that our diffusion measurements are in close agreement with the value predicted by the Mackie-Mears relationship, and that the presence of flow in the microchannel increases the dispersion of our tracer solution by two orders of magnitude, indicating the presence of convective transport within the porous medium of the agarose construct.

A.1.1.2.5. Discussion

Dispersivity is a parameter that characterizes the dispersion of solutes due to convective transport in porous media. Factors which influence dispersivity in include the size of the solute, the porosity of the material, temperature, tortuosity of the porous network, and the viscosity of the fluid. As the viscosity, solute size, and temperature were all unchanged in our experiments, we seek a relationship between the dispersivity and the physical properties of the porous media to obtain an estimate of the average pore-level velocity in our system. The dispersion coefficient is related to the effective diffusivity as follows (Equation A.4), where E is the dispersion coefficient, D_{eff} is the effective diffusivity, ς is the dispersivity, and u is the pore-level velocity.

$$E = D_{eff} + \varsigma u \tag{A.4}$$

If we our choice of channel spacing as a characteristic value of the dispersivity in agarose gels, the estimated average pore-level velocity for our system is 14 μm/s (0.3% of average channel velocity), which is in line with measurements from other laboratories (Chen et al. 2012) and estimates of interstitial flow velocities in articular cartilage in vivo (Mow et al. 1980), and seems reasonable even if our estimate of dispersivity was off by an order of magnitude in either direction.

APPENDIX B: BIOCHEMICAL PROTOCOLS

PAPAIN DIGESTION

Reagent

1) 35mg Cysteine
2) 20ml PBE
3) 0.lml Papain enzyme

Procedure

1) Add 35mg cysteine in 20ml PBE
2) Filter sterilization
3) Add 0.lml papain enzyme
4) Place 1ml of solution into each Eppendorf tube
5) Place in 60°C water bath for 17 hours
6) Store at -20°C (short term ~ 1 year) or -70°C (long term)

PICOGREEN DNA ASSAY

Reagents

1) Dilute 20X tris-EDTA solution to 1X with deionized water.
2) PicoGreen working solution
    a. Mix 100 µL of PicoGreen stock solution with 19.9 mL of diluted tris-EDTA buffer.
    b. Protect working solution from light using aluminum foil.
    c. The solution is stable for 1 day.
3) DNA working standards
    a. Dilute 30 µL of Lambda DNA standard with 1.47 mL of diluted tris-EDTA buffer (DNA stock solution: 2 µg/mL).
    b. Prepare the working standards based on the table below:

DNA stock volume (µL)	Diluted tris-EDTA volume (µL)	Final concentration (µg/mL)
1000	0	2
500	500	1
300	700	0.6
100	900	0.2
10	990	0.02
1	999	0.002
0	1000	0

Procedure

7) Dilute samples and controls with diluted tris-EDTA buffer (dilution factor = 1:60 ~ 1:120).
8) Add 100 µL of working standards, diluted samples and controls to each well of a 96-well plate in duplicate.
9) Add 100 µL of PicoGreen working solution to each well.
10) Incubate the plate in the dark at room temperature for 5 minutes.
11) Read the plate using a fluorescence plate reader with an excitation wavelength of 480 nm and an emission wavelength of 520 nm.

DMMB BLUE ASSAY

Reagents

1) DMMB dye solution
    a. Add 16 mg of DMMB to 5 mL of 100% ethanol and mix the solution for at least 12 hours until the DMMB is fully dissolved.
    b. Mix the dissolved DMMB solution with 950 mL of deionized water, 8.7 mL of 1 N hydrogen chloride, 3.04 g of glycine and 2.367 g of sodium chloride.
    c. Adjust pH to 3.0 using 1 N hydrogen chloride or sodium hydroxide.
    d. Thoroughly mix using a stir bar.
    e. Measure the absorbance of the DMMB dye solution using a spectrophotometer.
        i. $0.30 < A_{525} < 0.34$
        ii. $1.25 < A_{592} < 1.33$
            1. If the readings are too high, dilute the dye solution with deionized water.
            2. If the readings are too low, add one grain of DMMB to the dye solution and stir it for 12 hours.
            3. Re-measure the absorbance.
    f. Store in the dark for up to 3 months.

2) PBS-EDTA-cysteine solution
    a. Dissolve 0.372 g of EDTA and 0.175 g of cysteine in 100 mL of PBS.
    b. The solution is stable for 1 day.
3) Chondroitin sulfate working standards
    a. Dissolve 50 mg of chondroitin sulfate in 10 mL of PBS-EDTA-cysteine solution (chondroitin sulfate solution: 5 mg/mL).

b. Mix 2 mL of chondroitin sulfate solution with 48 mL of PBS-EDTA-cysteine solution (chondroitin sulfate stock solution: 200 μg/mL).

c. Prepare the working standards based on the table below (Table A.2).

Chondroitin sulfate stock volume (μL)	PBS volume (μL)	Final concentration (μg/mL)
0	1000	0
125	875	25
250	750	50
375	625	75
500	500	100
625	375	125
750	250	150
875	125	175
1000	0	200

Procedure

1) Dilute samples and controls with PBS (dilution factor = 1:15 ~ 1:50).
2) Add 8 μL of working standards, diluted samples and controls to each well of a 96-well plate in duplicate.
3) Add 200 μL of DMMB dye solution to each well.
4) Incubate the plate at room temperature for 2 minutes.
5) Read the plate using a spectrophotometer at 525 nm.
6) Assume a ratio of chondroitin sulfate to glycosaminoglycan of 1:1.

HYDROXYPROLINE ASSAY

Reagents

1) Assay stock buffer
    a. Dissolve 25.217 g of monohydrate citric acid and 60 g of sodium acetate trihydrate in 423.17 mL of deionized water.
    b. Add 6 mL of acetic acid, 70.83 mL of 6 N sodium hydroxide and 5 drops of toluene to the solution.
2) Assay working buffer
    a. Mix 10 mL of deionized water, 15 mL of isopropanol and 50 mL of assay stock buffer together.
    b. Adjust pH to 6.0 using 1 N hydrogen chloride or sodium hydroxide.
    c. Store at room temperature for up to several months.
3) Chloramine-T solution
    a. Mix 2 mL of deionized water, 2 mL of isopropanol and 16 mL of assay working buffer together.
    b. Dissolve 0.282 g of Chloramine-T in the mixture.
    c. Store in the dark at 4˚C for up to 1week.
4) pDAB solution
    a. Dissolve 3 g of pDAB in 12 mL of isopropanol.
    b. Add 5.2 mL of 60% perchloric acid slowly.
    c. Add 2.8 mL of n-propanol to the mixture.
    d. The solution is stable for 1 day.
5) Hydroxyproline working standards
    a. Dissolve 10 mg of hydroxyproline in 100 mL of deionized water (hydroxyproline stock solution: 100 μg/mL).
    b. Prepare the working standards based on the table below:

Hydroxyproline stock volume (µL)	Deionized water volume (µL)	Final concentration (µg/mL)
0	1000	0
100	900	10
200	800	20
300	700	30
400	600	40
500	500	50
600	400	60
700	300	70
800	200	80
900	100	90
1000	0	100

Procedure

1) Take 120 µL of working standards, samples and controls and place them in glass test tubes.
2) Add 120 µL of 12 N hydrogen chloride to each tube and vortex.
3) Cover the tubes with marbles and incubate them at 100˚C for 3 hours, followed by an 18-hour incubation at 95˚C using an oven in a fume hood.
4) Cool samples at room temperature.
5) Re-suspend the dried standards, samples and controls in 1 mL of deionized water and vortex.
6) Dilute samples and controls with deionized water (dilution factor = 1:2 ~ 1:10).
7) Add 50 µL of standards and diluted samples and controls to each well of a 96-well plate in duplicate.
8) Add 50 µL of chloramine-T solution to each well and incubate the plate in the dark at room temperature for 20 minutes.
9) Add 50 µL of pDAB solution to each well and incubate the plate in water bath at 60˚C for 30 minutes.
10) Cool the plate at room temperature for 15 minutes.
11) Read the plate using a spectrophotometer at 550 nm.
12) Assume a ratio of hydroxyproline to total collagen of 1:10.

COLLAGEN I ELISA

(*ADAPTED FROM CHONDREX, INC.)*

Reagents

1) Type II Collagen Standard 1 vial 100 µl, 100 µg/ml -20°C
2) Capture Antibody 1 vial 100 µl, 5 mg/ml -20°C
3) Detection Antibody 1 vial Lyophilized -20°C
4) Solution A - Capture Antibody Dilution Buffer 1 bottle 10 ml -20°C
5) Solution B - Sample/Standard Dilution Buffer 1 bottle 50 ml -20°C
6) Solution C - Detection Antibody Dilution Buffer 1 bottle 10 ml -20°C
7) Solution D - Streptavidin Peroxidase Dilution Buffer 1 bottle 20 ml -20°C
8) Streptavidin Peroxidase 2 vials 50 □l -20°C
9) OPD 2 vials Lyophilized -20°C
10) Chromagen Dilution Buffer 1 bottle 20 ml -20°C
11) Stop Solution - 2N Sulfuric Acid 1 bottle 10 ml -20°C
12) Wash Buffer, 20X 1 bottle 50 ml -20°C
13) ELISA Plate 1 each 96-well (8-well strips x 12) -20°C

Procedure

1) Add Capture Antibody: Dilute one vial of Capture Antibody with 10 ml of Capture Antibody Dilution Buffer (Solution A). Add 100 ml of capture antibody solution to each well and incubate at 4°C overnight.
2) 2. Dilute Wash Buffer: Dilute 50 ml of 20X wash buffer in 950 ml of distilled water (1X wash buffer). Wash the plate with 1X wash buffer at least 3 times using a wash bottle with manifold or an automated plate washer. Empty the plate by inverting it and blot on a paper towel to remove excess liquid. Do not allow the plate to dry out.
3) Prepare Standard Dilutions: The recommended standard range is 3.125-200 ng/ml. Prepare serial dilutions of the standard by mixing 20 ml of 100 mg/ml standard with 980 ml of Sample/Standard Dilution Buffer (Solution B) - 2000 ng/ml. Then mix 100 ml of the 2000 ng/ml standard with 900 ml of Solution B - 200 ng/ml. Then mix 250 ml of the 200 ng/ml standard with 250 ml of Solution B - 100 ng/ml. Then repeat this procedure to make five more serial dilutions of standard - 50, 25, 12.5, 6.25, and 3.125 ng/ml solutions. The 100 mg/ml standard stock may be stored at -20°C for use in a second assay. We recommend making fresh serial dilutions for each assay.
4) Prepare Sample Dilutions: Dilute tissue samples 1:1-1:1000 with Solution B depending on the estimated collagen content in the samples. Cell samples can

be used without further dilution. However, if it is necessary, dilute cell samples 1:1-1:100 with Solution B.

5) Add Standards and Samples: Mix samples and standard tubes well. Add 100 ml of Solution B (blank), standards and samples to appropriate wells. Incubate at room temperature for 2 hours.

6) Wash: Wash the plate with 1X wash buffer at least 3 times using a wash bottle with manifold or an automated plate washer. Empty the plate by inverting it and blot on a paper towel to remove excess liquid. Do not allow the plate to dry out.

7) Add Detection Antibody: Dissolve one vial of Detection Antibody in 10 ml of Detection Antibody Dilution Buffer (Solution C). Add 100 ml of detection antibody solution to each well and incubate at room temperature for 2 hours.

8) Wash: Wash the plate with 1X wash buffer at least 3 times using a wash bottle with manifold or an automated plate washer. Empty the plate by inverting it and blot on a paper towel to remove excess liquid. Do not allow the plate to dry out.

9) Add Streptavidin Peroxidase: Dilute one vial of Streptavidin Peroxidase in 10 ml of Streptavidin Peroxidase Dilution Buffer (Solution D). Add 100 ml of streptavidin peroxidase solution to each well and incubate at room temperature for 1 hour.

10) Wash: Wash the plate with 1X wash buffer at least 3 times using a wash bottle with manifold or an automated plate washer. Empty the plate by inverting it and blot on a paper towel to remove excess liquid. Do not allow the plate to dry out.

11) OPD: Dissolve one vial of OPD in 10 ml of OPD Dilution Buffer just prior to use. Add 100 ml of OPD solution to each well immediately after washing the plate. Incubate for 30 minutes at room temperature.

12) Stop: Add 50 ml of 2N sulfuric acid (Stop Solution) to each well.

13) Read Plate: Read the OD values at 490 nm. If the OD values of samples are greater than the OD values of the highest standard, re-assay the samples at a higher dilution. A 630 nm filter can be used as a reference.

APPENDIX C: HISTOLOGY & IMMUNOHISTOCHEMISTRY

SAFRANIN-O AND FAST GREEN STAINING

Procedure

Protocol Step	Reagent	Time (min : sec)
1	Distilled water	01 : 00
2	Weigert's hematoxylin working solution	02 : 00
3	Distilled water	05 : 00
4	0.2% aqueous fast green	01 : 00
5	1% acetic acid	00 : 03
6	0.5% safranin-O	05 : 00
7	95% alcohol	01 : 00
8	100% alcohol	01 : 00
9	100% alcohol	01 : 00
10	100% alcohol	01 : 00
11	Xylene substitute	01 : 00
12	Xylene substitute	01 : 00
13	Xylene	01 : 00

Results

GAG, nuclei and cytoplasm are stained pink/red, black and green, respectively.

IMMUNOFLUORESCENCE

Reagent Preparation

1) 1. Sodium citrate solution
    a. Dissolve 2.94 g of sodium citrate in 1 L of deionized water.
    b. Adjust pH to 6.0 using 1 N hydrogen chloride or sodium hydroxide.
    c. Add 500 µL of 20X PBS/Tween-20 solution.
    d. Store at room temperature for 3 months or at 4˚C for longer storage.
2) Blocking buffer
    a. Mix 150 µL of (goat) serum with 10 mL of PBS.
3) Diluted primary and secondary antibodies
    a. Mix primary antibodies with blocking buffer at a desired ratio.

Deparaffinization/Rehydration:

1) Wash three times in xylene for 5 min each.
2) Wash two times in 100% ethanol for 10 min each.
3) Wash two times in 95% ethanol for 10 min each.
4) Rinse sections two times in dH2O for 5 min each.

Antigen Retrieval

1) Bring slides to a boil in 10 mM sodium citrate buffer pH 6.0, then maintain at a sub-boiling temperature for 10 min. Cool slides on bench top for 30 min.

Staining Procedure

1) Block specimen in blocking buffer for 60 min.
2) While blocking, prepare primary antibody by diluting in blocking buffer to desired concentration
3) Aspirate blocking solution, apply diluted primary antibody.
4) Incubate overnight at 4°C.
5) Rinse three times in 1X PBS for 5 min each.
6) Incubate specimen in fluorochrome-conjugated secondary antibody diluted in antibody dilution buffer for 1–2 hr at room temperature in the dark.
7) Rinse three times in 1X PBS for 5 min each.
8) Coverslip slides with DAPI doped mountant.
9) For best results, allow mountant to cure overnight at room temperature. For long-term storage, store slides flat at 4°C protected from light.

APPENDIX D: QUANTITATIVE RT-PCR PROTOCOLS

RNA ISOLATION

Reagents

1) TRIzol® Reagent and PureLink™ RNA Mini Kit (included)
2) • Chloroform or 4–Bromoanisole
3) • 96-100% ethanol and 70% ethanol (in RNase-free water)

Procedure

1) Homogenize tissue samples in 1 ml TRIzol® Reagent per 50 – 100 mg tissue using a tissue homogenizer or rotor-stator. The sample volume should not exceed 10% of the volume of TRIzol® Reagent used for homogenization.
2) Phase Separation
    a. Incubate the lysate with TRIzol® Reagent (previous page) at room temperature for 5 minutes to allow complete dissociation of nucleoprotein complexes.
    b. Add 0.2 ml chloroform or 50 μl 4 – Bromoanisole per 1 ml TRIzol® Reagent used. Shake the tube vigorously by hand for 15 seconds**.**
    c. Incubate at room temperature for 2 – 3 minutes.
    d. Centrifuge the sample at 12,000 × g for 15 minutes at 4°C.
    e. Transfer ~400 μl of the colorless, upper phase containing the RNA to a fresh RNase – free tube.
    f. Add an equal volume of 70% ethanol to obtain a final ethanol concentration of 35%. Mix well by vortexing.
    g. Invert the tube to disperse any visible precipitate that may form after adding ethanol.
3) Binding, Washing and Elution

RNA QUANTIFICATION

Reagents and Supplies

1) Purified RNA
2) RNase, DNase-free water
3) Corning half area UV 96-well plates (VWR 33501-012)

Protocol

1) In each well of the UV plate, add 5 µL of purified RNA and 170 µL of water such that the dilution factor (D) is 35.
2) Add 175 µL of water to additional wells as the negative control (or blank).
3) Take absorbance readings at 260-nm, 280-nm and 320-nm lights.
4) Purity of isolated RNA can be calculated using the following equation: (the value should be between 1.5 and 2.0)

$$Purity = \frac{A_{260} - A_{320}}{A_{280} - A_{320}}$$

5) Quantity of RNA can be calculated using the Beer's Law with 1-cm pathlength of light:

$$ug\ RNA = \{average\ sample(A_{260}) - average\ blank(A_{260})\} \times 40 \times D \times \{volume\ in\ uL\}/1000$$

REVERSE TRANSCRIPTION

Reagents and Supplies

1) Purified RNA
2) QuantiTect Rev. Transcription Kit – 200 reactions (Qiagen 205313, -20°C)

Protocol

1) Thaw purified RNA and the RT kit on ice.
2) Mix each solution and centrifuge briefly to collect residual liquid from the sides of the tubes, and store on ice.
3) Prepare the genomic DNA (gDNA) elimination reaction on ice based on the following table:

Component	Volume / reaction (tube)	Final concentration
gDNA wipeout Buffer, 7X	2 µL	1X
RNA	Variable (1 ng – 1 µg)	
RNase-free water	Variable	
Total	14 µL	

4) Incubate the mixture at 42°C for 2 min and place immediately on ice.
5) Prepare the RT master mix on ice according to the following table:

Component	Volume / reaction (tube)	Final concentration
Reverse transcriptase	1 µL	
RT Buffer, 5X	4 µL	1X
RT primer mix	1 µL	
Total	6 µL	

6) Add 6 µL of RT mix to each of 14 µL of gDNA elimination tube from step 3 and result in a volume of 20 µL in total.
7) Mix and store on ice.
8) Incubate the mixture at 42°C for 15 min followed by 3 min of incubation at 95°C to inactivate the reverse transcriptase.
9) Store cDNA samples at -80°C.

POLYMERASE CHAIN REACTION

1) Thaw cDNA, primers and the SYBR Green kit on ice.
2) Mix each solution and centrifuge briefly to collect residual liquid from the sides of the tubes, and store on ice
3) Prepare PCR master mix on ice based on the following table:

Component	Volume/Reaction (well)	Final Concentration
SYBR Green, 2X	10 µL	1X
RNase-free water	3 µL	
10 µM forward primer	2 µL	1 µM
10 µM reverse primer	2 µL	1 µM
Total	18 µL	

4) Load 2 µL of cDNA or water (blank, negative control) into each well and add 18 µL of PCR master mix to each well and mix by pipetting up and down. (Total Volume= 20 µL)
5) Cover the plate with optical film and proceed to thermocycler.

LINREQ PCR PROTOCOL

1) Export the uncorrected amplification data from the thermocycler to Excel
2) Read data into LinReg-PCR:
    a. Select Step-One Plus (ABI) and DNA binding dye (SYBR Green).
    b. Select the columns and rows which hold the amplification data.
3) Setup Analysis for single stranded cDNA data with no baseline correction
4) Run baseline determination analysis
5) Check each sample to examine efficiencies and exclude poorly amplified samples as necessary
6) Set the log (fluorescence) threshold value on the left.
    a. Note: Make sure to keep this consistent between all plates with the same gene.
    b. Note: In StepOne, the threshold fluorescence is usually less than 1, which is why the log (fluorescence) value in LinRegPCR is negative.
7) Save this data to Excel.
8) Organize and perform Data Reduction in Excel
    a. Use geometric means when averaging data. (Taking the geometric mean is the same as taking the arithmetic mean of the cycle thresholds.)
9) Calculate the starting gene concentration, N0, based on each individual well's PCR efficiency:

$$N_0^* = \frac{\text{fluorescence threshold value}}{\text{Eff}^{C_q}}.$$

10) Calculate a manual ΔΔ method; that is, divide a sample's gene's starting concentration by the sample's housekeeping gene concentration, then divide by the geometric mean of your negative control.
11) Perform statistical analysis on the negative control normalized values.

REFERENCES

Albro MB, Chahine NO, Li R, Yeager K, Hung CT, Ateshian GA. 2008. Dynamic loading of deformable porous media can induce active solute transport. Journal of biomechanics 41(15):3152-3157.

Alhadlaq A, Elisseeff JH, Hong L, Williams CG, Caplan AI, Sharma B, Kopher RA, Tomkoria S, Lennon DP, Lopez A and others. 2004. Adult stem cell driven genesis of human-shaped articular condyle. Ann Biomed Eng 32(7):911-23.

Annabi N, Nichol JW, Zhong X, Ji C, Koshy S, Khademhosseini A, Dehghani F. 2010. Controlling the porosity and microarchitecture of hydrogels for tissue engineering. Tissue Eng Part B Rev 16(4):371-83.

Ateshian GA, Soslowsky LJ, Mow VC. 1991. Quantitation of articular surface topography and cartilage thickness in knee joints using stereophotogrammetry. Journal of Biomechanics 24(8):761-776.

Bal BS, Rahaman MN, Jayabalan P, Kuroki K, Cockrell MK, Yao JQ, Cook JL. 2010. In vivo outcomes of tissue-engineered osteochondral grafts. Journal of biomedical materials research. Part B, Applied biomaterials 93(1):164-74.

Bancroft GN, Sikavitsas VI, van den Dolder J, Sheffield TL, Ambrose CG, Jansen JA, Mikos AG. 2002. Fluid flow increases mineralized matrix deposition in 3D perfusion culture of marrow stromal osteoblasts in a dose-dependent manner. Proc Natl Acad Sci U S A 99(20):12600-5.

Bettinger CJ, Borenstein JT. 2010. Biomaterials-based microfluidics for engineered tissue constructs. Soft Matter 6(20):4999-5015.

Bettinger CJ, Weinberg EJ, Kulig KM, Vacanti JP, Wang Y, Borenstein JT, Langer R. 2005. Three-Dimensional Microfluidic Tissue-Engineering Scaffolds Using a Flexible Biodegradable Polymer. Advanced materials (Deerfield Beach, Fla.) 18(2):165-169.

Bi L, Li D, Liu J, Hu Y, Yang P, Yang B, Yuan Z. 2011. Fabrication and characterization of a biphasic scaffold for osteochondral tissue engineering. Materials Letters 65(13):2079-2082.

Bilgen B, Chang-Mateu IM, Barabino GA. 2005. Characterization of mixing in a novel wavy-walled bioreactor for tissue engineering. Biotechnology and Bioengineering 92(7):907-919.

Bilgen B, Sucosky P, Neitzel GP, Barabino GA. 2006. Flow characterization of a wavy-walled bioreactor for cartilage tissue engineering. Biotechnology and Bioengineering 95(6):1009-1022.

Biltz RM, Pellegrino ED. 1969. The chemical anatomy of bone. I. A comparative study of bone composition in sixteen vertebrates. Journal of Bone and Joint Surgery - Series A 51(3):456-466.

Boland T, Tao X, Damon BJ, Manley B, Kesari P, Jalota S, Bhaduri S. 2007. Drop-on-demand printing of cells and materials for designer tissue constructs. Materials Science and Engineering: C 27(3):372-376.

Borenstein JT, Megley K, Wall K, Pritchard EM, Truong D, Kaplan DL, Tao SL, Herman IM. 2010. Tissue Equivalents Based on Cell-Seeded Biodegradable Microfluidic Constructs. Materials 3(3):1833-1844.

Boschetti F, Cioffi M, Raimondi MT, Migliavacca F, Dubini G. 2005. NEW TRENDS IN TISSUE ENGINEERED CARTILAGE:: MICROFLUID DYNAMICS IN 3-D ENGINEERED CELL SYSTEMS. Journal of Mechanics in Medicine & Biology: World Scientific Publishing Company. p 455-464.

Bosnakovski D, Mizuno M, Kim G, Ishiguro T, Okumura M, Iwanaga T, Kadosawa T, Fujinaga T. 2004. Chondrogenic differentiation of bovine bone marrow mesenchymal stem cells in pellet cultural system. Experimental Hematology 32(5):502-509.

Brittberg M, Lindahl A, Nilsson A, Ohlsson C, Isaksson O, Peterson L. 1994. Treatment of Deep Cartilage Defects in the Knee with Autologous Chondrocyte Transplantation. New England Journal of Medicine 331(14):889-895.

Bruder SP, Jaiswal N, Haynesworth SE. 1997. Growth kinetics, self-renewal, and the osteogenic potential of purified human mesenchymal stem cells during extensive subcultivation and following cryopreservation. Journal of Cellular Biochemistry 64(2):278-294.

Buckley CT, Thorpe SD, Kelly DJ. 2009. Engineering of large cartilaginous tissues through the use of microchanneled hydrogels and rotational culture. Tissue Eng Part A 15(11):3213-20.

Buckwalter JA. 1992. Mechanical Injuries of Articular Cartilage. The Iowa Orthopaedic Journal 12:50-57.

Buckwalter JA. 2002. Articular cartilage injuries. Clinical Orthopaedics and Related Research(402):21-37.

Buckwalter JA, Brown TD. 2004. Joint Injury, Repair, and Remodeling: Roles in Post-Traumatic Osteoarthritis. Clinical Orthopaedics and Related Research 423:7-16 10.1097/01.blo.0000131638.81519.de.

Buckwalter JA, Mankin H. 1998. Tissue Design and Chondrocyte-Matrix Interactions. AAOS Inst Course Lect 47:477-86.

Buckwalter JAMHJ. 1997. Instructional Course Lectures, The American Academy of Orthopaedic Surgeons - Articular Cartilage. Part I: Tissue Design and Chondrocyte-Matrix Interactions*†. The Journal of Bone & Joint Surgery 79(4):600-11.

Bueno EM, Bilgen B, Barabino GA. 2005. Wavy-walled bioreactor supports increased cell proliferation and matrix deposition in engineered cartilage constructs. Tissue Eng 11(11-12):1699-709.

Bueno EM, Bilgen B, Barabino GA. 2008. Hydrodynamic Parameters Modulate Biochemical, Histological, and Mechanical Properties of Engineered Cartilage. Tissue Engineering Part A 0(0).

Bursac PM, Freed LE, Biron RJ, Vunjak-Novakovic G. 1996. Mass transfer studies of tissue engineered cartilage. Tissue Engineering 2(2):141-50.

Buschmann M, Gluzband Y, Grodzinsky A, Hunziker E. 1995. Mechanical compression modulates matrix biosynthesis in chondrocyte/agarose culture. J Cell Sci 108(4):1497-1508.

Campbell JJ, Lee DA, Bader DL. 2006. Dynamic compressive strain influences chondrogenic gene expression in human mesenchymal stem cells. Biorheology 43(3):455-470.

Cao T, Ho KH, Teoh SH. 2003. Scaffold design and in vitro study of osteochondral coculture in a three-dimensional porous polycaprolactone scaffold fabricated by fused deposition modeling. Tissue Eng 9 Suppl 1:S103-12.

Caplan AI. 2005. Review: mesenchymal stem cells: cell-based reconstructive therapy in orthopedics. Tissue Eng 11(7-8):1198-211.

Chang CH, Lin FH, Lin CC, Chou CH, Liu HC. 2004. Cartilage tissue engineering on the surface of a novel gelatin-calcium-phosphate biphasic scaffold in a double-chamber bioreactor. J Biomed Mater Res B Appl Biomater 71(2):313-21.

Chen T, Buckley M, Cohen I, Bonassar L, Awad H. 2012. Insights into interstitial flow, shear stress, and mass transport effects on ECM heterogeneity in bioreactor-cultivated engineered cartilage hydrogels. Biomechanics and Modeling in Mechanobiology 11(5):689-702.

Cheng SL, Yang JW, Rifas L, Zhang SF, Avioli LV. 1994. Differentiation of human bone marrow osteogenic stromal cells in vitro: induction of the osteoblast phenotype by dexamethasone. Endocrinology 134(1):277-86.

Chisti Y. 2001. Hydrodynamic damage to animal cells. Crit Rev Biotechnol 21(2):67-110.

Choi NW, Cabodi M, Held B, Gleghorn JP, Bonassar LJ, Stroock AD. 2007a. Microfluidic scaffolds for tissue engineering. Nature Materials 6(11):908-915.

Choi NW, Cabodi M, Held B, Gleghorn JP, Bonassar LJ, Stroock AD. 2007b. Microfluidic scaffolds for tissue engineering. Nature materials 6(11):908-15.

Cinbiz MN, Tığlı RS, Beşkardeş IG, Gümüşderelioğlu M, Çolak Ü. 2010. Computational fluid dynamics modeling of momentum transport in rotating wall perfused bioreactor for cartilage tissue engineering. Journal of Biotechnology 150(3):389-395.

Cohen NP, Foster RJ, Mow VC. 1998. Composition and dynamics of articular cartilage: structure, function, and maintaining healthy state. J Orthop Sports Phys Ther 28(4):203-15.

Concaro S, Gustavson F, Gatenholm P. 2009. Bioreactors for Tissue Engineering of Cartilage. Bioreactor Systems for Tissue Engineering. p 125-143.

Cuchiara MP, Allen ACB, Chen TM, Miller JS, West JL. 2010. Multilayer microfluidic PEGDA hydrogels. Biomaterials 31(21):5491-5497.

Cui W, Wang Q, Chen G, Zhou S, Chang Q, Zuo Q, Ren K, Fan W. 2011. Repair of articular cartilage defects with tissue-engineered osteochondral composites in pigs. Journal of Bioscience and Bioengineering 111(4):493-500.

Darling EM, Athanasiou KA. 2003. Articular Cartilage Bioreactors and Bioprocesses. Tissue Engineering 9(1):9-26.

Darling EM, Athanasiou KA. 2005. Rapid phenotypic changes in passaged articular chondrocyte subpopulations. Journal of Orthopaedic Research 23(2):425-432.

Datta N, P. Pham Q, Sharma U, Sikavitsas VI, Jansen JA, Mikos AG. 2006. In vitro generated extracellular matrix and fluid shear stress synergistically enhance 3D osteoblastic differentiation. Proceedings of the National Academy of Sciences of the United States of America 103(8):2488-2493.

Davisson T, Sah RL, Ratcliffe A. 2002. Perfusion increases cell content and matrix synthesis in chondrocyte three-dimensional cultures. Tissue Engineering 8(5):807-816.

Devarapalli M, Lawrence BJ, Madihally SV. 2009. Modeling nutrient consumptions in large flow-through bioreactors for tissue engineering. Biotechnology and Bioengineering 103(5):1003-1015.

Dietmar W H. 2000. Scaffolds in tissue engineering bone and cartilage. Biomaterials 21(24):2529-2543.

Engler AJ, Sen S, Sweeney HL, Discher DE. 2006. Matrix Elasticity Directs Stem Cell Lineage Specification. Cell 126(4):677-689.

Farndale RW, Sayers CA, Barrett AJ. 1982. A direct spectrophotometric microassay for sulfated glycosaminoglycans in cartilage cultures. Connective tissue research 9(4):247-248.

Fritsch A, Hellmich C, Dormieux L. 2009. Ductile sliding between mineral crystals followed by rupture of collagen crosslinks: Experimentally supported micromechanical explanation of bone strength. Journal of Theoretical Biology 260(2):230-252.

Fritton SP, Weinbaum S. 2009. Fluid and Solute Transport in Bone: Flow-Induced Mechanotransduction. Annu Rev Fluid Mech 41:347-374.

Fukuda A, Kato K, Hasegawa M, Hirata H, Sudo A, Okazaki K, Tsuta K, Shikinami Y, Uchida A. 2005. Enhanced repair of large osteochondral defects using a combination of artificial cartilage and basic fibroblast growth factor. Biomaterials 26(20):4301-8.

Galban CJ, Locke BR. 1999. Analysis of cell growth kinetics and substrate diffusion in a polymer scaffold. Biotechnology and Bioengineering 65(2):121-132.

Gao J, Dennis JE, Solchaga LA, Awadallah AS, Goldberg VM, Caplan AI. 2001a. Tissue-engineered fabrication of an osteochondral composite graft using rat bone marrow-derived mesenchymal stem cells. Tissue Eng 7(4):363-71.

Gao J, Dennis JE, Solchaga La, Awadallah aS, Goldberg VM, Caplan aI. 2001b. Tissue-engineered fabrication of an osteochondral composite graft using rat bone marrow-derived mesenchymal stem cells. Tissue Engineering 7(4):363-71.

Gemmiti CV, Guldberg RE. 2006. Fluid flow increases type II collagen deposition and tensile mechanical properties in bioreactor-grown tissue-engineered cartilage. Tissue Eng 12(3):469-79.

Ghosh S, Viana JC, Reis RL, Mano JF. 2008. Bi-layered constructs based on poly(l-lactic acid) and starch for tissue engineering of osteochondral defects. Materials Science and Engineering: C 28(1):80-86.

Golden AP, Tien J. 2007. Fabrication of microfluidic hydrogels using molded gelatin as a sacrificial element. Lab on a Chip 7(6):720-725.

Grad S, Loparic M, Peter R, Stolz M, Aebi U, Alini M. 2012. Sliding motion modulates stiffness and friction coefficient at the surface of tissue engineered cartilage. Osteoarthritis Cartilage 20(4):288-95.

Grayson WL, Bhumiratana S, Cannizzaro C, Chao PH, Lennon DP, Caplan AI, Vunjak-Novakovic G. 2008. Effects of initial seeding density and fluid perfusion rate on formation of tissue-engineered bone. Tissue Eng Part A 14(11):1809-20.

Grellier M, Bareille R, Bourget C, Amedee J. 2009. Responsiveness of human bone marrow stromal cells to shear stress. J Tissue Eng Regen Med 3(4):302-9.

Guilak F, Cohen DM, Estes BT, Gimble JM, Liedtke W, Chen CS. 2009. Control of Stem Cell Fate by Physical Interactions with the Extracellular Matrix. Cell Stem Cell 5(1):17-26.

Haasper C, Zeichen J, Meister R, Krettek C, Jagodzinski M. 2008. Tissue engineering of osteochondral constructs in vitro using bioreactors. Injury 39(1, Supplement):66-76.

Hollister SJ, Maddox RD, Taboas JM. 2002. Optimal design and fabrication of scaffolds to mimic tissue properties and satisfy biological constraints. Biomaterials 23(20):4095-4103.

Huang AH, Farrell MJ, Kim M, Mauck RL. 2010. Long-term dynamic loading improves the mechanical properties of chondrogenic mesenchymal stem cell-laden hydrogel. Eur Cell Mater 19:72-85.

Huang AH, Stein A, Tuan RS, Mauck RL. 2009. Transient exposure to transforming growth factor beta 3 improves the mechanical properties of mesenchymal stem cell-laden cartilage constructs in a density-dependent manner. Tissue Eng Part A 15(11):3461-72.

Huang CYC, Hagar KL, Frost LE, Sun Y, Cheung HS. 2004. Effects of Cyclic Compressive Loading on Chondrogenesis of Rabbit Bone-Marrow Derived Mesenchymal Stem Cells. STEM CELLS 22(3):313-323.

Huang GY, Zhou LH, Zhang QC, Chen YM, Sun W, Xu F, Lu TJ. 2011. Microfluidic hydrogels for tissue engineering. Biofabrication 3(1):012001-012001.

Hui TY, Cheung KMC, Cheung WL, Chan D, Chan BP. 2008. In vitro chondrogenic differentiation of human mesenchymal stem cells in collagen microspheres: Influence of cell seeding density and collagen concentration. Biomaterials 29(22):3201-3212.

Huiskes R, Ruimerman R, van Lenthe GH, Janssen JD. 2000. Effects of mechanical forces on maintenance and adaptation of form in trabecular bone. Nature 405(6787):704-706.

Hung C. 2003. Anatomically shaped osteochondral constructs for articular cartilage repair. Journal of biomechanics 36(12):1853-1864.

Hung CT, Lima EG, Mauck RL, Takai E, LeRoux MA, Lu HH, Stark RG, Guo XE, Ateshian GA. 2003. Anatomically shaped osteochondral constructs for articular cartilage repair. J Biomech 36(12):1853-64.

Huntley JS, Bush PG, McBirnie JM, Simpson AH, Hall AC. 2005. CHONDROCYTE DEATH ASSOCIATED WITH HUMAN FEMORAL OSTEOCHONDRAL HARVEST AS PERFORMED FOR MOSAICPLASTY. Journal of Bone and Joint Surgery 87(2):351-60.

Hunziker EB, Quinn TM, Hauselmann HJ. 2002. Quantitative structural organization of normal adult human articular cartilage. Osteoarthritis Cartilage 10(7):564-72.

Hutmacher DW, Singh H. 2008. Computational fluid dynamics for improved bioreactor design and 3D culture. Trends in Biotechnology 26(4):166-172.

Hwang CM, Sant S, Masaeli M, Kachouie NN, Zamanian B, Lee SH, Khademhosseini A. 2010. Fabrication of three-dimensional porous cell-laden hydrogel for tissue engineering. Biofabrication 2(3):035003.

Imhof H, Breitenseher M, Kainberger F, Rand T, Trattnig S. 1999. Importance of subchondral bone to articular cartilage in health and disease. Top Magn Reson Imaging 10(3):180-92.

Indrawattana N, Chen G, Tadokoro M, Shann LH, Ohgushi H, Tateishi T, Tanaka J, Bunyaratvej A. 2004. Growth factor combination for chondrogenic induction from human mesenchymal stem cell. Biochemical and Biophysical Research Communications 320(3):914-919.

James AM, Thomas B, Anneliese H, Joseph AB. 2004. Post-traumatic osteoarthritis: The role of accelerated chondrocyte senescence. Biorheology 41(3):479-491.

Jeon JE, Schrobback K, Hutmacher DW, Klein TJ. 2012. Dynamic compression improves biosynthesis of human zonal chondrocytes from osteoarthritis patients. Osteoarthritis Cartilage 20(8):906-15.

Johann RM, Renaud P. 2007. Microfluidic patterning of alginate hydrogels. Biointerphases 2(2):73-9.

Kandel RA, Grynpas M, Pilliar R, Lee J, Wang J, Waldman S, Zalzal P, Hurtig M. 2006. Repair of osteochondral defects with biphasic cartilage-calcium polyphosphate constructs in a sheep model. Biomaterials 27(22):4120-31.

Kapur S, Baylink DJ, William Lau KH. 2003. Fluid flow shear stress stimulates human osteoblast proliferation and differentiation through multiple interacting and competing signal transduction pathways. Bone 32(3):241-251.

Kenneth A. Williams SS, Timothy M. Wick,. 2002. Computational Fluid Dynamics Modeling of Steady-State Momentum and Mass Transport in a Bioreactor for Cartilage Tissue Engineering. Biotechnology Progress 18(5):951-963.

Khademhosseini A, Langer R, Borenstein J, Vacanti JP. 2006. Microscale technologies for tissue engineering and biology. Proceedings of the National Academy of Sciences of the United States of America 103(8):2480-7.

Khan IM, Gilbert SJ, Singhrao SK, Duance VC, Archer CW. 2008. Cartilage integration: evaluation of the reasons for failure of integration during cartilage repair. A review. European cells & materials 16(0):26-39.

Kim B-S, Mooney DJ. 1998. Development of biocompatible synthetic extracellular matrices for tissue engineering. Trends in Biotechnology 16(5):224-230.

Kreke MR, Huckle WR, Goldstein AS. 2005. Fluid flow stimulates expression of osteopontin and bone sialoprotein by bone marrow stromal cells in a temporally dependent manner. Bone 36(6):1047-1055.

Kreklau B, Sittinger M, Mensing MB, Voigt C, Berger G, Burmester GR, Rahmanzadeh R, Gross U. 1999. Tissue engineering of biphasic joint cartilage transplants. Biomaterials 20(18):1743-1749.

Kuo CK, Tuan RS. 2003. Tissue engineering with mesenchymal stem cells. Engineering in Medicine and Biology Magazine, IEEE 22(5):51-56.

Lawrence BJ, Devarapalli M, Madihally SV. 2009. Flow dynamics in bioreactors containing tissue engineering scaffolds. Biotechnology and Bioengineering 102(3):935-947.

Lee S-H, Moon JJ, West JL. 2008. Three-dimensional micropatterning of bioactive hydrogels via two-photon laser scanning photolithography for guided 3D cell migration. Biomaterials 29(20):2962-2968.

Lee W, Lee V, Polio S, Keegan P, Lee J-H, Fischer K, Park J-K, Yoo S-S. 2010. On-demand three-dimensional freeform fabrication of multi-layered hydrogel scaffold with fluidic channels. Biotechnology and Bioengineering 105(6):1178-1186.

Lees S. 2003. Mineralization of type I collagen. Biophysical Journal 85(1):204-207.

Lima EG, Mauck RL, Han SH, Park S, Ng KW, Ateshian Ga, Hung CT. 2004. Functional tissue engineering of chondral and osteochondral constructs. Biorheology 41(3-4):577-90.

Lin Z, Willers C, Xu J, Zheng MH. 2006. The chondrocyte: biology and clinical application. Tissue Eng 12(7):1971-84.

Ling Y, Rubin J, Deng Y, Huang C, Demirci U, Karp JM, Khademhosseini A. 2007. A cell-laden microfluidic hydrogel. Lab on a chip 7(6):756-62.

Mackay AM, Beck SC, Murphy JM, Barry FP, Chichester CO, Pittenger MF. 1998. Chondrogenic differentiation of cultured human mesenchymal stem cells from marrow. Tissue Eng 4(4):415-28.

Mahmoudifar N, Doran PM. 2013. Osteogenic differentiation and osteochondral tissue engineering using human adipose-derived stem cells. Biotechnology Progress 29(1):176-185.

Marklein RA, Burdick JA. 2010a. Controlling Stem Cell Fate with Material Design. Advanced Materials 22(2):175-189.

Marklein RA, Burdick JA. 2010b. Spatially controlled hydrogel mechanics to modulate stem cell interactions. Soft Matter 6(1):136-143.

Martin I, Miot S, Barbero A, Jakob M, Wendt D. 2007. Osteochondral tissue engineering. Journal of biomechanics 40(4):750-765.

Martin I, Wendt D, Heberer M. The role of bioreactors in tissue engineering. Trends in Biotechnology 22(2):80-86.

Massague J. 1990. The Transforming Growth Factor-beta Family. Annual Review of Cell Biology 6(1):597-641.

Mats B. 2008. Autologous chondrocyte implantation—Technique and long-term follow-up. Injury 39(1, Supplement):40-49.

Mauck RL, Soltz MA, Wang CC, Wong DD, Chao PH, Valhmu WB, Hung CT, Ateshian GA. 2000. Functional tissue engineering of articular cartilage through dynamic loading of chondrocyte-seeded agarose gels. J Biomech Eng 122(3):252-60.

Mauck RL, Yuan X, Tuan RS. 2006. Chondrogenic differentiation and functional maturation of bovine mesenchymal stem cells in long-term agarose culture. Osteoarthritis and Cartilage 14(2):179-189.

Maul T, Chew D, Nieponice A, Vorp D. 2011. Mechanical stimuli differentially control stem cell behavior: morphology, proliferation, and differentiation. Biomechanics and Modeling in Mechanobiology 10(6):939-953.

McCall J, Luoma J, Anseth K. 2012. Covalently tethered transforming growth factor beta in PEG hydrogels promotes chondrogenic differentiation of encapsulated human mesenchymal stem cells. Drug Delivery and Translational Research 2(5):305-312.

Melchels FPW, Domingos MAN, Klein TJ, Malda J, Bartolo PJ, Hutmacher DW. 2012. Additive manufacturing of tissues and organs. Progress in Polymer Science 37(8):1079-1104.

Merceron C, Portron S, Masson M, Fellah BH, Gauthier O, Lesoeur J, Chérel Y, Weiss P, Guicheux J, Vinatier C. 2010. Cartilage tissue engineering: From hydrogel to mesenchymal stem cells. Bio-Medical Materials And Engineering 20(3):159-166.

Miyanishi K, Trindade MC, Lindsey DP, Beaupre GS, Carter DR, Goodman SB, Schurman DJ, Smith RL. 2006. Effects of hydrostatic pressure and transforming growth factor-beta 3 on adult human mesenchymal stem cell chondrogenesis in vitro. Tissue Eng 12(6):1419-28.

Morgan EF, Bayraktar HH, Keaveny TM. 2003. Trabecular bone modulus–density relationships depend on anatomic site. Journal of Biomechanics 36(7):897-904.

Mow VC, Holmes MH, Michael Lai W. 1984. Fluid transport and mechanical properties of articular cartilage: A review. Journal of biomechanics 17(5):377-394.

Mow VC, Kuei SC, Lai WM, Armstrong CG. 1980. Biphasic Creep and Stress Relaxation of Articular Cartilage in Compression: Theory and Experiments. Journal of Biomechanical Engineering 102(1):73-84.

Nelson F, Billinghurst RC, Pidoux I, Reiner A, Langworthy M, McDermott M, Malogne T, Sitler DF, Kilambi NR, Lenczner E and others. 2006. Early post-traumatic osteoarthritis-like changes in human articular cartilage following rupture of the anterior cruciate ligament. Osteoarthritis and Cartilage 14(2):114-119.

Niederauer GG, Slivka MA, Leatherbury NC, Korvick DL, Harroff HH, Ehler WC, Dunn CJ, Kieswetter K. 2000. Evaluation of multiphase implants for repair of focal osteochondral defects in goats. Biomaterials 21(24):2561-74.

Nuttelman CR, Tripodi MC, Anseth KS. 2006. Dexamethasone-functionalized gels induce osteogenic differentiation of encapsulated hMSCs. Journal of Biomedical Materials Research Part A 76A(1):183-195.

Papachroni KK, Karatzas DN, Papavassiliou KA, Basdra EK, Papavassiliou AG. Mechanotransduction in osteoblast regulation and bone disease. Trends in Molecular Medicine 15(5):208-216.

Park JH, Chung BG, Lee WG, Kim J, Brigham MD, Shim J, Lee S, Hwang CM, Durmus NG, Demirci U and others. 2010. Microporous cell-laden hydrogels for engineered tissue constructs. Biotechnology and Bioengineering 106(1):138-148.

Park JS, Chu JS, Tsou AD, Diop R, Tang Z, Wang A, Li S. 2011. The effect of matrix stiffness on the differentiation of mesenchymal stem cells in response to TGF-β. Biomaterials 32(16):3921-3930.

Pittenger MF, Mackay AM, Beck SC, Jaiswal RK, Douglas R, Mosca JD, Moorman MA, Simonetti DW, Craig S, Marshak DR. 1999. Multilineage Potential of Adult Human Mesenchymal Stem Cells. Science 284(5411):143-147.

Porter B, Zauel R, Stockman H, Guldberg R, Fyhrie D. 2005. 3-D computational modeling of media flow through scaffolds in a perfusion bioreactor. Journal of Biomechanics 38(3):543-549.

Re'em T, Tsur-Gang O, Cohen S. 2010. The effect of immobilized RGD peptide in macroporous alginate scaffolds on TGFβ1-induced chondrogenesis of human mesenchymal stem cells. Biomaterials 31(26):6746-6755.

Roberts SJ, Tomlins PE, Faruqui N, Robinson JaJ. 2011. Diffusion of biologically relevant molecules through gel-like tissue scaffolds. Biotechnology Progress 27(1):251-61.

Roelen BAJ, Dijke Pt. 2003. Controlling mesenchymal stem cell differentiation by TGFB family members. Journal of Orthopaedic Science 8(5):740-748.

Saini S, Wick TM. 2003. Concentric Cylinder Bioreactor for Production of Tissue Engineered Cartilage: Effect of Seeding Density and Hydrodynamic Loading on Construct Development. Biotechnology Progress 19(2):510-521.

Schaefer D, Martin I, Jundt G, Seidel J, Heberer M, Grodzinsky A, Bergin I, Vunjak-Novakovic G, Freed LE. 2002. Tissue-engineered composites for the repair of large osteochondral defects. Arthritis Rheum 46(9):2524-34.

Schaefer D, Martin I, Shastri P, Padera RF, Langer R, Freed LE, Vunjak-Novakovic G. 2000. In vitro generation of osteochondral composites. Biomaterials 21(24):2599-606.

Schek RM, Taboas JM, Segvich SJ, Hollister SJ, Krebsbach PH. 2004. Engineered osteochondral grafts using biphasic composite solid free-form fabricated scaffolds. Tissue Eng 10(9-10):1376-85.

Scotti C, Buragas MS, Mangiavini L, Sosio C, Di Giancamillo a, Domeneghini C, Fraschini G, Peretti GM. 2007. A tissue engineered osteochondral plug: an in vitro morphological evaluation. Knee surgery, sports traumatology, arthroscopy : official journal of the ESSKA 15(11):1363-9.

Sengers BG, van Donkelaar CC, Oomens CWJ, Baaijens FPT. 2005. Computational study of culture conditions and nutrient supply in cartilage tissue engineering. Biotechnology Progress 21(4):1252-1261.

Sherwood JK, Riley SL, Palazzolo R, Brown SC, Monkhouse DC, Coates M, Griffith LG, Landeen LK, Ratcliffe A. 2002. A three-dimensional osteochondral composite scaffold for articular cartilage repair. Biomaterials 23(24):4739-4751.

Sikavitsas VI, Bancroft GN, Holtorf HL, Jansen JA, Mikos AG. 2003. Mineralized matrix deposition by marrow stromal osteoblasts in 3D perfusion culture increases with increasing fluid shear forces. Proceedings of the National Academy of Sciences 100(25):14683-14688.

Simon TM, Jackson DW. 2006. Articular Cartilage: Injury Pathways and Treatment Options. Sports Medicine and Arthroscopy Review 14(3):146-154.

Song YS, Lin RL, Montesano G, Durmus NG, Lee G, Yoo S-S, Kayaalp E, Haeggström E, Khademhosseini A, Demirci U. 2009. Engineered 3D tissue models for cell-laden microfluidic channels. Analytical and bioanalytical chemistry 395(1):185-93.

Spaulding GF, Jessup JM, Goodwin TJ. 1993. ADVANCES IN CELLULAR CONSTRUCTION. Journal of Cellular Biochemistry 51(3):249-251.

Sucosky P, Osorio DF, Brown JB, Neitzel GP. 2004. Fluid mechanics of a spinner-flask bioreactor. Biotechnology and Bioengineering 85(1):34-46.

Sugiura S, Sakai Y, Nakazawa K, Kanamori T. 2011. Superior oxygen and glucose supply in perfusion cell cultures compared to static cell cultures demonstrated by simulations using the finite element method. Biomicrofluidics 5(2):22202-22202.

Swieszkowski W, Tuan BHS, Kurzydlowski KJ, Hutmacher DW. 2007. Repair and regeneration of osteochondral defects in the articular joints. Biomolecular Engineering 24(5):489-495.

Szafranski JD, Grodzinsky AJ, Burger E, Gaschen V, Hung HH, Hunziker EB. 2004. Chondrocyte mechanotransduction: effects of compression on deformation of intracellular organelles and relevance to cellular biosynthesis. Osteoarthritis Cartilage 12(12):937-46.

Taguchi T, Sawabe Y, Kobayashi H, Moriyoshi Y, Kataoka K, Tanaka J. 2004. Preparation and characterization of osteochondral scaffold. Materials Science and Engineering: C 24(6–8):881-885.

Temenoff JS, Mikos AG. 2000. Review: tissue engineering for regeneration of articular cartilage. Biomaterials 21(5):431-40.

Tse JR, Engler AJ. 2001. Preparation of Hydrogel Substrates with Tunable Mechanical Properties. Current Protocols in Cell Biology: John Wiley & Sons, Inc.

Tuli R, Nandi S, Li WJ, Tuli S, Huang X, Manner PA, Laquerriere P, Noth U, Hall DJ, Tuan RS. 2004. Human mesenchymal progenitor cell-based tissue engineering of a single-unit osteochondral construct. Tissue Eng 10(7-8):1169-79.

Tuli R, Tuli S, Nandi S, Huang X, Manner PA, Hozack WJ, Danielson KG, Hall DJ, Tuan RS. 2003. Transforming Growth Factor-β-mediated Chondrogenesis of Human Mesenchymal Progenitor Cells Involves N-cadherin and Mitogen-activated Protein Kinase and Wnt Signaling Cross-talk. Journal of Biological Chemistry 278(42):41227-41236.

Vinatier C, Guicheux J, Daculsi G, Layrolle P, Weiss P. 2006. Cartilage and bone tissue engineering using hydrogels. Bio-Medical Materials And Engineering 16(4 Suppl):S107-S113.

Vunjak-Novakovic G, Obradovic B, Martin I, Freed LE. 2002. Bioreactor studies of native and tissue engineered cartilage. Biorheology 39(1-2):259-68.

Vuong J, Hellmich C. 2011. Bone fibrillogenesis and mineralization: Quantitative analysis and implications for tissue elasticity. Journal of Theoretical Biology 287(1):115-130.

Waldman SD, Spiteri CG, Grynpas MD, Pilliar RM, Hong J, Kandel RA. 2003a. Effect of biomechanical conditioning on cartilaginous tissue formation in vitro. J Bone Joint Surg Am 85-A Suppl 2:101-5.

Waldman SD, Spiteri CG, Grynpas MD, Pilliar RM, Kandel RA. 2003b. Long-term intermittent shear deformation improves the quality of cartilaginous tissue formed in vitro. Journal of Orthopaedic Research 21(4):590-596.

Waldman SD, Spiteri CG, Grynpas MD, Pilliar RM, Kandel RA. 2004. Long-term intermittent compressive stimulation improves the composition and mechanical properties of tissue-engineered cartilage. Tissue Eng 10(9-10):1323-31.

Wang EA, Rosen V, D'Alessandro JS, Bauduy M, Cordes P, Harada T, Israel DI, Hewick RM, Kerns KM, LaPan P. 1990. Recombinant human bone morphogenetic protein induces bone formation. Proceedings of the National Academy of Sciences 87(6):2220-2224.

Wang X, Grogan SP, Rieser F, Winkelmann V, Maquet V, Berge ML, Mainil-Varlet P. 2004. Tissue engineering of biphasic cartilage constructs using various biodegradable scaffolds: an in vitro study. Biomaterials 25(17):3681-8.

Worster AA, Brower-Toland BD, Fortier LA, Bent SJ, Williams J, Nixon AJ. 2001. Chondrocytic differentiation of mesenchymal stem cells sequentially exposed to transforming growth factor-β1 in monolayer and insulin-like growth factor-I in a three-dimensional matrix. Journal of Orthopaedic Research 19(4):738-749.

Wozney JM. 1992. The bone morphogenetic protein family and osteogenesis. Molecular Reproduction and Development 32(2):160-167.

Yang F, Williams CG, Wang D-a, Lee H, Manson PN, Elisseeff J. 2005. The effect of incorporating RGD adhesive peptide in polyethylene glycol diacrylate hydrogel on osteogenesis of bone marrow stromal cells. Biomaterials 26(30):5991-5998.

Yang YH, Barabino GA. 2011. Requirement for serum in medium supplemented with insulin-transferrin-selenium for hydrodynamic cultivation of engineered cartilage. Tissue Eng Part A 17(15-16):2025-35.

Yao H, Gu WY. 2004a. Physical signals and solute transport in cartilage under dynamic unconfined compression: finite element analysis. Annals of Biomedical Engineering 32(3):380-90.

Yao H, Gu WY. 2004b. Physical signals and solute transport in cartilage under dynamic unconfined compression: Finite element analysis. Annals of Biomedical Engineering 32(3):380-390.

Yu X, Botchwey EA, Levine EM, Pollack SR, Laurencin CT. 2004. Bioreactor-based bone tissue engineering: the influence of dynamic flow on osteoblast phenotypic expression and matrix mineralization. Proc Natl Acad Sci U S A 101(31):11203-8.